AN ABSTRACT OF THE DISSERTATION OF

Callie Branyan for the degree of Doctor of Philosophy in Robotics presented on August 24, 2020.

Title: Improving Soft Snake Robot Locomotion Through Targeted Environmental Interactions Using Artificial Snake Skin

Abstract approved: ______________________________

Yiğit Mengüç   Ross L. Hatton

This dissertation outlines the design and development of the first fully-soft, snake robot and its snake-inspired skin. Soft robotics takes advantage of soft materials to, among other things, improve robot interactions with complex, unstructured environments. Due to the interplay between the soft material and the environment, minor tweaks to the morphological design of the robot can produce major changes in behavior when using the same control input. The research goal of this dissertation was to determine how the locomotion a soft snake robot, using a lateral undulation gait, can be improved by targeting a specific environmental interaction through the confluence of body design, gait design, and interfacial mechanism design.

Understanding how these three areas of design can affect one another is key in developing robots that are adaptable in a range of environments. Each design area is addressed in a chapter of this dissertation to illustrate how changes to one area propagate to others, and how that can be an advantage to improving the locomotion of a soft robot. Chapter 3 examines how the body design of the robot changes its locomotion capabilities in granular media, focusing on interactions between the body and the ridges formed in the media. Chapter 4 illustrates how improvements to the gait can also be driven by interactions between the robot's body and the granular media.

The design and implementation of an interfacial mechanism to further improve locomotion is described in Chapter 5. Kirigami, a Japanese art form involving the patterning

of cuts in thin materials, is used to create a snake-inspired skin. The skin design targets directional friction, a morphological characteristic vital to snake locomotion in two axes. Most skins implemented for snake robots focus only on the longitudinal axis for creating directional friction. However, lateral undulation, the gait employed throughout this work, requires a significant lateral resistance to successfully create locomotion. This interfacial mechanism is designed specifically for the kinematics of the soft actuators as well as the production of directional friction in two axes, which required the creation of a new set of radial kirigami lattices.

Each chapter demonstrates how improvements to locomotion can come from designing the morphological characteristics of the robot alongside the development of a gait and interfacial mechanisms by targeting specific, bioinspired interactions between the robot and the environment. The final iteration of system resulted in a soft robot and it's snake-inspired skin with a 530% improvement in velocity over the original robot with no skin. The main contributions of this dissertation are:

1. The development of the first fully-soft snake robot.
2. A skin for lateral undulation with two axes of directional friction
3. A set of new kirigami lattice structures that can be used for bending actuators
4. A framework in which to investigate bioinspired design of robots in three areas of design: morphology, gait, and interfacial mechanisms.

Improving Soft Snake Robot Locomotion Through Targeted Environmental Interactions Using Artificial Snake Skin

by

Callie Branyan

A DISSERTATION

submitted to

Oregon State University

in partial fulfillment of
the requirements for the
degree of

Doctor of Philosophy

Presented August 24, 2020
Commencement June 2021

Doctor of Philosophy dissertation of Callie Branyan presented on August 24, 2020.

APPROVED:

Co-Major Professor, representing Robotics

Co-Major Professor, representing Robotics

Head of the School of Mechanical, Industrial and Manufacturing Engineering

---

Dean of the Graduate School

I understand that my dissertation will become part of the permanent collection of Oregon State University libraries. My signature below authorizes release of my dissertation to any reader upon request.

Callie Branyan, Author

ACKNOWLEDGEMENTS

This work was supported by the National Science Foundation, under award IIS-1734627, and the Office of Naval Research, under award N00014-16-1-2529. I received technical assistance from Chloe Flemming and Jacquelin Remaley in implementing the gaits used throughout this work. I also received guidance from Katia Bertoldi, and Ahmad Rafsanjani on working with kirigami to develop the skin. I worked with two excellent undergraduate researchers, Lily Orth-Smith and Gabriel Kulp in implementing the pneumatic control board used to drive the robots.

I of course have enormous gratitude for my advisors Yiğit Mengüç and Ross Hatton for their guidance and enthusiasm in propelling me through my doctoral program. All members of the mLab contributed their moral and intellectual support in many ways, and I greatly appreciate our time together. I thank my committee for their time and flexibility in working with my adjusted timeline upended by the global pandemic.

Finally, I thank my family for always supporting me through all the ups and downs that define a doctoral program.

TABLE OF CONTENTS

TABLE OF CONTENTS (Continued)

TABLE OF CONTENTS (Continued)

LIST OF FIGURES

LIST OF FIGURES (Continued)

LIST OF FIGURES (Continued)

LIST OF FIGURES (Continued)

LIST OF FIGURES (Continued)

Chapter 1: Introduction

Soft structures are ubiquitous in nature and are utilized by animals to navigate their respective environments. The morphology, including macro-scale body shape and micro-scale material features, of these soft structures allow the animal to adapt to complex environments without the need for large brains or complex control loops. Conversely, traditional robots are made with rigid materials that limit the flexibility and physical adaptability of the robot. The use of rigid materials allows for the completion of fast and precise control tasks when the task and environment are fully defined. When placed in dynamic, unstructured environments, these traditional robots tend to fail by falling over, getting stuck, or performing tasks on a loop that are unhelpful. However, undefined, and constantly changing environments are exactly the kinds of environments in which robots would be most useful.

Soft robotics takes advantage of soft materials to, among other things, improve robot interactions with complex, unstructured environments. For the purposes of this dissertation, soft refers to both the functional softness and the interactional softness of the robot. Functional softness refers to the compliancy of actuators and the method of actuation. Interactional softness refers to the material properties of the robot in which the body itself is soft and results in compliant and damped interactions with the environment. Therefore, the definition of "soft robot" used throughout this work refers to a robot made primarily of soft, elastomeric materials such that the actions of the robot are controlled by functional soft materials and interactions with the world are through a soft medium. Biological systems can successfully adapt to dynamic environments by coevolving morphological characteristics and behaviors with their environments. Potential applications for soft, bioinspired robots include urban search and rescue, exploration of unknown environments, and medical robotics. These applications require the ability to navigate narrow spaces, cross a range of terrains, enact a set of disparate motions, and interact with the environment without causing undue disturbances. These actions are difficult to realize with a traditional, rigid robot, but are (potentially) inherent with soft robots.

Most animals have a combination of rigid and soft structures that bring the advantages of both to successfully interact with their environment. However, there are certain families of animals that are mostly soft, and can produce a wide range of adaptable behaviors that would be impossible to do with a purely rigid structure. Snakes, which are primarily soft with only a rigid but highly flexible backbone, can navigate many disparate environments from tops of trees to burrowing in the sand. Worms, which are completely soft, can alter the cross-sectional area of their body to produce complex locomotion patterns, and anchor to their surroundings to crawl up vertical structures. These animals are successful in their specific tasks due to the flexibility and compliancy of their bodies. They are not as fast or strong as animals with more rigid components, but their adaptability to unstructured environments provides an advantage in their evolved ecological niche.

Snakes are an ideal candidate for the bioinspiration of a robot that can locomote in various environments. Rigid snake robots previously developed however, are unable to fully realize the flexibility and robustness that biological snakes exhibit in nature. There are morphological and behavioral examples seen in biological snakes that can inspire improvements to their design. Most improvements to locomotion have been implemented through increasing the complexity of gait design and control. The research goal of this dissertation is to determine how the bioinspired design and implementation of a soft snake robot can be improved by targeting a specific environmental interaction through the confluence of body design, gait design, and external mechanism design.

Snakes can move effectively in nearly all environments. Each species shares a general morphology of an elongated, limbless trunk, a head and tail, and a scale-patterned skin, but the specifics of each morphological characteristic changes depending on the environment in which the species evolved. There are a range of rigid snake robots that have been made in the past that focus on recreating the general morphology of the biological system and relying on the control over the gait to successfully navigate over a limited set of terrains [6]. The Series Elastic Actuator Snake from Carnegie Mellon University uses a soft element in their design to increase compliance and produce better torque control [7]. Though this robot is compliant across unstructured terrains, the robot is still considered rigid for the purposes of this dissertation as the primary interactions between the robot and the environment take place with rigid materials. Currently there is only one other soft snake robot in development. It too only produces the general morphology of a biological snake and relies heavily on the use of passive wheels to achieve locomotion, severely limiting the potential terrains it can traverse [8]. Most current rigid or soft snake robots rely on the development of a complex control system to implement gaits and attempt to optimize performance through the alteration of these gait. This strategy is contrary to the potential advantages provided by using soft materials.

Improvements to the robustness and adaptability of a soft robot need to go beyond the control strategy to take make use of the inherent advantages of using soft material. Due to the interplay between the soft material and the environment, minor tweaks to the morphological design of the robot can produce major changes in behavior when using the same control input. Therefore, when designing soft robots, the effects of body design, gait strategy, and external mechanism design need to be considered as a whole, rather than separate branches of investigation. Understanding how these three areas of design affect one another can also be explored through the lens of bioinspiration. Morphological characteristics of snakes can vary depending on their environment and, in combination with gait selection, snakes can produce a wide range of useful behaviors. By identifying how these changes in morphological characteristics affects locomotion capabilities, we can determine what set of characteristics would be useful to implement on a soft, snake-inspired robot.

One of the defining characteristics of snakes is their skin. The outer layer of snakeskin is covered in a pattern of overlapping scales that can be controlled by various muscles to engage with the surface the snake is navigating. Snakeskin is a unique adaptation to limbless locomotion utilizing frictional anisotropy to push the snake forward as it undulates its body. Frictional anisotropy refers to the characteristic that friction is higher when the snake slides backwards than when it slides forwards. Snakeskin varies depending on species as it has evolved its own set of characteristics based on the environment. Two characteristics of interest in the variance of snakeskin are microornamentation and the presence of keels. Microornamentation is the micro-ridges, nanoindentation, or other microstructures that can be found on the surface of scales. As with all morphological characteristics of snakes, microornamentation can vary across environment specific species and have their own frictional anisotropy. Arboreal snakes large denticulations/pits as well as raised ridges (sometimes referred to as keels) on their scales. Aquatic snake species have relatively smooth scale surfaces as the frictional properties are not as vital for locomotion through water [9]. Another definition of keels refer to raised ridges of scales on the ventrolateral position of the snake's body. They are a common attribute in arboreal species as these stiff ridges provide higher regions of friction and engagement that allow the snake to dig into bark and to prevent sliding when climbing vertically [10].

Friction is the key environmental interaction for the success of limbless locomotion through most terrestrial environments. Snakes have evolved an excellent external mechanism through their skin to engage with the terrain and promote useful behaviors. Animals are robust and adaptable to many terrains and situations because they work together with their environment to produce useful behaviors. Many state-of-the-art robots are designed and implemented as a separate entity from the environment in which they are placed. Or, in many cases, the environment is altered to better accommodate the robot. To get robots out of the lab and into real world situations where they will be most useful, they will have to adapt to a range of environments, most of which will not be known ahead of time. To improve a robot's capabilities, its design and control should be centered around a targeted environmental interaction. In the case of snake robots. I propose that designing the robot around enhancing directional friction will result in increasing its velocity through various terrains. The work presented in this dissertation examines how the locomotion of a snake-inspired robot is affected by the design of the robot's body, the gait the robot employs, and the design of a snake-inspired skin as an external mechanism targeting directional friction.

The structure of the dissertation is as follows. Chapter 2 covers background information on limbless locomotion strategies in nature and the soft robots designed to enact them, focusing on the advantages that snakes have in inspiring the design of robots to navigate variable terrains. Chapter 3 investigates how the design of the robot's body alters its behavior when employing the same control strategy. Chapter 4 presents a comparison of gait strategies across different terrains. Chapter 5 examines the design and implementation of a snake-inspired skin developed to target directional friction. The dissertation concludes with Chapter 6 summarizing the contributions of this work and future directions.

Chapter 2: Background

Improving the robustness and adaptability of robots in unstructured environments is a central goal in the field of robotics. Bioinpsiration is a common avenue of innovation for the design and control of robots. Most animals are a hybrid of soft and rigid structures that work together to make them successful in navigating and surviving their environment. It is rare to have an animal that is completely rigid, or completely soft. Considering how prevalent soft structures are in nature, fully understanding how animals utilize their softness to enact gaits and interact with their environment to produce useful behaviors will be essential in creating robots that can adapt to unknown terrain and survive unexpected conditions. Fully soft robots need to be further explored to determine the contributions of their soft structures to their locomotion.

Organisms in nature that are fully, or mostly soft, are often limbless and use the deformation of their soft bodies to produce locomotion and enact productive interactions with their environment. Snakes are one of the most adaptable animals that are mostly soft. They are found in almost all environments around the world and have a range of behaviors that allow them to deal with unexpected events and obstacles. Therefore, they are a useful source of bioinspiration to produce adaptable robots. However, there has not been extensive development of a soft snake robot, and those developed with traditional, rigid materials have focused more on the control and implementation of gaits. This chapter reviews soft robot technologies and current state-of-the art snake robots to identify the gaps that this work fills. It also introduces environment-specific snake morphology that can be applied to the design of a fully soft snake robot to improve its locomotion capabilities.

2.1 Body Design

2.1.1 Rigid vs Soft Robots

Traditional robots are made of rigid materials such as aluminum or carbon fiber. The exclusive use of these rigid materials is contrary to what is seen in nature. Biological systems are, for the most part, hybrid structures. In nature, these organisms make use of elastic and flexible materials to adapt to complex unstructured environments [11]. Scientists and engineers have developed traditional robots using rigid materials because they can perform repetitive tasks that require fast, strong, and precise actions [12]. In this realm, rigid robots are an excellent solution. However, as the field of robotics continues to grow, the environments in which robots would be most useful expands as well. These new potential environments are increasingly complex, unstructured, and impossible to account for as they are apt to change minute to minute. Traditional robots are consistently successful only in environments that are highly structured and well defined. These environments include factories, labs, and environments designed around the robot to ensure success [13]. When traditional robots are placed in complex, unstructured environments, they often cannot adapt to the changing conditions, and will likely fail after only a few disturbances. Rigid materials also limit robots in navigating narrow or confined spaces, complex manipulations of an object or the handling of delicate objects, and interacting safely with humans. The addition of soft materials could increase the adaptability and robustness of robots, making future state-of-the-art robots hybrid structures found throughout nature.

Soft materials allow robots to conform to their environment and deform into complex shapes. Their ability to realize these complex configurations would increase the complexity of manipulation skills, and their inherent softness would not cause undue damage to the object they are handling. For example, octopus tentacles, a completely soft structure, can deform into a large set of shapes due to their morphology and material properties. They can manipulate objects with the same dexterity as human hands, and can vary the force of interaction between powerful and delicate grips [14]. The natural compliancy of soft robots makes them suitable platforms for implementing locomotion through complex, unstructured environments. The softness of the robot allows them to adapt to their environment without requiring a complicated and robust control system to account for every disturbance. They can also interact with the environment without causing unnecessary disturbances or damage to said environment. Soft robots can absorb perturbations caused by interacting with an obstacle whereas rigid robots would likely bounce off the obstacle, likely displacing the obstacles, and causing a potential unrecoverable state of the robot. The flexibility and conformability of a soft robot means that they can strategically interact with obstacles to further their locomotion or manipulation tasks.

2.1.2 Review of Soft Actuators

The robots examined in this review are operated using three common actuation methods in soft robotics: fluidic actuation, dielectric elastomeric actuation (DEA), and shape memory alloy (SMA) actuation. The first, and most widely used, actuation method for soft robots is the use of pressurized fluids such as air or water to produce motion. The McKibben actuators [15] were the first fluidic actuator that proved such actuators can produce powerful actuation without the need for rigid structures. They inspired the development of fiber-reinforced actuators [16] and Pneu-nets [17], two of the most common fluidic actuators. By altering the morphology of the actuator, the desired shape of deformation can be produced [18], thereby mechanically preprogramming the actuator for a specific shape space [19]. However, these actuators require high power, and complex valving systems. These requirements limit soft robots in size, and untethering abilities although a successfully untethered robot developed solely on fluidic actuators was developed in [20].

DEAs are made from soft materials that actuate through electrostatic forces. They deform due to the electrostatic interaction between two electrodes with opposite electric charge. Though they do not require the use of pumps and valves like fluidic actuators, they do present their own limitations [21]. First, a rigid frame that pre-strains the elastomer is required. Though some designs have been developed without a rigid frame they produce lower forces than designs with rigid components, and the fabrication process is more complex [22]. Second, the reliability of the compliant electrodes needs improvement. Lastly, DEAs require high voltages to operate which is not ideal in many applications [12].

Shape memory alloys are common for soft actuation because of their high mass-specific force. They are wires that change shape when exposed to a temperature gradient. It is possible to program shapes into the alloys (commonly a nickel-titanium alloy) at different temperatures. It produces actuation by fluctuating temperature to cause the SMA to deform to the preprogrammed shapes at that temperature. Most SMA actuators are made from coils to amplify the overall strain [23]. This makes them easy to integrate into a soft structure. There are many limitations to SMA actuation. These include the challenge of maintaining robust temperature control in varying thermal conditions, the inefficiency of the actuators as most input energy is consumed by heat, and finally, overheating and over straining the actuators is easy and irreversible [12].

2.1.3 Snake Morphology

Soft snake robots can apply the advantages of biological snakes provided by their soft bodies to expand locomotion capabilities. Morphological characteristics that aid biological snake locomotion in a range of environments can be utilized on a new soft snake robot. Below is a review of these morphological characteristics based on three environments of interest: terrestrial, arboreal, and aquatic.

There are almost 3000 species of snakes worldwide, found in all habitats, all over the globe [24]. These different kinds of species have divergent morphologies associated with the environment in which they evolved [25]. The general morphology of a snake is a long, limbless trunk capped by a head and tail, and skin that provides frictional properties that vary depending on the material properties and morphology of the inner and outer skin and scale pattern. Determining how these differing species of snakes, and their subsequent morphologies, evolved, and how these changes in morphology affect locomotion, can provide a framework for improving snake robot locomotion capabilities. Snakes have a range of strategies for swimming, climbing, traversing tree tops, and crossing flat areas. Each strategy employed can be connected to differences in morphological characteristics such as body shape, scale pattern, muscle arrangement, and tail shape and length. These characteristics vary widely depending on the habitat in which the snake has evolved, primary gait pattern, and exposure to predators [26]. This thesis looks at the characteristics that aid in locomotion. These characteristics can be split into two general types. The first characteristic is the body type of the snake which includes the shape of the body, the shape and size of the tail, the aspect ratio, and the length-mass ratio. The second characteristic is the skin properties of the snake which includes the scale profile, texture, stiffness, the patterning of scales, and the addition of features like keels. The work described throughout this dissertation will treat these as two separate systems, examining the success of variations in morphological characteristics of both.

2.1.4 Body Type

The morphology of the trunk of different species of snakes can be broken down further into more discrete characteristics that have been examined by comparative biologists. The characteristics of interest for this thesis are: cross-sectional geometry, aspect ratio, and length-mass ratio. These vary widely depending on the environment the snake inhabits. Tail morphology is also important and becomes most useful in aquatic environments. This thesis focuses on terrestrial environments and a tail was not implemented on the root. However, differences in tail morphology depending on environment show how minor changes in design can lead to major changes in behavior.

Cross Section Geometry

The cross sectional shape of the snake's body changes its ability to interact with the substrate it is navigating. Aquatic snake species are vertically flatter (cross sectional height > width) to increase the cross sectional area of the lateral bends to "push" against the water [27] like an oar. Arboreal snakes are slender and more oblong than cylindrical [10], where as terrestrial snakes are stockier and can be horizontally flatter (cross sectional height < width), or more cylindrical depending on the fluidity of the terrain [24].

Aspect Ratio

The aspect ratio, or the average width of the cross section of the snake to the total length of the snake varies depending on the environment in which the snake evolved. The aspect ratio of the snake's body is linked to the cross sectional shape of its body so the trend between environments is maintained. Terrestrial snakes have wide bodies compared to their length and therefore have smaller aspect ratios [28]. Arboreal snakes on the other hand have high aspect ratios as their bodies are slender and long to increase their ability to navigate tree tops and support their bodies during climbing [10]. Aquatic snakes also have high aspect ratios due to their paddle-like cross section [29].

Length-Mass Ratio

The length-mass ratio of the snakes body is also linked to to its cross sectional shape and its aspect ratio, maintaining the trend between species. Across environments, terrestrial snakes tend to be heavy-bodied compared to their total length, arboreal species are lighter, and aquatic species have a moderate length to mass ratio [25].

Tail Morphology

The size and shape of the tail in snakes also change across environments. The major variations in shape are the differences between terrestrial and aquatic snake species. Aquatic snakes have a more paddle-like tail [29] where as terrestrial snake tails are more conical [30]. The size of tails across species varies as well, but the locomotion trends caused by the variation within species show that the lighter the tail the faster the locomotion [30]. Terrestrial snakes have longer tails than aquatic species [27]. However, arboreal snakes have longer and stiffer tails than terrestrial snakes. It has been shown this is to assist with blood circulation of arboreal species due to the increased effect of gravity on the snake, but it was also proposed that it lends to interacting with branches for anchoring during locomotion [31].

The general trends by studying the body type of snakes across different species shows that despite the shared general morphology, variations such as shape, size and mass are prevalent depending on the environment. These variations can be implemented on a soft snake robot to determine their effectiveness in aiding locomotion across terrestrial environments.

2.1.5 Snake Skin

Snakes have a unique skin that allows them to have useful interactions with their environment to aid locomotion. Determining the differences in morphological characteristics of the skin across species found in terrestrial, arboreal, and aquatic environments can lead to the development of skins for a soft snake robot that aids in traversal through the respective terrains. The morphology of the scales can change across species, and additional stiffening structures like keels can assist snakes in highly specialized environments. The control the snake has over its scales means that they can also vary their frictional properties on command.

Types of Scales

Snakes have a set of dorsal and ventral scales along their body. The ventral scales, along the belly of the snake, are vital to producing the frictional anisotropy that helps snakes move through their environment. They are large and rectangular to oblong shaped, and form a single row along the belly. The dorsal scales can vary in geometry and form overlapping rows along the length of the body. These scales are not vital to the propulsion of the snake through the terrain, but they occasionally are used when interacting with obstacles or during burrowing. Depending on the environment, the morphological characteristics of the scales can vary as well. Microornamentation on the scales can vary across environmentally-specific species and have their own frictional anisotropy due to micro-ridges or nanoindentations. Arboreal snakes usually have large micro-structures (ridges, pits, etc.) to dig into bark for climbing. Aquatic snake species have relatively smooth scale surfaces as the frictional properties are not as vital for locomotion through water [9].

Scale Activation

Snake skin was previously thought to be a passive mechanism to assist snakes in navigating most terrains. However, recently it has been proven that snakes can "activate" their scales in order to latch onto surfaces to propel themselves forward [32]. Depending on that activation, they can decouple their frictional properties from the deformation of their bodies during locomotion.

Keels

Snakes in arboreal habitats have keels, or stiff ridges, that are offset from their belly to help their interactions with bark and branches. These keels can also prevent them from sliding backwards as they crawl vertically up trees. Both the ledge the keels form on the body, and the additional stiffness lend advantages to climbing [10].

The evolution of snake skin depending on the environment shows how important the morphological characteristics are in assisting useful interactions between the morphology and the environment to aid locomotion. Exploring these different characteristics as a separate system from the body can lead to the development of environment specific artificial skins that can be implemented on the robot to improve its behavior in the respective terrains.

2.1.6 Design of Snake Robots

The morphology of biological snakes consists of an elongated body with a rigid and flexible backbone used to create a traveling wave of lateral bends from head to tail. The simple morphology, and its ability to produce locomotion in a variety of terrains is appealing to produce with robots as the traversal of unstructured environments is a highly sought after goal. Snake robots have been developed since the early 1970s introduced by Shigeo Hirose and his work on the Active Cord Mechanism [1]. The required curvature and fluidity of movement seen in biological snakes is replicated on rigid robots through the use of numerous actuators combined in series to discretize the propagating bends. Hirose's early work also developed the serpenoid curve, which is a representation of the fundamental shape function describing the backbone of biological snakes as they execute common gaits [1]. Both the design and locomotion of snake robots has been advanced using Hirose's work as its foundation. The design of rigid snake robots can be organized based on the mechanisms used to produce locomotion.

A common method to produce locomotion in snake robots is to use the serpenoid curve gait and passive wheels to resist lateral movement of the robot's segments. Hirose's rigid snake robots use passive wheels to produce displacement (see Figure 2.1 a). The advantage of using passive wheels is the ability to produce fluid movement that approximates the biological snake gaits well. However, the wheels significantly limit the terrains that can be traversed by the robot, and the level of serpentine motion is limited by how many actuators are used in series, increasing control complexity. Hirose's snake robot requires 20 actuators to approximate snake locomotion and has low functional softness and no interactional softness. Additional mechanisms were used to lift the robot's body to expand the set of traversable terrains, but still requires a relatively flat surface to allow the wheels to roll smoothly [1].

To reduce the number of segments needed to replicate fluid serpentine locomotion, the use of active wheels was implemented by Hirose (see Figure 2.1 b) [1]. Active wheels could provide propulsion, the serpentine pattern of movement was produced by the multi-segment configuration of the robot. Active wheels could also traverse non-smooth terrains. Though active wheels do provide flexibility in terms of active degrees of freedom, it does add complexity to control to coordinate the wheels with the actuated joints.

Howie Choset's group developed a rigid snake robot without wheels to increase the

Figure 2.1: **a)** Original snake robot developed by Hirose using passive wheels [1]. **b)** Active wheel design implemented by Hirose [1]. **c)** Choset's modular snake robot [2].

amount of traversable terrains. Choset's modular snake robot relies on the undulation of the robot, and its interactions with the ground to produce locomotion (see Figure 2.1 c). The robot is made from a chain of single-DOF modules that are combine in series offsetting the joint axis of each module by 90 degrees with respect to the previous joint [2]. This robot can navigate a wide variety of environments, but relies heavily on the design of the gait and real-time control to produce effective locomotion. This robot is limited by the number of modules to produce fluid snake-like locomotion as it takes upwards of 16 modules. Soft snake robots also need several modules to enact snake locomotion, but the number of actuators can be reduced as the actuators are combined in series only to propagate the wave along the backbone, not produce the bends of the wave. Rigid snake robots need at least three segments (two actuators) to produce approach constant curvature whereas soft snake robots need only one for constant curvature.

A series elastic actuator was added to the modules on the Choset snake robot to enable compliant motion and fine torque control [7]. The more compliant motion and torque control enable low impedance motions allowing the robot to naturally comply with obstacles and unstructured terrains. This increase in functional compliance improves the interactions between the robot's body and the environment as is seen with biological snakes [33]. Thought this actuator and control combination has high functional softness, but is still limited in interactional softness.

These robots can approximate snake-like locomotion very well. They are however, limited in terms of the fluidity of geometries they can produce as they rely on a high number of links working in coordination to produce the propagation of lateral bends along the backbone of the robot. The use of multiple modules and rigid materials limits the mechanisms that aid in interacting with the environment to produce effective locomotion. Many rigid snake robots use wheels to ensure net forward displacement, which reduce the applicable environments. The complexity in behavior is also dependent on the coordinated control of the numerous modules to produce the desired gaits.

2.2 Gait Design

2.2.1 Limbless Locomotion in Nature

Limbless locomotion is seen throughout nature. Even some animals with limbs (like lizards) will abandon the use of their limbs and opt for a limbless strategy for traversing especially dense (tall grass) or fluidic (sand, water) environments [34]. Limbless locomotion specifically developed through years of evolution to perform well in environments that are constrictive (tunnels), debris ridden (forest floors), fluidic (sand, mud, water), and highly variable (tops of trees) that do not require speed [35]. There is a broad range of locomotion patterns used by limbless organisms. Snakes will use different forms of undulation to locomote and the specific type of undulation is dependent on the environment. There are crawling locomotion patterns that are used by a variety of animals. Other strategies such as jet propulsion or rolling have been replicated in soft robots, but will not be reviewed here as they are not as common. The wide range of navigable environments with such a simple morphology is of profound interest to scientists and engineers looking to develop systems that can traverse complex and variable terrains.

2.2.2 Undulation

Undulation consists of the propagation of s-shaped bends along the length of the animal's body. The amplitude of the bends may change as they travel, and the curves can be symmetric or asymmetric. Snakes are the most common limbless animal utilizing undulation for terrestrial locomotion. There are three types of snake locomotion that are derivatives of undulation and used in specific environments: lateral undulation, concertina, and sidewinding.

Lateral Undulation

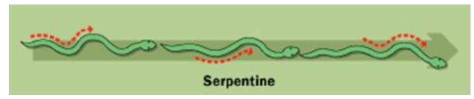

Figure 2.2: Lateral undulation [3]

Also referred to as serpentine locomotion, lateral undulation is the most common way in which snakes produce locomotion and can be used in nearly all terrains. It involves flexing muscles to produce lateral waves that propagate along the snake's backbone [35]. The bends formed can push against debris or rough areas on the surface [36]. On flat, smooth surfaces, snakes use the anisotropy of their scales to create the necessary frictional forces to propel themselves forward. Lateral undulation can also have a lifting pattern where the snake will lift certain parts of its body as the wave propagates creating sliding contact points that remain static as the wave passes through them, and then slide forward with the body [37].

There are many mechanical strategies that have evolved with locomotion and morphology that makes lateral undulation effective. Previous theories were based on the utilization of protruding features in the surface as push-points for the lateral bends of the snake's body to create a resultant vector tangent to the propagating curves [36]. However, this did not explain why snakes could traverse featureless surfaces while using lateral undulation. There has been significant research looking how snakes use their scales and shifting their weight distribution onto specific points. Snake scales can snag asperities in the surface they are traversing and create frictional anisotropy to propel themselves forwards [34]. However, this is not the only reason snakes can slither so quickly. An increase in speed can be explained by the alteration to the frictional forces. Frictional forces are proportional to the weight applied, when the snake lifts parts of its body concentrating its weight on only a few contact points, it generates more thrust.

Concertina Locomotion

Figure 2.3: Concertina gait [3]

Concertina locomotion is often used by snakes for climbing through trees, over especially smooth surfaces, or when traveling through tunnels. It involves the cycling of coiling and sliding (see Figure 2.5) of each half of the body. One half of the body anchors, while the other half slides across the substrate to crawl forwards. The frictional properties of the snake's skin are required to anchor the snake as it coils the other half of its body. This strategy also allows for the traversal of any firm sites and is especially effective in tunnels [38]. Concertina locomotion is very energetically costly and slow in comparison to the other snake locomotion strategies [39].

The snake exerts most of the applied energy to pushing their body against the tunnel walls to ensure stability. On an incline, concertina locomotion is also effective as snakes will use a combination of friction-enhancing techniques such as digging their scales into the ground, as well as wedging against obstacles using a force up to nine times their body weight to push themselves along [40].

Sidewinding

Sidewinding is mainly used by snakes in loose terrains like soil or sand. The snake lifts part of its body off the ground and moves it sideways pushing against static contact points along the ground. Laterally directed slippage is counteracted by the twisting of the body so that the posterior edge digs into the media providing more potential reaction force [35]. The static contact points are actually, from the frame of the body, rolling or peeling points, where the bends of the snake distribute the shear force to prevent slipping. Sidewinding has also been observed as an intermediate gait when transferring from land to water. Sidewinding is the fastest locomotion and most efficient form of snake locomotion [41].

Figure 2.4: Sidewinding gait [3]

Aquatic Undulation

Most aquatic animals use a form of lateral undulation to propel themselves through water. Aquatic undulation has a higher magnitude velocity than terrestrial undulation, but is similar in terms of body-lengths/s [42]. Whereas snakes use their scales to break symmetry and direct motion, eels and other elongated fish use their heads and tails. The morphology of the tail is important as for most aquatic snakes and eels, the tail becomes paddle-like to have more surface area in contact normal to the direction of displacement. These animals will also vary the angle of attack of their tails during the gait cycle, though for the most part it is negative [43].

2.2.3 Crawling Locomotion

Crawling locomotion is another common strategy in limbless locomotion and includes several different gait types. Peristalsis and two-anchor crawling are utilized by caterpillars, worms, and leeches. Snakes use a rectilinear gait which produces crawling, optimizing the use of their scales to produce locomotion. These methods have a generally lower magnitude of velocity than undulation, but are similar in terms of body-lengths/s [4].

Peristalsis

Peristalsis is unique amongst the other gaits described in that it is used by completely soft organisms like worms. It is characterized by a coupled propagation of radial contraction and axial elongation moving down the length of the body. [44]. The radially expanded regions anchor the organism to the substrate while the radially contracted regions advance over the substrate via axial elongation [45]. Unlike most limbless locomotion strategies, peristalsis does not need anisotropic friction to produce locomotion. If the forward and backward friction coefficients are equal, locomotion is produced by altering the percentage of simultaneous body contraction (<50%).

Two Anchor Crawling

Two-anchor crawling is achieved through the cycling of lengthening and shortening of the entire body. As compared to peristalsis, the body of the organism contracts as a whole rather than a wave of contraction propagating along the body. The anchoring is a result of anisotropic friction. As the body slides forward, the anisotropy produces a net forward displacement as the friction in the forward direction is less than that in the backwards direction. The biological solutions for creating this anisotropic friction vary over distinct species. Caterpillars often utilize seta, or bristles, that protrude when the respective body segment is activated. Some organisms have prolegs or suckers that anchor the body during locomotion [46].

Rectilinear Locomotion

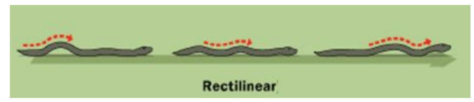

Figure 2.5: Rectilinear gait [3]

Rectilinear locomotion is a hybrid between peristalsis and two-anchor crawling used by large snake species. It is especially useful for climbing and traveling through narrow burrows. It is similar to peristalsis in that it is characterized by a wave of lifting of body segments down the length of the snake. It does not, however, have a mode of radial contraction as seen in peristalsis. Without this couple change in cross-sectional shape, rectilinear locomotion relies on anchoring via frictional anisotropy like two-anchor crawling. The snake contracts certain muscles that pull its belly scales forward producing an angle of attack. The scales then latch onto the asperities in the surface. It then contracts other muscles to push forwards against the latched scales (see Figure 2.5). Snakes that use rectilinear movement have developed scales especially suited for efficient latching [35].

2.2.4 Soft Robot Species Locomotion

Soft robots can conform to surfaces or objects, absorb energy to maintain stability, and present physical robustness at a potentially low cost. These advantages can be applied to broaden the applications of robots in unstructured environments. The scope of this review encompasses robots that are primarily soft and rely on deformations of the body to produce locomotion. This mechanism for locomotion is utilized by many limbless organisms in nature. From snakes to caterpillars, biological, limbless locomotion comes in many forms and inspires many different soft robots currently in development.

To compare locomotion abilities across the field, soft roboticists use body-lengths per second (BL/s) as a quantitative measure of locomotion. A chart of the speeds expressed as BL/s is shown in Figure 2.6 [4]. The velocity in terms of body-lengths per second allows for the comparison of different locomotion strategies across different size scales. The size of robots developed in the soft robotics community vary and using BL/s allows for a direct comparison on performance in terms of speed. The review of robots used to make this chart had an expanded definition of soft robots to include compliant, but mostly rigid, mechanisms as well as limbed robots. Though the scope of this review is strictly soft-bodied, limbless robots, this chart is helpful in showing how limbless locomotion compares to that of other

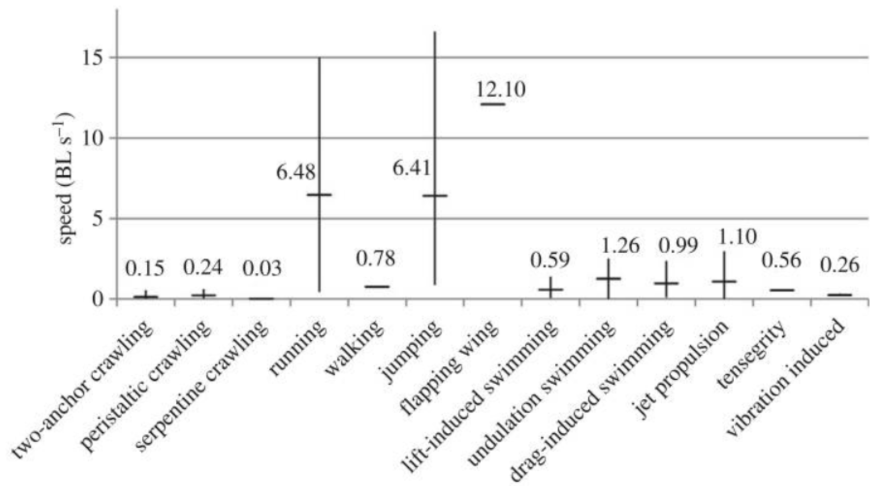

Figure 2.6: Chart of soft robot locomotion in terms of body-lengths per second to allow comparison of these different locomotion strategies across different sized robots [4].

locomotion patterns within soft robotics.

There are several "species" of soft robots that have been developed and studied throughout the literature. Many limbless soft robots produced thus far are worm-inspired using two-anchor crawling or peristalsis as their modes of locomotion. Aquatic soft robots have been developed based on eels, lampreys, and fish. There have been two snake-inspired robots produced in the literature; one using lateral undulation, the other using rectilinear locomotion.

Worms

Many worm-inspired soft robots use two-anchor crawling at their mode of locomotion. Most robots inspired by two-anchor crawling strategies focus on replicating the cycling of elongation and shortening and the differential friction necessary for anchoring. Trimmer et. al. developed worm-inspired robot using two-anchor crawling with actuators made from shape memory alloy springs embedded in a silicone wall [47]. They did not implement a solution for frictional anisotropy until the next generation of the robot in [48] where they designed and implemented prolegs. This strategy for locomotion is effective, but limitations with SMA actuation prevent scaling of the robot using this strategy. Calderon et. al developed a robot inspired by burrowing worms where they used the two-anchor technique to climb a vertical pipe [49]. This utilization of two-anchor crawling would be useful in many applications, but because of the mechanical preprogramming of the robot, it could only climb a pipe of a predetermined size. Expanding capabilities to include pipes of varying sizes or utilizing a different mode of locomotion would be useful for bringing this robot into unstructured environments.

Peristalsis is the other primary mode of locomotion for worm-inspired soft robots. Many of these robots have produced the contraction/elongation gait sequence by creating braided structures using SMA actuators [50, 51, 52]. Though on the more rigid end of the definition of soft robot, these robots were effective in both scaling up the size of the robot and navigating various environments with the locomotion strategy. A study to minimize friction alongside peristalsis production was conducted with Softworm in [53] to define what mechanical strategies could be employed in robots that is not seen in nature. Though peristalsis does not need to employ additional mechanical strategies to deal with friction, its speed is slow enough to opt for other locomotion strategies. It would be useful in combination with another mode of locomotion as its ability to produce locomotion in constrictive or vertical terrains would be advantageous in many robotic applications.

Aquatic Species

Lamprey-inspired robots using SMAs to produce actuation have been developed to enact aquatic undulation [54, 55]. There are very few soft, self-contained, underwater robots as many soft actuators, like SMAs, need to stay dry. Marchese et. al. developed a mostly soft robotic fish where a single rigid section in the middle of the body was used to contain the onboard electronics and power supply [56]. They used fluidic actuators and compressed gas to actuate the soft tail to produce aquatic undulation. They showed that continuum body motion resulted in locomotion underwater which was not achievable with rigid fish-like robots as they were discretized by their rigid actuators. However, their robot's performance was suboptimal as they did not optimize the locomotion pattern in terms of combining variations of undulation with morphology and interactions with the water. They showed a successful self-contained soft robot which is uncommon in the field, and outlined the importance of understanding how gait parameters, morphology, and environmental interactions are necessary to produce a more efficient, better-performing robot.

2.2.5 Control of Snake Robots

A survey of snake-inspired robots from 2009 showed that most snake robots had some degree of functional softness, as they had the flexibility to produce undulation through of use of many discrete links [6]. However, none of these robots had a high degree of interactional softness we use as our definition for "soft robot." They were unable to capture the smooth propagation of the traveling wave produced by continuous curving along the backbone. The use of many rigid actuators limited the conformability to obstacles seen in biological snakes when interacting with their environment. Therefore, the reviewed robots had limitations in what environments they could operate. However, the review emphasizes that production of lateral resistance, employed by biological snakes bracing against obstacles or using the anisotropy of their skin, are required for producing successful terrestrial undulation.

There is only one "soft" snake robot using lateral undulation that has been developed before this thesis. Onal and Rus created a fluidic elastomer robotic snake in [8]. Their robot consists of eight actuators paired antagonistically to achieve bidirectional bending that creates the wave propagation along the backbone. Onal's robot uses passive wheels to create anisotropic friction. This technique allows them to move efficiently on hard, flat surfaces, but severely limits their ability to traverse over any other terrains and limits their interactional softness. Their work elucidates the idea that morphological strategies in replicating anisotropic friction generated from snake scales is necessary to develop a successful soft snake robot.

Katia Bertoldi's group at Harvard developed a crawling soft snake robot to study the contributions of a kirigami snake skin in producing effective locomotion [57]. The robot was inspired by the frictional properties found with snake species using rectilinear locomotion. They replicated the lengthening and shortening of a single body in the form of one fiber-reinforced actuator, therefore, producing two-anchor crawling rather than rectilinear locomotion. However, they showed that the simple addition of an anisotropic snake skin, where scales are activated upon pressurization of the actuator, created locomotion where there was none previously.

Rigid snake robots are implemented by a series of active joints that can create locomotion through the coordinated actuation of these joints producing bends that propagate from head to tail. These coordinated movements are called gaits which are motions that produce a desired net displacement. To achieve the amplitude of bending required for snake locomotion, the rigid robot must have a large number of actuators. However, it is not feasible to produce a control program for each individual actuator to enact an overall gait. The number of actuators and the parameters of control increase the complexity of the design of the gaits as well as its implementation. Therefore, the trend in rigid snake robot locomotion is to rely on parameterized or scripted gaits to produce locomotion. Parameterized gaits can be described by a relatively simple parameterized function, like a sinusoid. Bioinspired gaits like lateral undulation can be represented by a parameterized function. Scripted gaits cannot be represented by a single function, and instead step the robot through a series of predefined shapes. Traversing a unique environment such as climbing stairs can be categorized as a scripted gait [58]. Current snake robots can usually implement gaits based on the fundamental serpenoid curve defined by Hirose [1]. However, to expand the complexity of behavior, other gaits can be designed and implemented on the robots.

There are two approaches to designing gaits, either through setting the series of shapes the robot's backbone transfers between, or by driving the joint angles as functions of joint number and time. The design of backbone curves is more intuitive as the gait can be visualized in the real world, but it does not identify what the low-level actuator control inputs are without further characterizing how the actuators can be sequenced to reach a desired backbone curve. The actuator inputs can be limited to bidirectional bending to make producing the control sequence easier, but it limits the applicability of the robot in 3D motions. Specifically setting the joint angles to produce locomotion bypasses this complication, but is an unintuitive process to produce real-world effects.

A hybrid approach has been developed that uses a fitting algorithm, annealed chain fitting, to specify high-level backbone curves that can produce 3D motion. To determine the low-level parameters to control individual actuators, "key frames" can be pulled from static backbone curves. This strategy, keyframe wave extraction, discretizes the target curve in time. A trajectory of positions for each joint can then be produced by sequencing these key frame positions. The gait is then produced by determining a parameterized function that captures the basic form of these sequences. The advantage of this method is that a gait can be designed that is intuitively realized in the real world, without having to explicitly control the joint angle of each actuator [59]. This hybrid method can produce bioinspired gaits commonly seen with snakes, as well as highly specialized, non-biological gaits such as rolling, to navigate complex environments. Using such methods does expand the locomotion capabilities of the robot, but relies heavily on controlling a large set of actuators. Any unexpected obstacles or features of an unstructured environment would require a unique gait to be designed if the common gait fails the traversal. Increasing the complexity of the control system does not inherently increase the adaptability of the robot in unknown environments.

The principles of snake robot locomotion and design can be implemented using soft robots. As was seen in this brief review, complex behaviors of rigid snake robots are produced through the control of the robot. These rigid robots could produce effective snake locomotion, but relied heavily on their control systems to present any adaptability or robustness in unstructured environments. Soft robots, because of the nonlinearities in the material, are inherently difficult to control through gaits alone. The hybrid design method from [59] can still be successfully implemented on soft snake robots to produce a variety of simple gaits, but novel research can be done in determining how the morphology of a soft snake robot affects locomotion. The morphology of the robot can be designed to keep the control simple while still producing adaptable behaviors. This review shows there is a gap that can be filled by developing a soft snake robot that produces a variety of gaits, and focuses on how the morphology of the robot and its interactions with the environment affects its locomotion capabilities.

2.3 Interfacial Mechanism Design

2.3.1 Interactions with Environment

The behaviors produced by soft robots are dynamic and are a result of the combination of control, morphology, and environment. The relationship between these areas is defined by morphological computation (MC). Specifically, MC is the behavior produced in soft robots because of the interactions between its morphology and its environment [60]. MC is the attempt in the soft robotics field to understand how the mechanics of the soft robot, and its interaction with the world, alter behavior. However, a method for identifying the key factors in the produced behavior has not been well defined within the field. Most of the understanding, and subsequent improvements to the robot are intuitive and come from observations of the robot in a specific environment.

Traditional, rigid robots are limited in their ability to interact with their environment. For example, if a legged bipedal robot were to collide with an unknown obstacle protruding from the ground large enough to knock it over, the robot would have difficulty in maintaining its desired trajectory and could potentially damage itself in a fall. A robust reactive controller is necessary to deal with perturbations if the body cannot absorb them effectively. Unlike their rigid counterparts, soft robots can absorb perturbations because of the damping qualities of the material. Soft robots can also conform smoothly around obstacles and can use them in advancing through the terrain as snakes do when they push off of rocks. Traditional robots cannot effectively operate in unstructured environments without robust and adaptive control systems, whereas soft robots can use the compliant properties of their materials to remove the complexity of control in reacting to perturbations in the environment. For the most part, the behavior of the robot as it conforms to its environment can be advantageous as soft materials can absorb disturbances better than rigid materials. However, because the interactions between the robot and the environment cannot be predicted or exploited consistently, some produced behavior is unwanted, or undermines what the initial control of the robot accomplished. Therefore, understanding how soft-bodied robots interact with the environment, and then developing mechanical solutions to prevent the unhelpful MC and promote the useful MC is necessary to further develop soft robotics as a field.

Soft-bodied, limbless organisms deal with environmental disturbances by changing the shape of their body, varying the stiffness throughout their body through muscle activation, and the use of mechanical strategies such as scales to exact control over the environment in which they evolved. Currently, several strategies exist to develop successful interactions between soft robots and their environment based on the observations of limbless organisms. However, they are still heavily dependent on the specific robot, environment, and intuition of the designer. Determining the fundamental mechanical advantages provided by morphological characteristics in nature, can inform the design of soft robots to produce interactions with the environment to aid locomotion.

2.3.2 Deformation Strategies

Limbless animals navigate and interact with their environment through the deformation of their bodies. Snakes will vary the speed of the propagating wave, as well as its amplitude depending on what environment they are traversing. They can lift their bodies, stiffen their body, or activate their scales to interact with their environment. Those strategies can be used in escaping obstacles if the snake becomes entangle in weeds or wedged under heavy debris [36].

Current methods for enacting shape changes within the body of a soft robot are linked to actuation, and usually have only one or two achievable shapes. The soft snake robot developed by Onal et. al. was designed for bidirectional bending (2D motion) [8]. The cyclic deformation of the actuators and the lateral resistance provided by attached passive wheels enabled lateral undulation locomotion. The parameters of locomotion they could control were frequency and amplitude of the propagating wave. The use of passive wheels limited the terrains they could traverse, as well as the set of propagating waves they could produce. Though they enacted continuum curvature during wave propagation, something not achievable with rigid links, they had no explicit strategies for exploiting advantageous MC other than the properties of the propagating wave. Tolley et. al developed an untethered, quadruped robot that could walk based on cyclic deformations of the legs through inflation/deflation [20]. The desired stiffness of the body could be controlled by further inflating the legs, but deformation and stiffness were coupled, therefore altering the crawling gait by changing the leg shape. This coupling limited the forces the leg could enact, and consequently the speed varied over different terrains.

The need for wheels on the soft snake robot [8] and variable stiffness on the legs of the soft quadruped robot [20] provide evidence that deformation is not enough to enact the range of forces on the environment necessary to operate robustly through many environments. Current actuation methods used in the field are coupled to shape deformation. This means that to increase the stiffness of an actuator, the deformation of that actuator will change. To ensure the environment does not impede, but rather facilitates locomotion, is to decouple the relationship between stiffness and shape deformation thereby increasing the production of good MC.

Many invertebrates can morph the shape of their body or limbs to better interact with the environment [61]. This is an extraordinary advantage over rigid animals and robots. Margheri et. al. developed an invertebrate robot inspired by the octopus tentacle that could extend and shorted the length of the arm, and vary the cross-sectional area of the arm [62]. These are invaluable capabilities for soft robots over their rigid counterparts that can be applied to interact with unstructured environments.

Controlled shape changing is necessary to expand the framework of exploiting morphology, dynamics, and the transient behavior of the environment defined within terradynamics to produce better MC. Therefore, more research is required in understanding how limbless animals deform their body in response to environmental interactions.

2.3.3 Variable Stiffness Strategies

Variable stiffness will be key in developing soft robots for the real world. Soft robots would become more capable in unstructured environment by replicating the way animals vary the stiffness of their muscles to perform different behaviors appropriate for interaction with the environment. However, variable stiffness remains an open problem in soft robotics. Two approaches used currently are material jamming and the use of smart fluids.

Jamming-based systems are useful for modulating stiffness as they provide the capability of a reversible transition from fluid-like to solid-like materials with limited volume variation. There are two common jamming-based systems: particle jamming, and layer jamming. Both operate on the same principle; a vacuum triggers the shift from fluid to solid, which increases the relative shear resistance experienced by the particles or layers embedded in the elastic membrane [63].

Particle jamming, both active and passive, has been used frequently for manipulation and gripping. Brown et. al. produced an active jamming gripper made from a balloon filled with a granular material. The gripper could conform to the shape of an object, and when the jamming was activated it would increase the stiffness of the mechanism, grasping the object with enough force to pick up [64]. Passive jamming has been implemented on a soft, bending actuator that relies on the deformation of the actuator to jam the particles into a stiffer state [65]. Passive jamming couples the variation of stiffness to the deformation of the actuators. Particle jamming has high deformability in the fluid state with a drastic increase in stiffness upon vacuum, without a significant volume change. However, it does require a large volume of granular material to achieve any significant stiffness modulation which limits scaling of soft robots.

Layer jamming is based on overlapping surfaces presenting a large contact area that translates into an increased friction force upon vacuuming [63]. Though scaling is still limited, it is more versatile than particle jamming. Locomotion abilities using jamming-based systems are difficult as jamming itself cannot do net external work on the environment, but it can modulate the work done by another actuator. For instance, a jamming skin can be wrapped around a fluidic actuator that controls the shape and stiffness upon actuation.

This skin can be used for rolling locomotion by alternating the vacuuming sequence of the actuator [66]. However, it is not an efficient method for producing locomotion and would be more ideal in combination with other actuation methods. Layer jamming can be used in addition to fluidic actuators to maintain the shape of a pneumatic actuator, even after the pressure on the actuator is released, successfully decoupling stiffness from actuation [67].

Smart fluids such as magneto- and electrorheological fluids can also be used for varying the stiffness of a soft robot. These materials can change their rheological properties when a magnetic (MR) or electric (ER) field is applied. Fluidic channels can be created within an elastomer to inject the MR or ER fluid. When the correct field is applied, the fluid becomes more viscous and effectively stiffens the actuator. They can also act as valves and be used to control actuation of a multi-actuator system [68]. The limitations lie mostly in applying the corresponding field to the fluid which requires high voltage power sources. Also, sealing issues, particle settling, and environmental contamination problems are present [63]. Finally, any actuation or stiffening produced by these fluids are slow, and for locomotion purposes they are not ideal.

Modulating stiffness throughout the actuators of the robot will greatly improve the robot's ability to interact with all environments. Further research is necessary in both defining what actions produce good MC and how best to enact them utilizing variable stiffness.

2.3.4 Surface Interaction Strategies

Morphology-based mechanical strategies is another method employed to create soft robots that can better interact with the environment. The most obvious mechanical strategies in use are contact-based. Most limbless locomotion capabilities are made possible through the animal's frictional properties of their body. This is highlighted by the use of scales in snakes. By activating certain sections of muscles along their body, snakes can alter the angle of attack of their scales. By patterning the activation and release of scales, they can be used to dig into the asperities of the surface the snake is traversing. This creates more friction in the backwards direction than that in the forward direction. This anisotropy allows the snake to achieve a net forward displacement. The production of anisotropic friction for soft snake robots has been accomplished using passive wheels [8], and more recently, a kirigami skin for rectilinear locomotion [57]. Patches of high friction material have been used to aid two-anchor crawling in a worm-inspired robot [69]. To enable peristalsis in earth worm-inspired robots, adhesive pads have been used on various segments of the robot's body to produce discrete contact points of high friction along the body [70, 71]. Directional friction strategies have also been used for climbing robots using directional spines on the feet of the robot to compliantly engage with surface asperities [72].

All of these strategies utilize mechanical additions to promote friction instead of relying solely on body deformation. They were designed for the specific locomotion pattern of the robot in order to promote MC that advanced the locomotion abilities. However, they cannot easily be transferred to robots that use other locomotion strategies, or alternate through different modes of locomotion. This again shows how dependent the design of soft robots is on the intuition of the designer, the selected locomotion strategy, and the morphology of the robot.

In more fluidic environments such as water and sand, the simple mechanical addition of a tail increases the robot's ability to produce effective locomotion. In addition to adhesive pads used to create high friction points, Lin et. al. used tail skids to increase lateral stability to improve the peristaltic locomotion they were employing [70]. For the soft fish robot used to produce aquatic undulation, Marchese et. al relied on the the morphology of the tail to ensure propulsion through the water [56] . Although it has not been implemented on a soft snake robot for subterranean environments, it has been found that the snout and tail on a sand fish lizard are vital in its ability to alter its angle of attack within sand to either bury itself, or surface during subterranean locomotion [34].

Mechanical strategies through variations in morphology are key to producing effective limbless locomotion. Though current implementations on soft robots are few and highly dependent on the robot and the selected operating environment, there are many biological examples that prove their viability.

2.4 Summary

Bioinspiration is a useful tool to develop robots that are robust and adaptable in complex environments. Considering how prevalent soft structures are in nature, further investigation of soft implementation of bioinspired robots is warranted. This chapter has provided context for state-of-the-art the development of snake robots in the literature and what soft robot technologies can be utilized to further evolve soft snake robots. A review of limbless locomotion in nature shows that snakes are incredibly versatile in the range of gaits they can employ, as well as how they can adapt those gaits to changes in their environment. There are many aspects of snakes that make them useful models for robots in unstructured environments, including:

- Elongated body with continuous deformation
- Mostly soft with rigid, but highly flexible backbone for compliance and force
- Soft body results in compliant interactions with the environment
- An array of useful gaits
- Skin with frictional anisotropy

Rigid snake robots have produced the general body shape of snakes to realize the serpentine locomotion snakes use. However, the use of rigid materials has limited the functional and interactional compliancy of the robot. reducing the applicable environments. These robots cannot produce continuous deformation, and the curvature they can realize requires the use of many discrete actuators. The usefulness of the snake's soft body and skin has not yet been investigated, as only one soft snake robot using lateral undulation has been developed before this work and was limited in its interactional softness by the use of passive wheels. A skin has been executed on a soft robot, but for a crawling locomotion which has differing dynamics than lateral undulation. This chapter reviewed what has been accomplished in limbless soft robots and snake robots in general and the main contributions are listed below:

- Worms are the most common inspiration for limbless soft robots
- Only one soft snake robot has been published previously
- Rigid snake robots rely on control complexity to create compliancy
- An anisotropic skin for crawling locomotion was developed for extending soft actuators

These contributions have not yet fully realized the versatility and adaptability of biological snakes. Through the review of useful characteristics of snakes and current state-of-the-art snake robots we have determined that a soft snake robot with high functional and interactional compliancy justifies further investigation. Actuators made from elastomeric materials would allow for continuous deformation and would better represent the soft body of biological snakes. Rigid snake robots have relied on complex gait implementations to improve locomotion in complex environments. Shifting to soft robot technology will require exploration of morphological contributions to improve locomotion as there is a more coupled relationship between the soft robot and its environment. Snakes in disparate ecological niches have evolved different morphological characteristics, that when examined through the lens of environmental interactions, can be engineered to increase the soft robot's capabilities in a wider range of environments. The review of soft robot strategies for environmental interaction has shown that the frictional properties of the robot are a major contributor to the success of the robot. Snakes have evolved skin that exhibits frictional anisotropy, but this external mechanism has yet to be employed on an undulating soft snake robot. The main contributions of this dissertation that address the gaps identified in this review are listed below:

- First *fully-soft* snake robot to improve locomotion through high functional and interactional softness
- Explanation of how the morphological design of snake robot changes its behavior in addition to the gait design
- First implementation of frictional anisotropic skin for lateral undulation on a soft robot

The material reviewed in this chapter provides a starting point for the design and implementation of a *fully-soft* snake robot. The proceeding chapters will address how the morphological characteristics of the robot can change its behavior, how the design of a gait unique to the dynamics of the robot and its coupled behavior with the environment can improve its locomotion in that environment, and how the design of an external mechanism targeting a specific environmental interaction can improve its locomotion. Studying the effects of the combination of morphology, gait, and environmental interactions on the velocity of locomotion through relatively simple environments, and its adaptability to more complex environments can aid in further development of bioinspired soft robots.

Chapter 3: Morphology of Snake Robot Changes Behavior

Based on the literature reviewed in the previous chapter, snakes provide an excellent model on which to design a soft robot. Though rigid snake robots have been widely developed, there has only been one previous soft snake robot developed [8]. However, its designers have reduced both its functional and interactional compliancy by using wheels to provide resistive forces during locomotion. Therefore, it is of interest to develop of a fully-soft snake robot with high functional and interactional compliancy to study how targeted interactions with the environment could aid in locomotion.

Designing the morphology of the robot, the gait, and the method of interacting with the environment have to be done somewhat in tandem to increase the versatility of the robot. Snakes use a variety of gaits in nature, but we focus on lateral undulation, the most common gait, to implement on the robot. The gait used to initially test the robot prototypes presented in this chapter is an optimized (based on cost of travel) sinusoidal traveling wave function specified by the amplitude of sine and cosine curvature modes we refer to as a "circular gait" [73]. Further definition and modification of this gait is discussed in Chapter 4. For the purposes of this chapter, the circular gait represents an implementation of lateral undulation relying on the shape space generated by the robot in a granular media.

3.1 Extensible Actuators in Soft Snake Robots

This chapter examines how the morphology of the soft snake robot changes its behavior when implementing the same gait and control scheme across prototypes. The selected circular gait requires the production of a specific series of shape changes the actuator must enact. These shape changes, which make up the shape space of the robot, drive the design of the soft actuators. In addition to producing the necessary shape space, the design of the robot needs to account for implementation in real environments as well as manufacturability. Below are the design requirements that ensure the above criteria is met:

- Bidirectional bending capabilities

- Cross-sectional area geometry that prevents rolling
- An aspect ratio that produces a 2:1 drag ratio (lateral:longitudinal)
- Modularity of robot to ensure propagation of bends along length

3.1.1 Design

Our initial design of our soft snake robot is driven by the shape space required to perform the circular gait, our representation of lateral undulation. To implement this shape space, as illustrated in Fig. 3.1, the robot must be capable of achieving a set of S- and C-shaped poses. Therefore, each actuator must exhibit bidirectional bending to at least a 90° arc without producing significant twisting or rolling. The robot should be modular because locomotion will require at least one pair of bidirectional bending actuators in tandem, thus each actuator must have a connecting mechanism that does not require excessive use of rigid parts. Fiber-reinforced actuators were selected because they have been well characterized [18], and because they are highly modifiable due to the use of molds. A typical fiber-reinforced actuator has one chamber used for actuation. A strain-limiting layer can be added for bending, and different fiber wrapping techniques can be used for extending or twisting [19]. For this first prototype, bending is achieved through the strain limitation created by the uninflated side of the actuator. Including a strain-limiting layer between air chambers adds complexity to the manufacturing process, that in its initial stages, would have reduced the reliable production and replication of actuator capabilities.

To meet the design requirements above, we implemented the following designs: 1) The mold design was modified to create two air chambers for bidirectional bending. 2) A double-helical thread wrapping pattern was used to prevent twisting upon inflation, which disrupts the gait pattern significantly enough to prevent any forward displacement. 3) An elliptical cross section geometry was selected to approximate the typical body shape of a snake, and prevent the actuators from rolling during actuation. 4) Magnets were embedded into the silicone caps used to seal the ends of the chambers, so that an arbitrary number of actuators can be linked together. Placing them in the caps prevents them from interfering with inflation. The final actuator designed is 110mm in length, and has an elliptical cross section with a semi-major axis of 30mm, semi-minor axis of 20mm, and a wall thickness of 3mm. The actuator design is shown in Fig. 3.2.

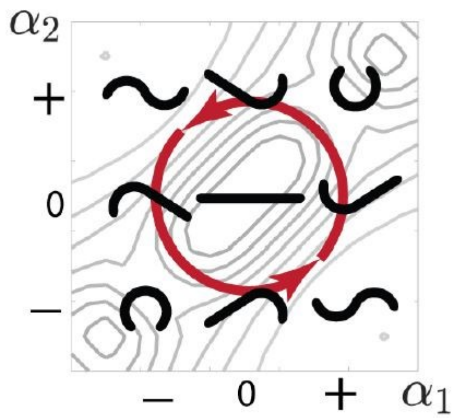

Figure 3.1: Shape space required for circular gait.

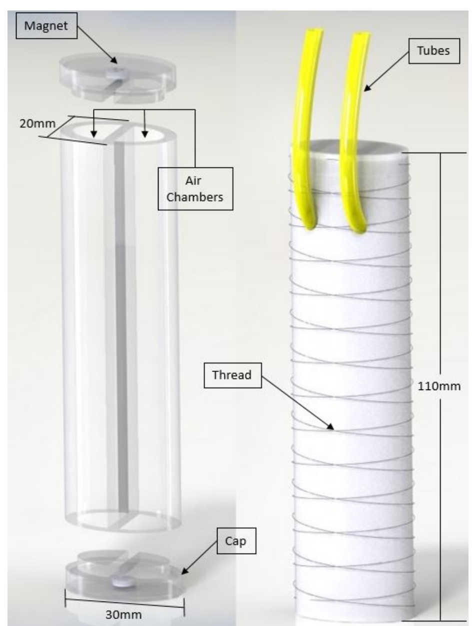

Figure 3.2: Assembly and dimensions of silicone actuator

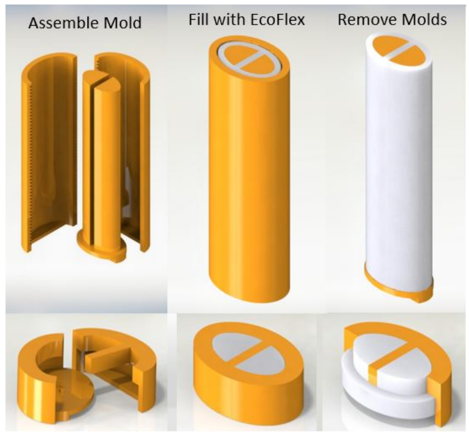

Figure 3.3: Fabrication procedure to mold silicone actuators

3.1.2 Manufacturing

Manufacturing of soft robots is an open problem in the field, and can therefore effect the design and implementation of the robot. The use of elastomeric materials introduces nonlinearities from material properties that are sensitive to any imperfections (bubbles, inconsistent wall thickness, etc.). If any imperfections are introduced during manufacturing, the actuator could out right fail, or produce inconsistent intended, or non-intended behaviors. State-of-the-art pneumatic soft actuators are manufactured through molding of the selected elastomeric material. Therefore, every design change to the actuator requires a design change to the molds which can propagate to a change in the assembly procedure of the actuators. A fully enclosed structure cannot be molded unless using materials for the internal structures that can be removed later. The removal of internal structures requires pulling those structures through a hole in the outer wall of the actuator, which would require patching after removal, leading to a likely point of failure or decrease in performance capabilities. Another option is lost wax casting, which utilizes wax for the internal structures of the mold, that can then be melted and drained through a small hole. Again, the hole would require patching, but more significantly, the internal structures would also need to be molded from wax. This process, on top of the jigs necessary to ensure alignment of these internal structures would potentially introduce a number of imperfections making it almost impossible to create identical actuators to pair together to build the snake robot.

The goal of the manufacturing process was to produce actuators that behave as similarly as possible to prevent asymmetries during locomotion that would inhibit locomotion. The strategy we employed was to make the actuator in parts for assembly. The more individual parts you have to make for the actuator, the greater possibility of introducing imperfections. The most common failure modes for fiber-reinforced, bending actuators are listed below:

- Inconsistent wall thickness
- Misalignment of internal air chambers
- Misalignment of strain limiting material
- Wrinkling of strain limiting material
- Imperfect seal between air chambers (bubbles or capping)
- Misalignment of fiber reinforcement

To prevent these failure modes, we fabricated the two air chambers in a single mold to ensure the wall thickness and alignment of the chambers were consistent. The mold had a pattern that would embed a grid on the outer surface of the actuator to align the thread used for fiber-reinforcement. We had a separate mold to fabricate the caps that had plugs in the shape of the air chambers to provide a seal. The mold designs can be seen in Fig. 3.3. Molding the body with both air chambers embedded in a single mold made it extremely difficult to include a strain limiting layer between air chambers to promote bending. However, the strain differential between the inflated side and uninflated side was enough to produce bending along the length of the actuator as it extended upon inflation. Therefore, the potential deficiencies leading to inconsistently-performing actuators — or total failure — introduced by embedding a strain limiting layer were deemed too detrimental for the first prototype of the robot. The bidirectional bending requirement was still met by the strain differential introduced between the inflated and uninflated chambers on the actuator, and all other failure modes were minimized by the mold design.

The molds were 3D printed using MeltInk3d 2.85mm PLA on an Ultimaker 2+ using a 0.6mm nozzle. The actuators were made from EcoFlex®00-30 which was poured into the molds and set to cure (about 3 hours at room temperature). Before the elastomer was poured into the cap molds, a magnet was placed 1mm above the bottom of the mold. The magnets were used to meet our modular requirement so we could connect different actuators together as desired. The magnets were placed so opposite poles were at each end of the actuator so they could be paired with any other actuator. When the main body was cured, the outer walls of the mold were removed (see Fig. 3.3) and the double helical thread pattern was wrapped by hand following the grid line imprinted into the outer surface of the soft actuator by the mold. The caps were glued to both ends of the main body with SilPoxy® and the seam was sealed with a thin layer of the EcoFlex®00-30. Each actuator was characterized to determine which actuators behaved similarly enough to pair together for the robot.

3.1.3 Characterization of Extensible Actuators

During the iterative prototyping and testing procedure used to determine a final design for the soft actuators, it was confirmed that actuators that had similar pressure-curvature relationships in testing reproduced the desired gait pattern better (more symmetric). We used an Optitrack Prime 13 motion capture system to track the arc angle (bending upon inflation) and length (extending upon inflation) of each actuator at known values of input pressure, using a syringe to inflate each chamber from 0 to 24 kPA in 3.4 kPA increments. The results of these tests are summarized by the Pressure-Angle and Pressure-Length curves for the two closest performing actuators in Fig. 3.4. The final manufacturing process greatly reduced the number of inconsistencies between actuators. About 1 in 8 actuators failed completely, and 1 in 5, though functioning, behaved too differently from the other actuators to be paired up for a robot. This characterization phase was essential to ensure that the robot could enact the pose sequences of S- and C-shaped backbones, and also provided us with a mapping between input pressure and shape that helped with tuning the control inputs to drive the gait.

The drag ratio was an important parameter in the geometric model used to generate the predicted results of the circular gait. The drag ratio can be adjusted by altering the aspect ratio (length:width) of the actuator. The aspect ratio of the actuators was 110cm:30cm. The drag ratio was measured using the Mark-10 force measurement system. To measure the lateral drag force of the actuator, a cord was attached to 3 points along the actuator (both ends and the middle), and dragged along the top of the millet. The same was done to measure the longitudinal drag force, but the cord was attached to just one end. The recorded drag ratio was 1.8:1 which was close to the intended 2:1 drag ratio as specified

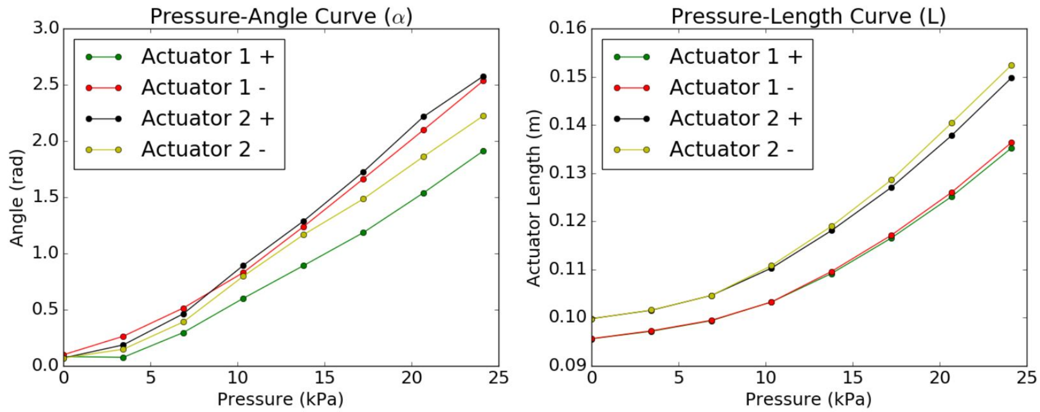

Figure 3.4: Characterization of pressure vs. bending and pressure vs. elongation for each chamber of each actuator.

suggested drag ratio listed in the requirements above.

3.1.4 Preliminary Locomotion in Granular Media

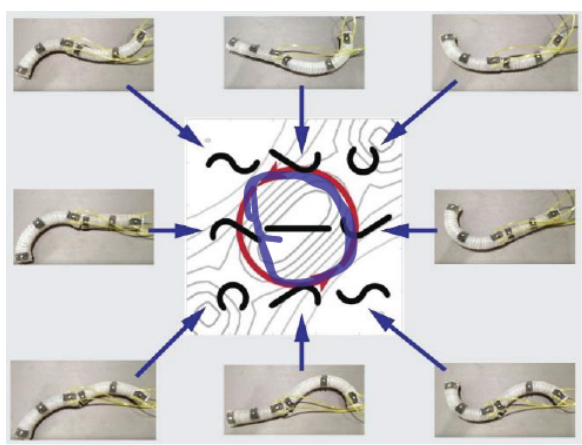

Figure 3.5: Snapshots of robot prototype #1 enacting shape space and corresponding experimental production of circular gait.

The circular gait was implemented on the extensible robot in millet (a small seed) to represent a granular media. Fig. 3.5 shows the robot reproducing the required shapes, as

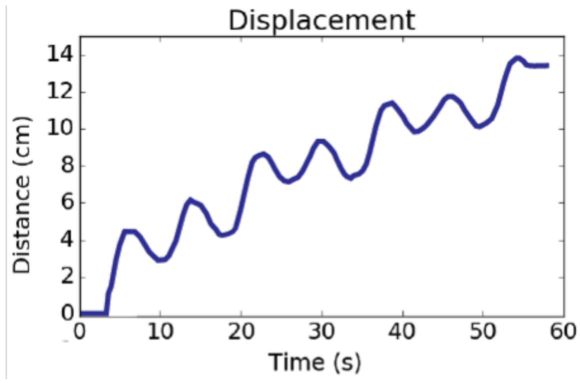

Figure 3.6: Total displacement of robot prototype #1 using circular gait in millet.

well as the experimental results of driving the circular gait. The experimental production of the circular gait (blue circle) is not a perfect reproduction of the driven gait (red circle). As can be seen from the snapshots of the robot forming each shape, the C-shapes were not well replicated, and that is where the experimental data deviates most from the circular gait. The extension of the actuators and the interference of the magnets are likely responsible for the poor production of C-shapes. The extension of the actuators prevented full curvature. The magnets were heavy in comparison to the rest of the robot and made the connection points cumbersome to deform around and drag along during locomotion.

The total displacement of the robot through the granular media driving the circular gait is shown in Fig 3.6, and had a maximum velocity of 0.2 cm/s (0.001 body-lengths/s). The trend of displacement shows that though the gait pattern resulted in a forward movement, there was a small backward movement for each stroke. These backward movements were caused by the contraction of the actuators as they deflated, as well as slipping backwards in the grains as the actuators straightened upon deflation. However, each step backward was smaller than the step forward so the robot was still able to propel itself through the terrain. Removing this backward step phenomenon is explored in Chapter 4.

The geometric model used to define the circular gait predicted a velocity of 0.09 body-lengths/gait-cycle when using the measured drag ratio of 1.8:1. The experimental velocity of the robot using the OptiTrack motion capture system resulted in 0.23 body-lengths/gait-cycle. The largest difference between the robot and the model is the fact that the robot has a mode of extension and contraction during each gait cycle. Therefore, a second prototype would need to be constructed that removed the extensibility of the robot in an effort to better represent the geometric model.

3.2 Inextensible Actuators in Soft Snake Robots

A second prototype of the robot was developed to determine whether the mode of extension of the original soft robot was aiding in the overall locomotion capabilities of the robot as the actual displacement of the robot was larger than the model's prediction. The new design of the soft actuators would include inextensible fabric embedded in between the two air chambers in the main body of the actuator to prevent extension. This change in design greatly increased the complexity of the manufacturing process requiring a complete redesign of the molds and assembly procedure.

3.2.1 Design

The new actuators still had two chambers for bidirectional bending, and an elliptical cross section to prevent rolling. The only difference is the addition of an inextensible backbone to prevent extension and promote bending. Embedding the backbone material required precision in placement as well as the ability to bond well with the silicone elastomer (EcoFlex®00-30). Therefore, a 0.25mm thick, woven fiberglass mesh was used as the backbone material. The openness of the weave allowed for the silicone to seep into the holes and bond the backbone to the chamber walls.

The dimensions of the actuator were 110mm in length, with an elliptical cross section with a semi-major axis of 30mm, semi-minor axis of 20mm, and a wall thickness of 3mm. These are the same dimensions as the first prototype, keeping the aspect ratio equivalent. The magnets were removed from the caps as we no longer required modularity, and they seemed to interfere with the robot's ability to cleanly form the C-shapes needed to realize the shape space for the circular gait. All actuators, before being permanently affixed to one another, would be characterized to ensure symmetric behavior.

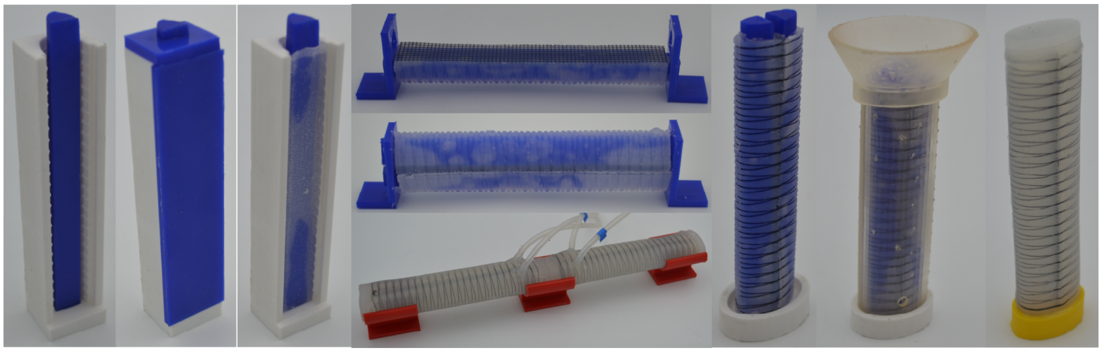

Figure 3.7: Assembly of inextensible actuators and robot. Actuators are made in halves, an inextensible material is embedded between halves and the two halves are bonded. After threading the actuator, following the imprinted grid, the actuators is overmolded to secure fibers and capped. Two actuators are bonded to form a full robot.

3.2.2 Manufacturing

The inclusion of an inextensible layer between air chambers required a complete redesign of the molds. In addition to altering the design of the molding and assembly process to embed the inextensible fabric into the actuator, we made further design changes to reduce errors that arose from the first design of molds. The two internal structures that created the air chambers in the original mold design started to warp after many uses. The warping resulted in a tapering wall thickness between chambers which drastically changed the behavior of the actuator. This made it difficult to produce actuators that behaved similarly. There were also bubbles that were produced during curing in the wall separating chambers that were inaccessible after curing to fix, and resulted in a complete failure of the actuator. Therefore, the design of the new molds would take into account the necessity of consistent wall thickness between the chambers, and make those walls accessible to fix any bubbles that arise during curing.

The resulting design of the molds can be seen in Fig. 3.7. To embed the inextensible fabric between chambers required molding each half of the actuator separately. The assembly procedure was also improved to ensure that the two halves of each actuator would be held in proper alignment during curing. A jig was also implemented to keep the two actuators that made up the robot held in alignment during the curing process. The new manufacturing strategy, other than allowing for the insertion of an inextensible backbone,

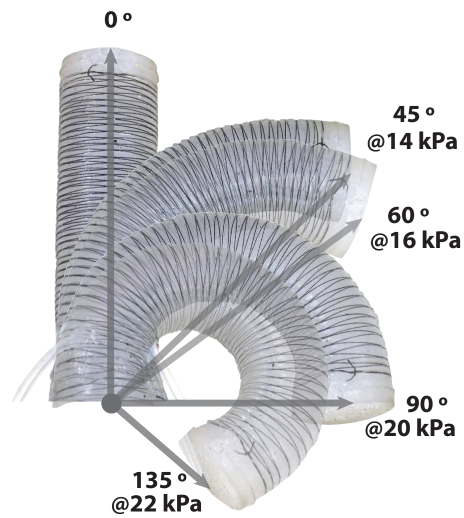

Figure 3.8: Range of curvatures tested in gaits. Measured as the angle of the arc swept by the actuator when inflated.

also increased the reproducibility of the actuators. The assembly process eliminated full failure of the actuators by eliminating the production of the failure modes listed above. About 1 in 15 actuators behaved too differently to pair up with another actuator to form a full robot.

3.2.3 Characterization of Inextensible Actuators

The behavior of the robot is dependent on the relationship between the input pressure and the resulting curvature of the actuator. Here, curvature is defined as the amplitude of the input wave, and is measured as the angle of the arc swept by the actuator upon inflation. To properly compare curvature to locomotion capabilities, this relationship needs to be determined. Based on lateral undulation performed by snakes, a range of curvatures is expected to result in locomotion. However, different curvatures are expected to be more effective in different terrains as snakes vary the amplitude of their propagating wave as they traverse through different environments [29]. Therefore, a set of maximum amplitudes can be tested to determine its contribution to locomotion. The respective input pressures for each air chamber were measured to inform the control of the robot. The set of curvatures

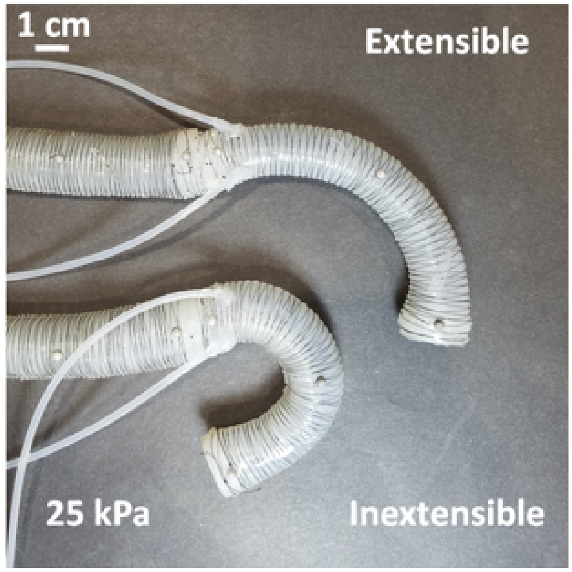

Figure 3.9: Difference in curvature of the two robots inflated to the same pressure

and corresponding pressure inputs can be seen in Figure 3.8.

A comparison of the two robot prototypes is shown in Fig. 3.9. As can be seen, at the same input pressure the two robots have very different deformation behavior. The only difference between the two robots is the addition of the inextensible backbone material. The addition of a backbone provides a strain limiting layer on the soft actuator. This layer prevents extension, and promotes bending of the actuator. The inextensible robot has a much larger curvature than the extensible robot because the forces from inflation are being used for pure bending, rather than having a mode of extension along the bend. This minor tweak in mechanical design resulted in a significant change in behavior, underlying how sensitive soft robots are to the design and implementation of physical embodiment.

3.2.4 Preliminary Locomotion in Granular Media

The new inextensible prototype was tested in millet using the same circular gait tested on the first prototype. The result of this preliminary test is shown in Fig. 3.10. The significant different in deformation behavior resulted in a much larger displacement in comparison to the original, extensible prototype.

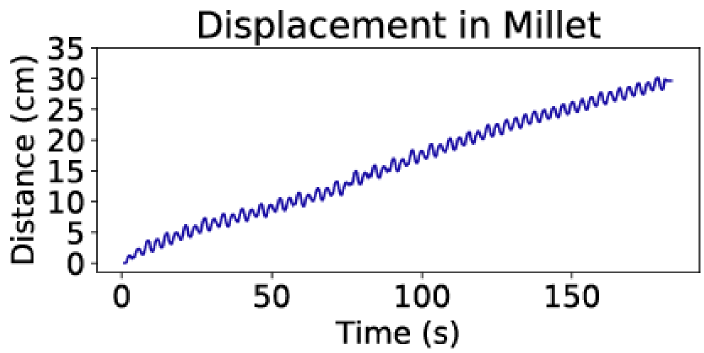

Figure 3.10: Result of the inextensibile prototype driving the circular gait in millet.

Further analysis and comparison between the locomotion capabilities of the extensible and inextensible robots is presented in Chapter 4.

3.3 Summary

This chapter has outlined the design and manufacturing of two prototypes for a soft snake robot, an extensible robot and an inextensible robot. The design of the robots was directed by the shape space requirements necessary to successfully produce lateral undulation. The complexity of manufacturing soft actuators resulted in the first, extensible prototype as consistently embedding an inextensible layer in between air chambers was difficult. However, when the robot was tested in millet, a granular media, it produced a larger displacement/cycle than that which was predicted by the model. It was then hypothesized that the extensibility of the robot, which introduced a mode of peristalsis to the locomotion, was aiding the robot's capability. A second prototype of the robot with an inextensible backbone helped determine how peristalsis could be contributing in the extensible prototype. The manufacturing process was redesigned to accommodate the inextensible backbone material by building the actuators in halves, and combining them with the inextensible layer placed between the two halves. The redesign of the manufacturing and assembly process of the actuators allowed for further reduction of failure modes, increasing the reproducibility of the actuators. The addition of the inextensible backbone changed the deformation behavior of the actuator. In comparison, at equal pressures, the two robot prototypes resulted in very different shapes. The inextensible robot was able to reach much larger curvatures than the extensible robot, and completely removed the peristaltic mode of locomotion during testing. The inextensible robot displaced further in millet than its extensible counterpart, and provides an excellent platform to further explore effects of gait parameters and interactions with the environment on the locomotion capabilities of the robot.

Chapter 4: Gait Design for Locomotion in Granular Media

4.1 Development of Gait for Extensible Robot

The previous chapter showed how the design of the robot can change its behavior when implementing the same gait and control parameters. This chapter will fully define the circular gait used in the previous chapter. Variations of this gait were all tested on the original extensible robot. The deviations from the model's predictions of displacement with the extensible robot called for the design and implementation of an inextensible robot to better represent the kinematic model used to derive the gaits. This second prototype was tested using the circular gait, as well as modified gaits that take advantage of interactions with the environment.

4.1.1 Snake-inspired Gait Selection

A primary goal of this work was to demonstrate the effectiveness of using a well-defined geometric gait model to develop a control sequence for the locomotion of our soft snake robot. Soft robots are not easily modeled, making it difficult to generate control strategies that can be generalized for many designs. They are also coupled to their environment as their behavior is sensitive to interactions with the environment altering their deformation capabilities. Using a geometric gait model that accounts for the kinematics of the "backbone" of the robot, and which can be separated from the nonlinear dynamics through which the system achieves the sequence of shapes, reduces the impact of design and potential imperfections of the system. The dynamics of interactions with the environment are reduced to characterizing a drag ratio, as the model was intended for a low Reynolds number environment, where drag forces are dominate during the production of locomotion. Therefore, this method reduces the nonlinearities inherent with soft robots, and accounts for a simplified model of their interactions with the environment. Our selection of shape sequences that are likely to form an effective gait is guided by the soap-bubble [73] model of gait performance which geometrically balances the displacement achieved over a gait cycle against the cost

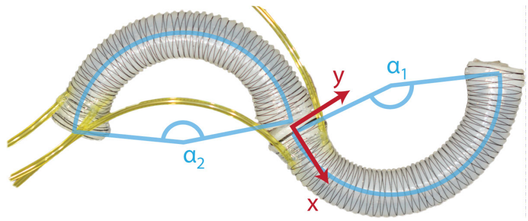

Figure 4.1: Geometry of shape variables in two-actuator soft snake system. The origin of the body frame coordinate system is placed at the center point along the spine between the two actuators, with the x-dimension of position parallel to the spine and y-dimension perpendicular. The turning angle θ is defined relative to the x-axis.

(measured in time or effort) required to execute that cycle. The set of assumptions for the model are listed below:

- The environment is a viscous fluid where drag forces are dominate
- The drag ratio is 2:1
- The actuators have constant curvature along their length

The pose set for backbones of biological snakes can be represented by sinusoidal traveling wave functions [1, 59]. The serpenoid-curve gait for this system can be specified by the amplitude of sine and cosine curvature modes [73]. Our soft snake robot is a two-link, piecewise-continuous-curvature system which can approximate a subset of the biological snake's backbone shape space and thus can implement locomotion with select serpenoid-curve gaits. The soft robot's shape space can be parameterized by the arc angle of each link, α_1 and α_2. See Fig. 4.1 for an illustration of these shape parameters on the robot's body and Fig. 4.2(a) for example backbone shapes produced by varying α_1 and α_2. Displacement and orientation of the robot are measured as the displacement of the *body frame*, a coordinate system positioned at the center of the spine at $t = 0$ as shown in Fig. 4.1, from its initial position.

The configuration of the soft snake robot can be denoted by a position space G that describes the location and orientation of the robot in the world, and a shape space R that defines the relative placement of points on its body. The position of the robot is given by $g = (x, y, \theta)$ relative to a choice of origin frame, and the shape of the robot is given by

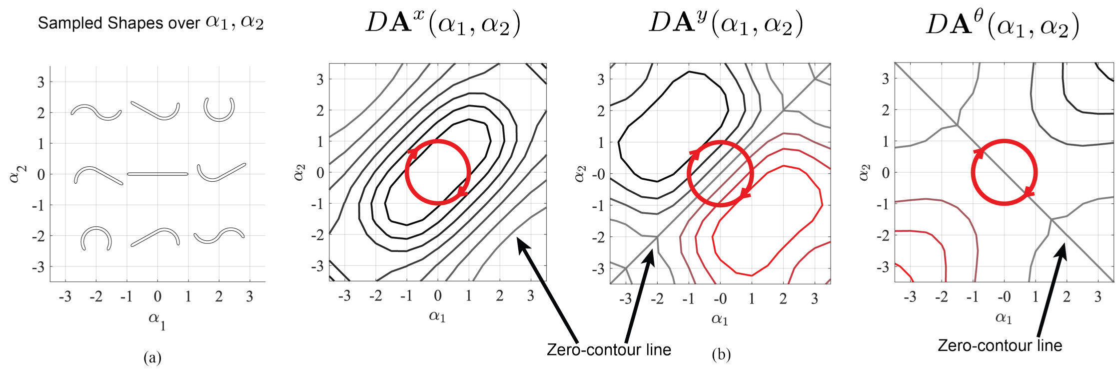

Figure 4.2: (a) Sampled backbone shapes for the soft serpenoid system visualized as a function of α_1 and α_2. (b) Constraint curvature ($D\mathbf{A}(\alpha_1, \alpha_2)$) for the soft serpenoid system in a granular substrate with a lateral-to-longitudinal drag ratio of 1.8:1, visualized as contour plots with respect to x, y, and θ. An example gait stroke that varies α_1 and α_2 sinusoidally and 90 degrees out of phase to produce a "circular" stroke is plotted. Note that the gait cycle encloses part of a sign-definite region $D\mathbf{A}^x(\alpha_1, \alpha_2)$, indicating that there will be net displacement per cycle along the longitudinal axis of the body. The gait cycles encloses equal positive and negative regions on the contours $D\mathbf{A}^y(\alpha_1, \alpha_2)$ and $D\mathbf{A}^\theta(\alpha_1, \alpha_2)$ and thus will not produce any lateral or rotational displacement.

$r = (\alpha_1, \alpha_2)$. We model the relationship between changes in shape and position as a *local connection* matrix $\mathbf{A}$,

$$\overset{\circ}{g} = -\mathbf{A}(r)\dot{r}$$

where $\overset{\circ}{g}$ is the system body velocity ($\dot{g}$ expressed in forward, lateral, and rotational components) and $\dot{r}$ is the rate of change of body shape. The model holds under the assumptions that gliding cannot occur and that displacement is locally proportional to the amount of shape change. A local connection matrix summarizing an appropriate dynamics model for this system can be constructed by taking a ratio between lateral and longitudinal drag forces and assuming quasistatic equilibrium [74]. The local connection matrix can be visualized as a set of vector fields on R relating changes in x, y, and θ to changes in shape $r = (\alpha_1, \alpha_2)$. Over a cyclic trajectory in the shape space (a gait), the net integral along the vector fields (i.e. the net displacement over the cycle) can be approximated by the area integral of the curvature of the constraints, $-D\mathbf{A}$, in the region enclosed by the gait. $D\mathbf{A}$ is the total Lie bracket of $\mathbf{A}$, and is closely related to its row-wise curl [75, 76].

The components of the constraint curvature $D\mathbf{A}(\alpha_1, \alpha_2)$ for the soft serpentine system are shown in Fig. 4.2 as contour plots, overlaid with an example gait that traverses the shape space by varying α_1 and α_2 sinusoidally and 90 degrees out of phase to produce a "circular" stroke. Note that there is an elliptical sign-definite region surrounding the origin in the contour plot for the x-component of position, whereas the y- and θ- plots have symmetric positive and negative regions around the origin. Gaits that enclose this region will thus produce net displacement along only the x-dimension of the body position. Previous work in geometric mechanics has demonstrated the utility of gait selection by choosing a stroke cycle that encloses sign-definite regions of these contour maps [77] [78] [74].

A gait cycle that encloses the entire sign-definite region should produce the largest displacement per cycle, but the shape sequence required to do this might have a high energy cost. The soap-bubble method [73] is an extension of this algorithm that attempts to optimize the gait cycle in terms of the displacement gained relative to the cost of the stroke. Curvature enclosed near the zero-contour is of low value, and so contributes relatively little to the net displacement and the shape changes required to encompass it require more time or effort in each cycle, meaning that a stroke that is contracted away from this contour is often more cost-efficient in terms of time and power.

We select gait cycles for our soft snake robot that enclose portions of the sign-definite region of the x-dimension contours of curvature to 1) demonstrate that the robot is able to achieve net longitudinal displacement with these gaits and 2) validate the displacement against the model based on the portion of sign-definite region enclosed by the cycle. The gaits tested all vary α_1 and α_2 in an elliptical stroke of the general form

$$\begin{bmatrix} \alpha_1(t) \\ \alpha_2(t) \end{bmatrix} = R(\phi) \begin{bmatrix} a\cos(t) \\ b\sin(t) \end{bmatrix} \tag{4.1}$$

where $2a$ and $2b$ are the widths of the major and minor ellipse axes and $R(\phi)$ is a rotation of the ellipse about the origin by an angle of ϕ. The optimal gait generated by this model is the circular gait, used to compare behavioral changes across robot design in Chapter 3. It is determined as optimal due to enclosing maximum sign-definite area while minimizing the cost to travel along that path.

4.1.2 Gait Testing Procedure

To implement gait strokes and evaluate their performance, we developed methodologies for directly controlling the shape parameters α_1 and α_2 of the robotic system, tracking progression through the shape space, and measuring net displacement of the robot. The experimental procedure we followed used the OptiTrack Prime 13 motion capture system (Natural Point Inc.) to quantify the robot's shape and position changes for each gait stroke based on reflective markers placed on the robot.

The snake's pneumatic control system is based on an open source design [16] that utilizes a single micro-compressor with separate air lines for the actuator chambers. They can be driven to a separate pressure with solenoids valving at variable PWM rates. An Arduino Mega operates the solenoids by receiving control instructions from a separate computer via a serial data connection. Using the relationship between pressure and shape previously established, we developed Python scripts to drive PWM rates (and hence angles of curvature) sinusoidally in an appropriate pattern to realize elliptical gait stroke sequences.

We used the OptiTrack motion capture system to track reflective markers placed in three locations on each actuator (a total of six markers along the robot). The markers were placed on the dorsal surface of each cap and at the center of the actuator's elastic spine, so that the three points could be used to fit a circle to the actuator and thus yield a numerical approximation of its arc angle. The body frame of the two-actuator system was identified as the center point of the line formed by the two markers adjacent to each other where the actuators were clasped together by magnets. All motion capture data was saved and post-processed to compute and plot the body frame coordinates and curvature angles observed during a gait test.

A test area was created inside the motion capture stage by filling a large bin with millet, which was selected as the granular medium for these experiments because of its relatively low density ratio of 0.78 to 1 compared with the robot. The lateral-to-longitudinal drag ratio for the substrate was measured as 1.8 to 1. The drag ratio of the surface medium contributes considerably to net displacement, since lateral resistance translates lateral waves of bending along the backbone into forward movement, and so this ratio is crucial to estimating expected displacement.

We tested gait strokes described by Equation (1) with varying values of b and ϕ. The value of a was fixed in all tests to limit actuator bending to about 2 radians in either

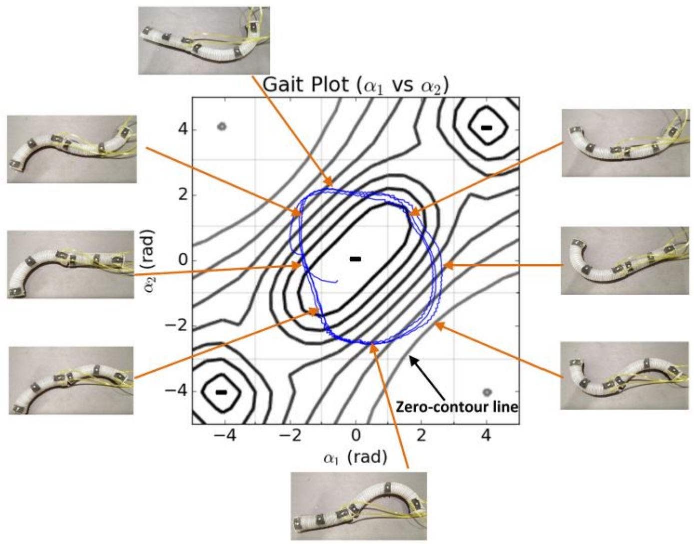

Figure 4.3: Motion capture data from the soft robot demonstrating a circular gait stroke ($a : b = 1$) plotted on top of the $D\mathbf{A}_x(\alpha_1, \alpha_2)$ contour plot for the two-link soft serpenoid system. Key frames in the shape cycle are indicated with pictures.

direction. Parameter values were selected empirically to enclose various regions within the zero-contour line, with rotations of $\phi = \frac{\pi}{4}$ or $\phi = \frac{3\pi}{4}$ to evaluate the impact of enclosing lengthwise and transverse regions of the elliptical area.

4.1.3 Initial Locomotion Results for Extensible Robot

Five different elliptical gaits were examined, with each test cycling through about 3 repetitions of a gait stroke during a total test duration of roughly 54 seconds or 18 seconds per stroke. Actual variations in shape parameters as observed with the motion capture system and calculated during post-processing of data are plotted on top of the $D\mathbf{A}^x(\alpha_1, \alpha_2)$ contour plot in Fig. 4.3 and Fig. 4.4. The plot in Fig. 4.3 includes snapshots of backbone shapes that correspond to select points on the gait stroke to illustrate the pose sequence. Displacement is visualized as a function of time in Fig. 4.5. Net x- and y- displacement measurements for all gaits are shown in Table 4.6.

All gait strokes examined in these experiments achieved measurable forward displacement, and it should be noted that these gaits were within the boundaries of the sign-definite

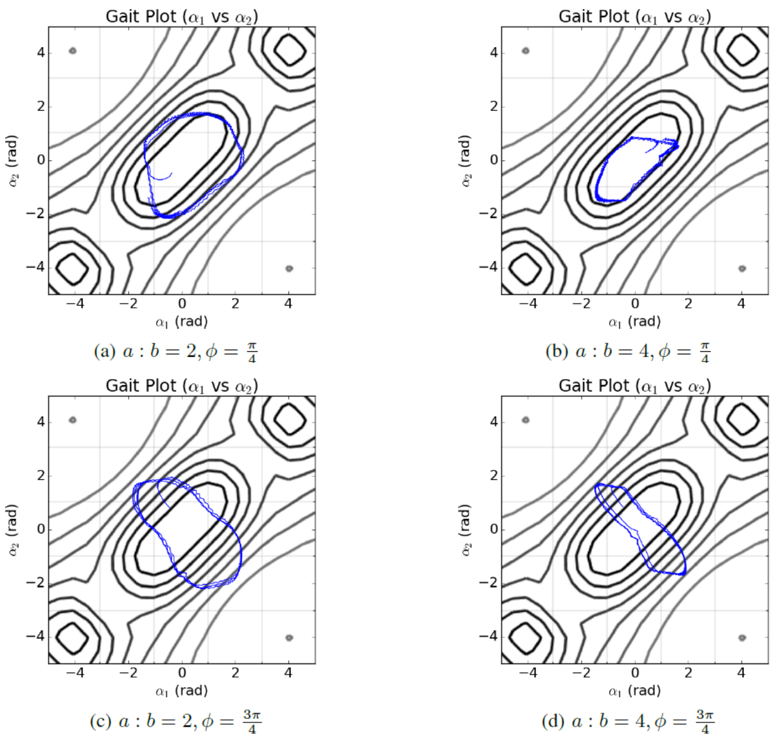

Figure 4.4: Gait stroke plots for four different elliptical gaits collected with the motion capture system. The observed gait strokes are plotted on top of the $D\mathbf{A}_x(\alpha_1, \alpha_2)$ contour plot.

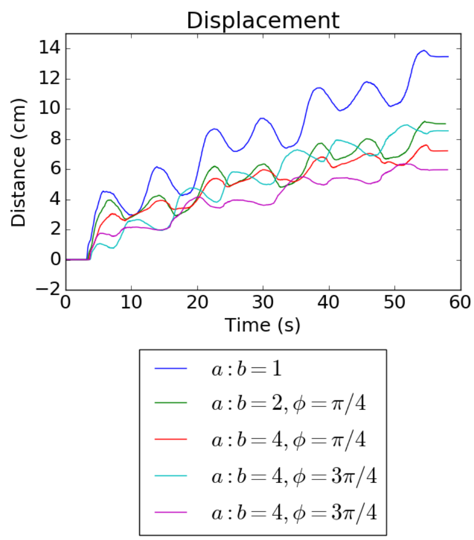

Figure 4.5: Displacement along the longitudinal (x) body axis visualized as a function of time for all gait strokes examined with the motion capture system.

Gait Parameters	Measured Δx	Measured Δy	Average Disp (x)	Predicted Disp (x)	Cost	Efficiency
$a:b=1$	13.5 cm	3 cm	0.23 L/cycle	0.09 L/cycle	29.91 rad	0.0077 L/rad
$a:b=2, \phi=\frac{\pi}{4}$	9.0 cm	0.6 cm	0.15 L/cycle	0.07 L/cycle	22.96 rad	0.0065 L/rad
$a:b=4, \phi=\frac{\pi}{4}$	7.3 cm	0.4 cm	0.12 L/cycle	0.03 L/cycle	17.85 rad	0.0067 L/rad
$a:b=2, \phi=\frac{3\pi}{4}$	8.7 cm	1.6 cm	0.15 L/cycle	0.06 L/cycle	23.26 rad	0.0064 L/rad
$a:b=4, \phi=\frac{3\pi}{4}$	6.0 cm	0.25 cm	0.1 L/cycle	0.03 L/cycle	20.53 rad	0.0049 L/rad

Figure 4.6: Net displacements along the longitudinal (x) and lateral (y) body axes during the gait tests. The displacements are measured over 3 cycles of the gait stroke and the time elapsed for each test was roughly 54 seconds. Average displacement in body lengths (L) per cycle are also given for comparison with displacements predicted by area integral of D**A**. The gait cost is the magnitude of shape change in a cycle (estimated perimeter of the actual elliptical trajectory, measured in radians), and efficiency normalizes average displacement against the cost of the stroke.

region with respect to $D\mathbf{A}^x$. For comparison with the displacement measurements observed with the motion capture system, we estimated the area integrals of $D\mathbf{A}^x$ based on the 1.8:1 drag ratio over each of the five regions enclosed by the actual shape trajectories. These predicted displacement values are also given in Table 4.6 in units of body lengths (L) per cycle. The cost for a gait stroke in this system was taken as the magnitude of the total shape change incurred over the cycle, which is the estimated perimeter length of the elliptical trajectory. To assess relative efficiency of each gait pattern, the average displacement was normalized against cost, and both cost and efficiency metrics are reported in Table 4.6 as well.

The circular stroke ($a : b = 1$) performed significantly better than the other gaits in terms of net displacement per cycle, and only somewhat better than the others in terms of efficiency. Net displacement appears to scale with size of the elliptical area enclosed about the origin and does not have a strong dependency on the orientation of that ellipse, although the elliptical gaits oriented at $\phi = \frac{\pi}{4}$ perform slightly better. It is worth noting that efficiency gains diminish as the size increases, which is consistent with the soap-bubble heuristic for gait selection. The measured displacements agree with the area integral predictions in terms of which gaits offer the most displacement, though not on the magnitude of the displacement. The soft snake actually produced more net forward movement by a factor of 2-3 over the predictions. The peristaltic mode of locomotion caused by the cycles of elongation and retraction that accompany the bending in C- and S-shaped backbones could have contributed to this extra net forward displacement. This explanation is also supported by the displacement plots and visual qualitative analysis of the gait, which show cycles of stretching and pulling forward on retraction. Another explanation could be that the drag coefficient measurement is incomplete which would affect the magnitude of the predicted displacement while having a minimal effect on the size of the sign-definite region.

A key trend to note across all gait plots is the contraction of the stroke curve in either quadrants I and III. As shown in Fig. 4.3, a C-shaped backbone is produced when α_1 and α_2 have the same sign (quadrants I and III), and an S-shaped backbone when they have opposite signs (quadrants II and IV). The orientation of the elliptical sign-definite region of $D\mathbf{A}^x$ with its semi-major axis along $\alpha_1 = \alpha_2$ indicates that an "ideal" gait would include tight arc angles in the C-shapes and relatively shallow angles on the S-shapes. All gait plots gathered with motion capture show a somewhat concave curve in quadrant I, quadrant III, or both, highlighting that the soft robot was not as successful at achieving high-curvature

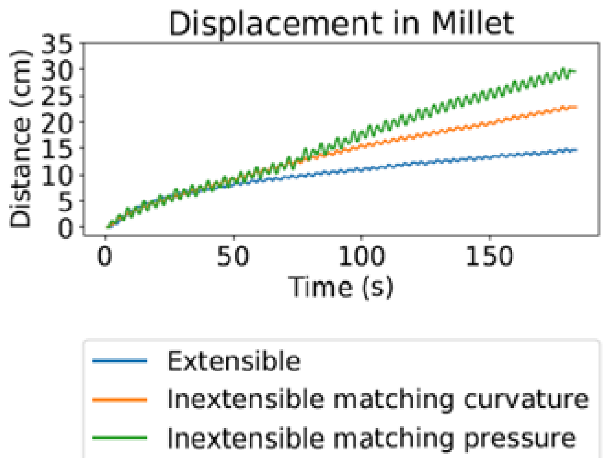

Figure 4.7: Results locomotion of both robots in millet comparing both matching curvatures and matching input pressures.

C-shapes as it should be to perform a maximum-displacement gait stroke.

The strong S-shape backbones consistently demonstrate arc angles of about 2 radians from both actuators, which indicates that each is capable of achieving strong arcs in both positive-direction and negative direction curvature and suggests that the explanation for weaker C-shapes is unrelated to their bending capabilities. Forming a C-shape is usually a higher-cost operation than forming an S-shape of similar amplitude, since both ends of the body are moving in the same direction in a high-lateral-drag medium. We noticed the actuators pivoting slightly outwards about the magnetic fastener when forming C-shapes, probably at least partially due to this high drag force condition.

4.1.4 Comparing Locomotion in Granular Media

To compare the locomotion behaviors of both robots, we performed gait tests matching both the shape deformation (curvature) of the robot as well as the control parameter (input pressure). Both robots were tested in millet, our granular media, using the same circular gait to represent lateral undulation. The results from the inextensible robot run at matching curvature and matching input pressure were compared to the results of the extensible robot. The reason for comparing results of the matching input pressure is due to the larger

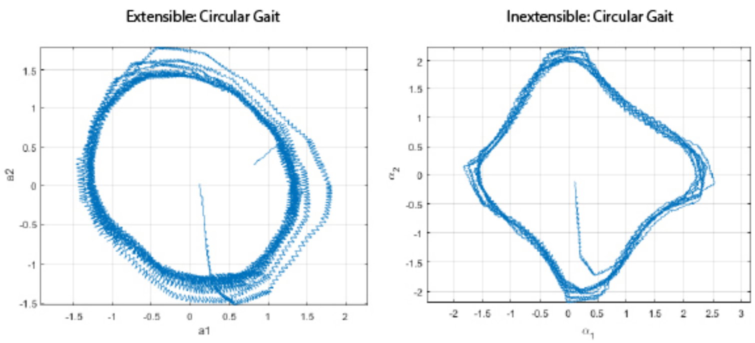

Figure 4.8: Comparison of the experimental circular shape spaces of the extensible and inextensible robot prototypes.

curvature achieved by the inextensible robot at the same pressure. Since our gait is defined by the shape space enacted by the robot, to make a proper comparison, the robots need to produce the same shapes. However, to demonstrate how major behavioral changes can be produced by implementing minor design changes with the same control input, we wanted to compare the performance of the robots with matching control parameters. These results can be seen in Figure 4.7, and show that in either case, the new inextensible robot produced a larger displacement over the original extensible robot. The comparison of the experimental data on generating the shape space is shown in Fig. 4.8.

We expected the displacement/cycle of the new inextensible robot to be closer to the predictions output by the geometric mechanics model since we had removed the mode of extension during locomotion. However, the difference between experimental displacement/cycle and predicted displacement/cycle only grew. Further possibilities behind why the experimental results did not match the predicted results can be defined by the assumptions made for the model.

Both prototypes of our system did not adhere to all assumptions for the model. Although close, the actuators did not exhibit constant curvature, especially when interacting with the environment. The use of elastomeric material means that the environment has a significant impact on the deformation of the actuators. If enough of the granular media was in contact with the actuator, the actuator would change shape in response to the obstacle. The actuators also had a reasonable cross-section (470 mm^2). This meant that were considerable end forces on the actuators that the model did not account for that could be contributing

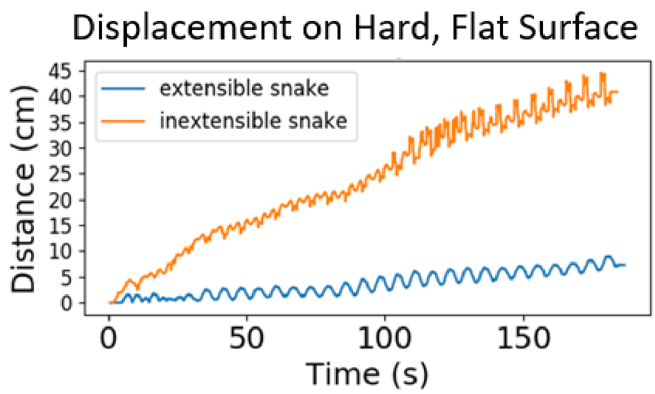

Figure 4.9: Results locomotion of both robots on a hard, flat surface.

to the displacement of the granular media around the robot. As the environment shifts around, the robot can produce both positive and negative behaviors upon interactions. A considerable cross section increases the interaction capabilities of the robot with the environment.

The only remaining significant difference between the robot and the geometric mechanics model is the softness of the body and its associated dynamics. The purpose of the geometric mechanics model and its implementation for a soft robot was to design gaits for the robot without having to account for the nonlinearities originating in the elastomeric materials used to build the robot. The circular gait, as an implementation of lateral undulation, is still a valid and useful gait to employ, but it seems likely that the nonlinearities of a soft robot cannot be ignored to accurately predict displacement/cycle. As simplified control scheme for producing a useful gait, the circular gait can continue to be used and modified to further improve locomotion capabilities.

Another unexpected result of the addition of an inextensible backbone was that the robot could successfully move across hard, flat surfaces. The millet, a fluidic medium, was chosen as the testing environment for the previous work precisely because we had not implemented any frictional anisotropy on the robot's morphology. Fluidic media removes the necessity of frictional anisotropy to produce displacement using lateral undulation [34].

When the inextensible robot was tested using the same circular gait on a hard flat surface, it was found that it could produce considerable displacement. The results of a comparison of the two robot prototypes can be seen in Figure 4.9. The results show that the extensible robot produces very little displacement across a hard, flat surface, whereas the inextensible robot produces a large displacement, almost doubling its displacement through millet. Usually, on a flat, hard surface, snakes rely on frictional anisotropy to propel themselves forward. The inextensible robot had no frictional anisotropy, as only the elastomer was in contact with the surface.

Qualitative observation of the inextensible robot showed that it was much more dynamic on a hard surface, than in granular media. When the robot inflated to large curvatures and then uncurled during deflation, it tended to push itself up off the surface producing out-of-plane motion. When the inextensible robot is in a granular media the pushing force was disseminated by the grains as they flowed away in response to the reactive forces. The original, extensible robot did not produce out-of-plane motion because the mode of extension/contraction absorbed the reactive energy upon deflation.

There are also the micro-mechanical interactions between the elastomer and the hard, smooth surface that could be a contributing factor to successful locomotion with directional friction. The fact that the inextensible robot had some lifting meant parts of the body were smearing against the surface and acting as an anchor to push off against. The extensible robot had no lifting, and had equal motions of extending and contracting canceling out the adhesion effects. Therefore, the successful propulsion across relatively smooth, hard surfaces is likely a combination of a stiffer interaction with the terrain resulting in more dynamic movement, and the adhesion between the elastomer material of the robot's body and the surface acting as push-off points for propulsion.

4.2 Modifying Gaits for the Inextensible Robot

Snakes will vary their gait patterns depending on what environment they are traversing. The more fluidic the environment, the faster the travel speed of the propagating wave along the backbone and the larger the wave amplitude grows as it moves down to the tail [36]. The circular gait is simply a sinusoidal traveling wave function where the sine waves for each actuator are 90 degrees out of phase and the amplitude of the sine wave corresponds to the magnitude of curvature of each actuator. The sinusoidal function can be modified to reflect different amplitudes and phase offsets as performed in nature. As seen in 4.7, the gait with a larger amplitude (more curvature) produced a larger displacement through the environment. Therefore, comparing the effects of curvature on the locomotion capabilities of the robot will be useful.

The deviation of the experimental results from the model predictions may also be caused by the complex coupling between the robot and its environment. Therefore, varying the environment while holding the gait constant would also provide useful information on how interactions between soft robots and terrain are vital in producing effective locomotion. Identifying effective locomotion strategies is also necessary to determine the robustness of the robot in unstructured environments such as confined spaces and under heavy debris. Though we have evidence that the inextensible robot can operate on hard, flat surface (as described in Chapter 3), we continued to focus on granular media as the robot had no frictional anisotropy and adhesion forces would be negated in a fluidic medium. The experiments were performed in environments that can be considered granular media with varying grain sizes. The selected environments were: paper, to represent a hard, flat surface, sand (10^{-4} m), millet (10^{-3} m), BB pellets (10^{-2} m), and rocks (10^{-1} cm). Paper (a hard, flat surface) was tested to compare against the granular media and determine how effective contributions from out-of-plane motion would be on the locomotion capabilities of the robot.

The soft robot was operated with a pneumatic control system based on an open source design [16]. The board utilizes a microcompressor with separate air lines for each actuator chamber, and each line is driven by a solenoid valving at a specified PWM rate. This system allows control of the max duty cycle of the solenoids, the timing and patterning of the solenoids opening and closing, and how long the solenoids stayed open. Therefore, the amplitude (curvature) of each actuator could be controlled by how long the solenoid valves were open, and the sequence of chamber activation could be controlled by when the solenoid valve would open/close. The control over these parameters is similar to the snake's ability to alter the amplitude of the propagating wave as it encounters various terrains, as well as altering its muscle activation to vary the speed and phase of the propagating wave [79].

4.2.1 Varying Gait Parameters

The first parameter varied was the phase offset between the two sine waves driving the two actuators of the robot. This was varied in our control scheme by patterning the opening and closing of the solenoid valves that delivered air to the robot. The phase offset was defined by percentage of overlap shown in the chart in Fig. 4.10. Each gait was tested using a medium amplitude of 60 degree arc sweep in millet, the medium particle size terrain. Each experiment used the OptiTrack motion capture system to collect position data from the reflective markers located on each end and middle of each actuator. The position data was then used to determine the net displacement of the robot. The results of the phase offset experiments can be seen in Figure 4.11.

During testing, it was consistently noted that all gaits had a small step backward during each cycle. This is caused by the symmetric gait and considerable slipping between the robot's body and the media. The granular media flowed as it came in contact with the body of the robot. The grains could be packed together and form ridges for the robot to push off of, as intended, or they could flow apart, resulting in the robot digging a channel preventing any further displacement. The experiments in which the robot dug itself into a channel were ignored as they did not happen frequently.

The robot is soft and relatively light in comparison to the dense millet. These qualities meant that though the robot could act on the environment, the environment also acted on the robot. Dense piles of millet would prevent the actuators from reaching the shape driven by the gait as the weight of the millet became greater than the output force of the actuator. If the piles around the robot were too small, the robot would slip on the grains, and slide backward. It was also noted that large piles of millet would form in non-ideal positions to the robot, so when the actuators deflated (unfurled) they would impact the newly formed pile, pushing itself backwards instead of a simple lateral push.

Interactions with the environment, especially if the environment changes over time, is important to take into account when designing gaits, and in future work, when the robot is sensorized and closes the feedback loop, it can respond accordingly. This is another open problem in the field of soft robotics as there is a complex coupling between soft bodied robots and creatures and their respective environments.

The current design of the robot cannot alter its behavior based on how it is interacting with a time-history-dependent environment, and is therefore easily perturbed by it. However, by employing an asymmetric gait, we can reduce the unintended behaviors produced by unfavorable interactions. All gaits employed by any animal or robot have some form of asymmetry, usually through interactions with the terrain via frictional forces. The asymmetry in our robot-environment system was supposed to come from laterally pushing off ridges formed by the millet, but as we could not directly control how the robot came in contact with the ridges and where the ridges would form, we were not maximizing our asymmetric interactions.

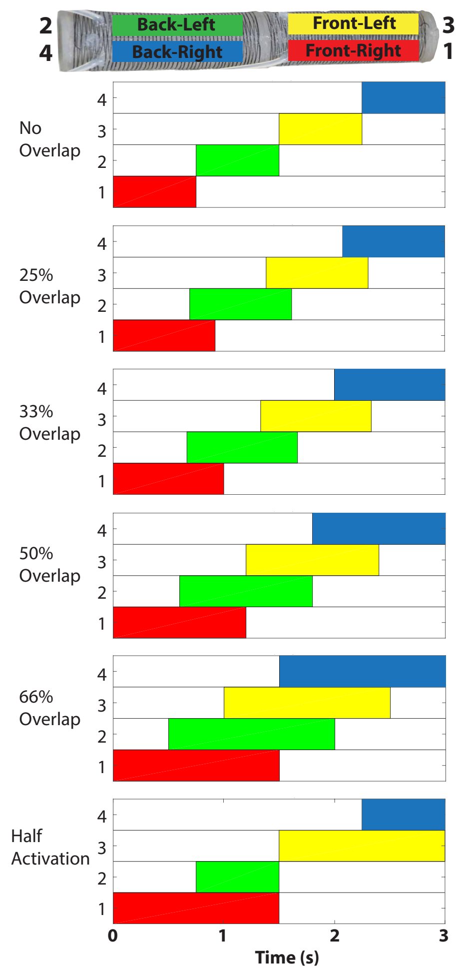

Figure 4.10: Illustration of gait sequences to show when each chamber is inflated and for how long.

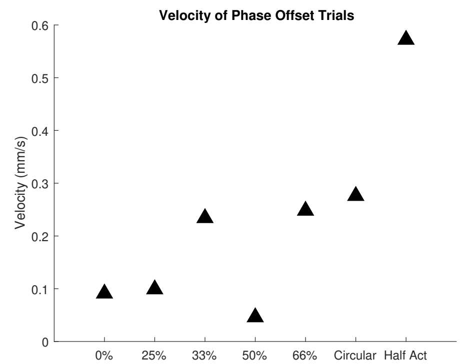

Figure 4.11: Plot of the velocities of the gaits varying the phase offset. Included is the circular gait developed in [5]

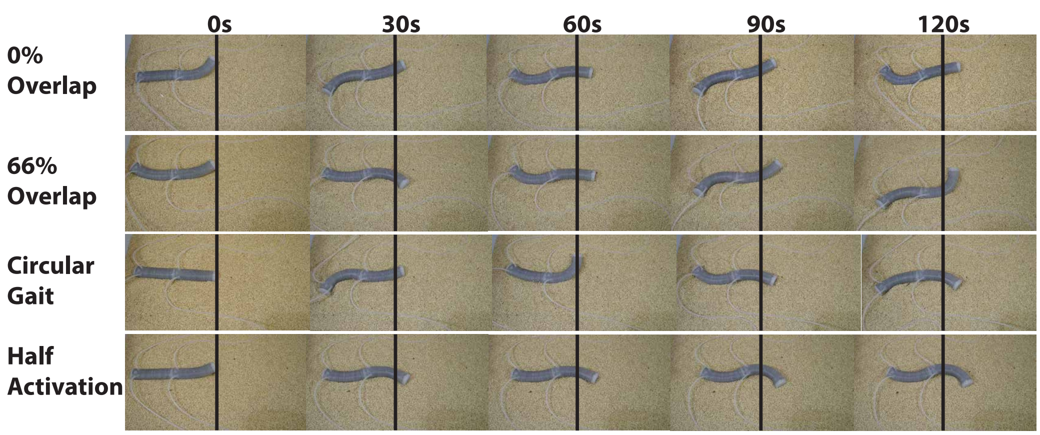

Figure 4.12: Time lapses of some of the gaits in which the phase offset of the traveling wave was varied by a percentage overlap. The circular gait from [5] is included for comparison.

An asymmetric gait was developed to account for these non-ideal interactions with the environment, and ensure positive behaviors were consistently performed. This asymmetrical gait is referred to in this work as the “half-activation gait”. This refers to the back actuator being activated half as long as the front actuator (as shown in the bottom plot of Fig. 4.10). This asymmetrical activation resulted in the back actuator returning to a neutral position, where its lateral resistance was maximized, while the front actuator was deflating. A comparison of the shape space enacted by the robot performing the half-activation gait

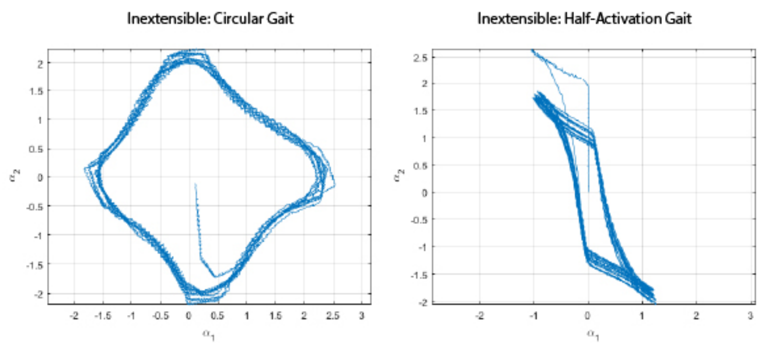

Figure 4.13: Comparison of experimental shape space data of robot enacting each gait.

versus the circular gait is shown in Fig. 4.13.

The half-activation gait reduced the backward sliding of the robot as a larger anchoring force was likely applied by the back actuator reducing slip. A comparison of achieved velocity between the half-activation gait, the circular gait, and the other symmetric variations to the circular gait is shown in Fig. 4.11. Introducing asymmetry through the gait instead of relying on ideal environmental interactions that could not be controlled, resulted in a much large velocity and net displacement. The circular gait, the optimal gait for our kinematic model, was the second best gait, verifying that though the model does not fully capture the robot-environment system, it is still a valid gait to use.

Due to the success of the half-activation gait, further experiments in varying amplitude (curvature) of the front actuator were carried out with this gait over our selected terrains. Changes in amplitude were implemented by changing the max duty cycle of the solenoid valves in our control system. Four amplitudes, measured as an angle of the arc swept by the actuator upon inflation (see Fig. 3), were selected; 45°, 60°, 90°, and 135°. These curvatures were enacted by the front actuator whereas the back actuator curved to only half the angle. It was expected that the more the front actuator curved the more forward displacement would be achieved. This prediction comes from the observations in [36] that snakes in fluidic environments will increase the amplitude of the propagating wave as it travels towards the tail. Though the half-activation gait halves the amplitude of the wave as it travel caudally, the idea was that an increase in velocity can be achieved by increasing the overall amplitude of robot.

The results of how amplitude affects locomotion for each terrain can be seen in Figure

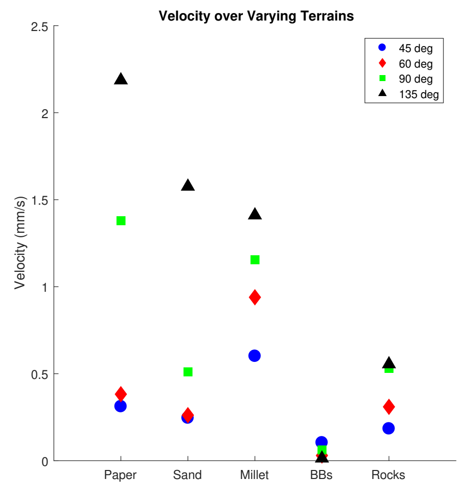

Figure 4.14: Velocity results of the curvature testing in all terrains

4.14. As is seen in the graph, the 135° amplitudes performed best in all terrains except the BBs. The BBs terrain had almost no displacement for every amplitude tested. The BBs were much more dense than the robot which prevented the robot from sinking into the media. Snapshots from the 135° gait over all terrains can be seen in Figure 4.15.

As previously described, the inextensible robot had out-of-plane motion when deflating from high curvatures when on a solid surface. This out-of-plane motion was not achieved in granular media because the grains absorbed some of the forces, dampening its effects. The gaits, originally designed for granular media, were therefore effective on packed surfaces because of this dynamic behavior, and the adhesion between the elastomeric body and the surface. The half-activation gait, though designed specifically to deal with the unfavorable interactions between the unfurling actuators, and the ridges of grains, was most effective on paper, than in any of the granular environments. This is likely because the strategy of maintaining a neutral position (maximizing lateral resistance) of the back actuator because more surface area of the elastomer was in contact with the terrain, providing a more stable anchor. The sand, the most packed granular media tested, had the second best result as the robot had some out-of-plane motion due to the grains not sliding as much as they did in the other granular environments.

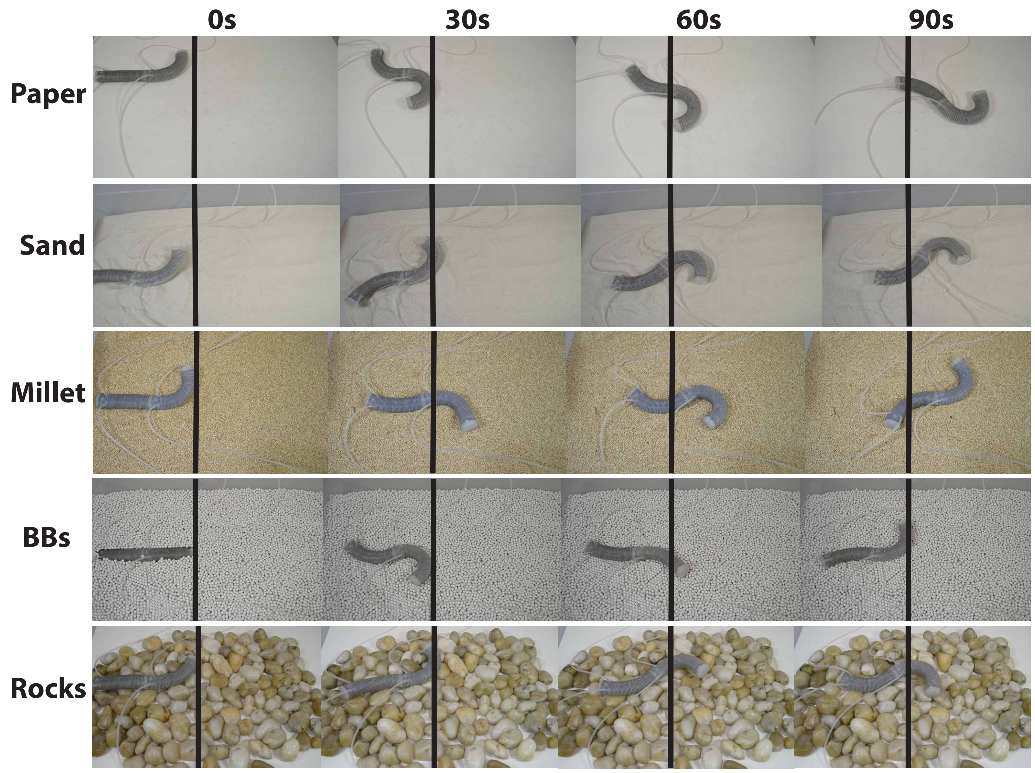

Figure 4.15: Snapshots from all terrains with the 135°, half activation gait

4.2.2 Demonstrations of Robustness

The capabilities of the robot in more complex, and specific terrains to examine its usefulness in potential applications was also explored using the half-activation gait. The first experiment tested the robot's ability to extract itself when buried, and to continue to progress along the terrain. The robot was able to extract itself and move 5cm (half its body length) in 40 seconds when buried in millet. The second experiment included dumping a pile of rocks onto the robot while in motion to examine its ability to withstand trauma, and escape unexpected changes to its environment. These are practical demonstrations to show how effective soft snake robots would be in navigating urban disaster zones. The robot also traversed the length of a 60 cm, 7.62 cm diameter pipe. The robot was placed partly in the pipe, and it took one minute to pull itself all the way into the pipe. It traveled the 60 cm in four minutes and finally extricated itself completely in one minute. Though progres-

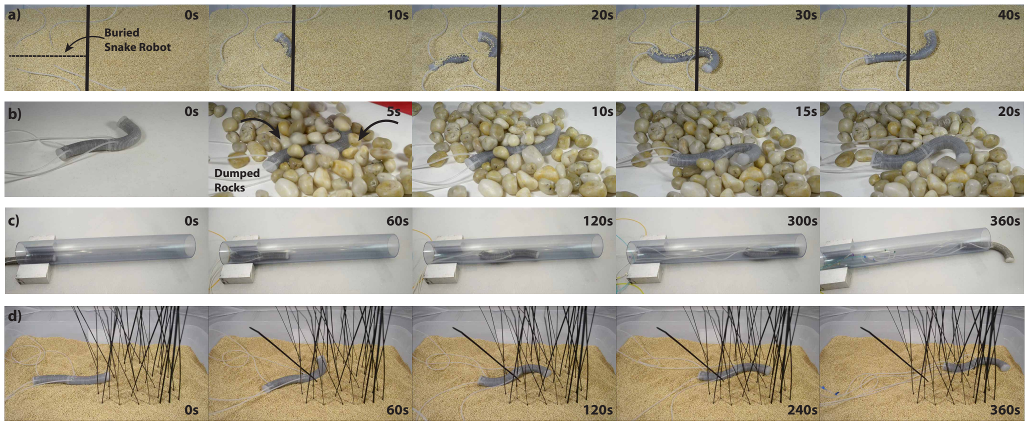

Figure 4.16: **a)** Robot unburying itself in millet and traversing 5cm **b)** Demonstrating the ability to dump heavy items on the robot and have it dig itself out **c)** Robot enters, traverses, and exits a 60cm long, 7.62cm diameter pipe **d)** Robot traversing 20 cms through a long grass substitute (30.5 cm) long zipties

sion was slow, the robot was able to move through the confined space. Lastly, the robot's ability to navigate environments that present random obstacles that could potentially entangle the robot was tested. 30.5cm long plastic zip-ties were embedded into the millet to represent long weeds. It traversed 20cm of the "weeds" in six minutes. Snapshots of these demonstrations can be seen in Figure 4.16.

4.3 Summary

This chapter outlined the development of the circular gait, a geometric gait model representing lateral undulation. The gait is optimized based on the sequence of backbone shapes the robot has to enact and the cost of travel as it transitioned from one shape into the next. This strategy for modeling the gait and predicting displacement through a granular media separates the shape space of the backbone from the nonlinear dynamics through which the robot-environment system achieves this sequence of shapes. Soft robots, because of the use of elastomeric materials, are inherently nonlinear. There is also a complex coupling between the robot and its environment that can change with each step. The model is an attempt to generalize undulatory locomotion of a soft robot without having to know the design of the robot, or the discrete interaction with the environment, as well as any imperfections that might be present in the system.

Initial locomotion experiments using this circular gait on an extensible robot show that the gait model was viable, but the robot was displacing further than the model predicted. Other than not adhering strictly to all assumptions for the model, the initial prototype extended/contracted each cycle. Our original hypothesis was that the extra displacement was due to this peristaltic mode of locomotion unique to an extensible robot. It was believed that this extension/contraction was aiding the robot in its traversal of the granular environment. We therefore design a second prototype of the robot that removed this peristalsis mode. However, when testing this new, inextensible robot with the circular gait in a granular environment, it produced an even larger displacement, deviating further from the model's predictions. It was therefore determined that though the geometric gait model still produced successful locomotion, it was not fully capturing the complexities of the soft material and its coupling to the environment.

Snakes can modify the speed of wave propagation, and the amplitude of their lateral bends to increase their speed through a range of environments. With our new inextensible robot we varied the phase offset (speed of propagation) and amplitude (magnitude of curvature) of the sinusoidal waves foundational to the circular gait. Observations of a range of gaits varying phase offset resulted in an insight that the robot was not successfully breaking gait symmetry through interacting with the ridges formed in the granular environment. This breaking of gait symmetry is necessary for forward propagation, but because the robot was slipping due to non-ideal interactions, each undulatory cycle resulted in a small backward step. A custom gait, referred to as the half-activation gait, was developed to ensure asymmetry was present. This gait outperformed its symmetric counterparts both in granular environments and hard, flat terrain by reducing the amount of slip experienced each gait cycle. Using this gait to determine how changes in amplitude effected locomotion, we found that maximizing the curvature of the robot, maximized displacement.

It is uncommon for animals to utilize asymmetrical gaits. They instead rely on their morphology and interactions with the environment, usually through frictional forces, to create the necessary asymmetry to produce effective locomotion. Snakes, when in environments devoid of obstacles to push off against, will rely on their skin, and its frictional anisotropy to create the asymmetry necessary to use lateral undulation effectively. The current design of the robot can effectively locomote through a range of environments with an asymmetrical gait, but that is contrary to nature. The next chapter will look at breaking gait symmetry with the morphology of the robot targeting the environmental interaction between the terrain and scales embedded in a skin wrapped around the robot.

Chapter 5: Snake-Inspired Kirigami Skin for Lateral Undulation

5.1 Frictional Anisotropy in Snakes and Snake Robots

Limbless locomotion strategies couple the deformability of the organism's body and the frictional properties of the organism's skin to successfully locomote across a wide range of terrains. As lateral bends of the snake's body propagate down the backbone, these bends can brace against obstacles to push the snake forwards [35]. However, when obstacles are absent in the environment, significant displacement using lateral undulation depends on the interactions between the snake's scales and asperities on the terrain's surface [80]. Here, frictional forces become dominant (see Fig. 5.1), requiring both a longitudinal (axial) force vector, and a lateral (tangential) force vector to provide proper reaction forces to produce forward propagation. The production of both axial and tangential forces between the body of a snake robot and its environment is vital to the success of locomotion.

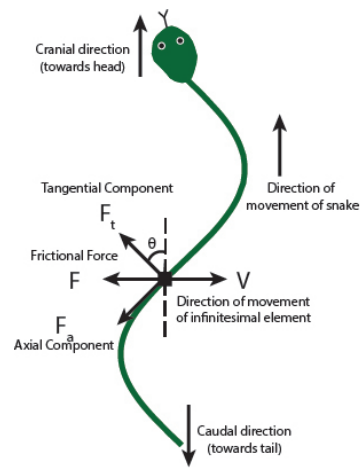

Figure 5.1: FBD of forces acting on snake during lateral undulation.

The anisotropic properties of snake skin originate in the morphology and activation of their ventral scales. At the macro-level, snake skin exhibits longitudinal (along the backbone) anisotropy through the overlapping pattern of the scales allowing for smooth gliding forwards (with the scales) and resistance sliding backwards (against the scales). Snakes also exhibit high friction in the lateral axis (across the scales) that in combination with the deformation of their body can provide lateral resistance to push off against surface asperities similar to pushing off an obstacle [81]. This can be represented as a lateral-longitudinal anisotropy which is the ratio between resistance across the scales and resistance when moving forwards with the scales. Close examination of snake skin revealed that at the micro-level snake scales exhibit microornamentation (micro-ridges, nanoindentations, or fibular components), that may contribute the lateral resistance needed to traverse environments containing only surface asperities in which to interact.[9].

To ensure the successful propagation of the robot through its environment, both the kinematic production of the gait and the environmental interactions must be considered. Many snake-inspired robots use wheels to provide the lateral resistance necessary for lateral undulation [82, 8, 83]. However, the addition of wheels limits the traversable terrains to hard, flat surfaces. There has been success in improving locomotion of a rigid snake robot with the addition of artificial scales to provide longitudinal anisotropy [84], but that work did not examine friction in the lateral direction.

The skin developed in this chapter is based on kirigami, a Japanese art form that involves cutting patterns into thin sheets of material. Patterning cuts into a material to produce a desired behavior is a common design mechanism (e.g expanded sheet metal). By implementing a specific parallel lattice of cuts into a material, the kirigami structure can then produce out-of-plane buckling when uniaxially stretched. The profile cut into the sheet, and the patterning of these profiles can be varied to alter the feature that pops out of plane (see Fig. 5.2b) [85]. Recently, kirigami has been used to develop skin for soft robots utilizing a rectilinear gait [57] and a two-anchor crawling gait [86], both of which involve the cycling of elongation and contraction of a soft actuator. However, a skin had not yet been developed for a snake-inspired robot using a lateral undulation gait, which introduces novel skin mechanics – such as asymmetric buckling and gradients of strain.

This chapter covers the development of kirigami skins for our soft, bending actuators to improve the robot's velocity when performing a lateral undulation gait. The skin needs to provide the advantages of frictional anisotropy without interfering with the deformation required to propagate bends along the soft robot's body. Using kirigami allowed for the activation and deactivation of scales as the soft actuators deform – similar to biological snakes activating their scales to increase friction [32]. Though lateral friction is regarded as an important feature of snake skin in the biology literature [81], no one has yet directly designed and tested a skin with lateral friction as its focus. Understanding how bioinspired adaptations have coevloved with their environment to produce positive interactions is necessary to engineer these systems for robotics. Therefore, the skin developed for this soft robot will specifically target lateral friction, and determine how it could be contributing to locomotion. The first prototype of skin uses gaps in the lattice pattern to achieve bending, and uses microornamentation to augment lateral friction production. All skins that are implemented on bending actuators will have an in-plane rotation of the scales w.r.t the surface. Therefore, this rotation of scales from a longitudinal orientation towards a lateral orientation will produce some lateral friction. However, the first prototype augments the production of lateral friction through the microornamentation on the surfaces of the scales. The second prototype of skin redefines traditional kirigami lattices in an effort to further increase lateral friction. A radial pattern of scales is used (compared to rectilinear) to orient the tips of the scales closer to an ideal lateral force vector. This adds a further rotation to the already-present in-plane rotation of the scales w.r.t the surface. Bending is achieved through the gradient of hinge widths which is an inherent property of the radial lattice structure.

5.2 Kirigami Skin with Microornamentation

For the initial, proof-of-concept skin design, the previously published kirigami skin [57] needed to be altered to allow for bending. Typical kirigami lattices are axially stiff along the axis of applied strain. When that uniaxial strain is experienced by the pattern of hinges, they buckle popping out the cut profile attached to the hinge. This property results in a large bending stiffness. To use these lattices for lateral undulation, we needed to reduce the

DEFINITIONS

Coefficient of friction (COF): Ratio between frictional force and the applied normal force.

Angle of attack (AOA): A model that can be used to simulate a variety of sizes and designs of a soft robot.

Cranial: Direction moving towards the head. Forward direction.

Caudal: Direction moving towards the tail. Backward direction.

Longitudinal anisotropy: Frictional ratio between the two directions on the longitudinal axis. Backwards (Caudal) : Forwards (Cranial).

Lateral-longitudinal anisotropy: Frictional ratio between the lateral axis and the forward longitudinal axis. Lateral : Forwards (Cranial).

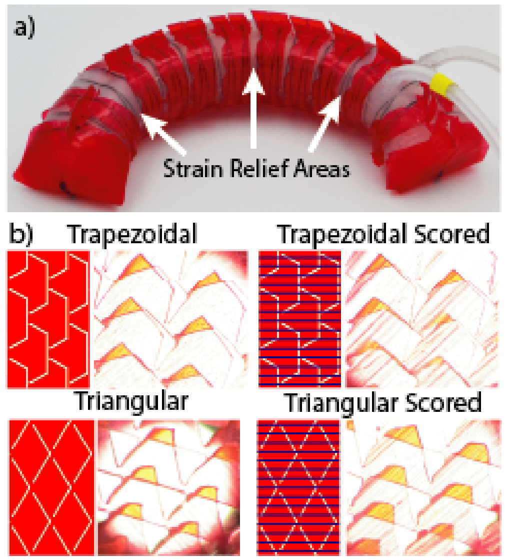

Figure 5.2: a) Strain relief areas allow for curvature of soft actuator. b) Kirigami scale profile geometries and microornamentation.

bending stiffness of the skin, requiring a redesign of the lattice. Additionally, we wanted to implement a specific strategy for lateral friction that also did not interfere with the deformation of the actuator and the overall performance of the skin. Our strategy for increasing lateral friction is microornamentation as seen on biological snake scales. This bioinspired mechanism has not previously been investigated for robots. Micro-ridges, a common form of microornamentation, were implemented on this first prototype of skin by scoring polyester plastic sheets along the longitudinal axis of the skin.

Fig. 5.2 illustrates bending strategy and microornamentation employed on the skin. The coefficients of friction (COF) were experimentally determined and the corresponding anisotropic ratios were calculated. The scale profile shape, and scale microornamentation were varied to measure their contributions to the robot's locomotion capabilities. The angle of attack (AOA) of the scales coupled to the curvature of the robot's actuators was also examined for contributions to the frictional properties of the robot, and locomotion in general.

5.2.1 Design and Fabrication

The inextensible robot, with a new cross-sectional area (264 mm^2), was used to test the skin developed in this chapter. The smaller cross-sectional area was employed to reduce the weight of the robot in an effort to further increase the velocity of locomotion. The fabrication processes for implementing microornamentation, and wrapping the skin around the soft actuator are shown in Fig. 5.3. The skin consisted of a lattice pattern, originally developed in [57], cut into polyester plastic sheets (Practi-Shim™ #222, AccuTrex Products Inc., PA) with a thickness of 0.002" (51 μm) using a Silhouette Cameo 3 knife plotter (Silhouette America, Inc., UT). Two shape profiles, triangular and trapezoidal, were selected based on previous high coefficient of friction results [57]. Microornamentation was implemented by scoring ridges into the plastic sheets before cutting the scale pattern. The ridges were plastically deformed into the sheets using an EK Tools mini scoring board (EK Success Ltd, UT) with score lines 1.25mm wide and 1.25mm deep with 1mm spacing.

Kirigami patterns produce out-of-plane deformation when a uniaxial strain is applied across the lattice. An extending actuator is ideal for producing uniaxial strain, however, actuators that can only extend cannot produce lateral undulation. Previous skins were for extending actuators and do not allow for curvature as they restrict the biaxial deformability of a bending actuator [57]. Bending was enabled by introducing strain relief along the length of the skin (see Fig. 5.2a). To promote consistent activation of the scales, these areas of strain relief had to be relatively small, and embedded uniformly along the skin. The introduction of these negative spaces in the lattice also reduced the self-collision of scales along the inner side of the actuator upon bending which also impedes curvature.

The skin needed an assembly method for adhering that would keep the skin on the actuator without further impeding deformation. The assembly method is shown in Fig. 5.3. The skin was wrapped around the elliptical actuator and the edges were adhered to create a cylinder. The edges were adhered to form a "spine," which needed to be adhered out-of-plane from the strain to prevent the edges from pulling apart due to shearing. The spine was cut along the kirigami pattern, separated at the strain relief areas to allow the skin to slide along the actuator. To fully contain the soft actuator, the plastic sheet was cut to reduce creases at the ends of the elliptical body, and adhered (SuperGlue® Gorilla Glue) to the plastic on the body of the actuator. The tubing for air supply was fed through the closest strain relief area. The actuators were adhered to one another using SilPoxy™

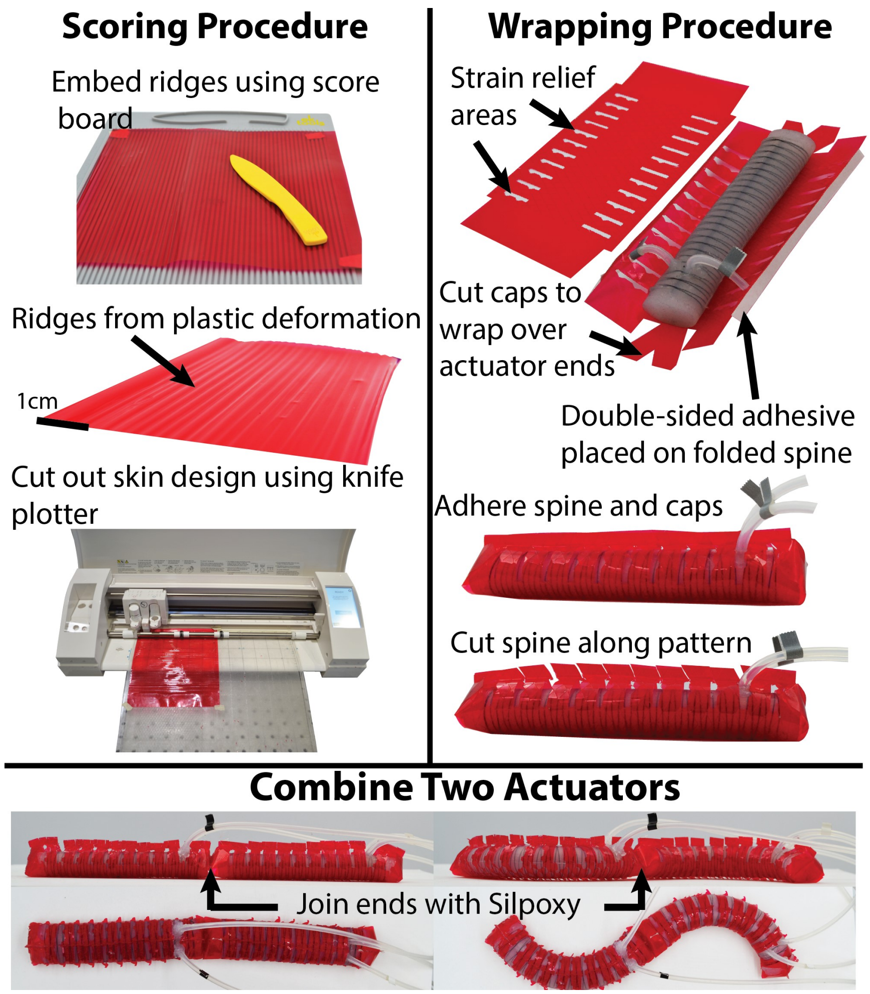

Figure 5.3: Fabrication processes for preparing skin and wrapping around an actuator.

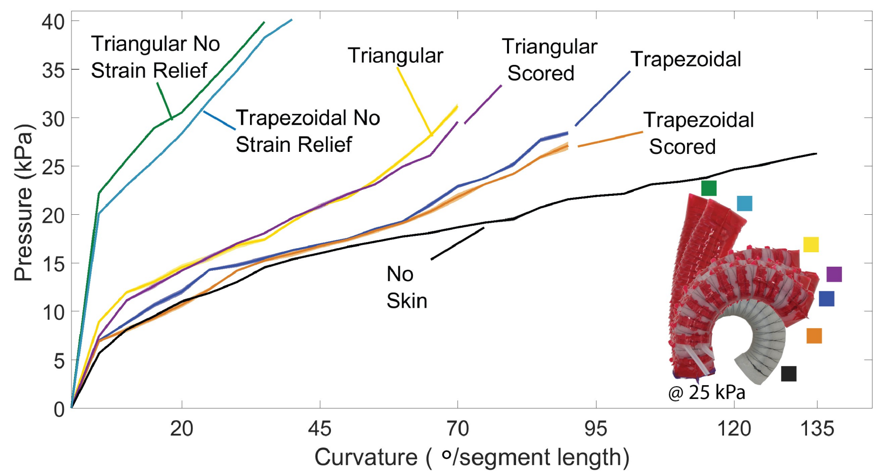

Figure 5.4: Effect of strain relief designs on curvature vs. pressure relationship. Inset shows the achievable curvature of each skin when the actuator is inflated to the same pressure.

placed on the capped ends and allowed to cure.

Fig. 5.4 shows the relationship between pressure and curvature to illustrate how the strain relief design allowed for more curvature of the actuator. The four skins tested in this work are compared to an actuator with no skin, and actuators with no strain relief design. The characterization shows that the skin does restrict curvature as expected, but that the actuator with skin can still reach moderate curvatures. The actuators without strain relief take larger pressures to reach their maximum curvatures. The maximum curvature achieved by the trapezoidal profile actuators before failure was 90° at around 28 kPa, and for the triangular profile actuators was 70° at around 30 kPa. Failure modes of the skin-actuator combination were the skin ripping along the hinges, or the junction point of the tubing and the soft body of the actuator. At higher curvatures, the plastic skin would rip along the hinges as the plastic skin drew tighter around the elastomeric body of the actuator. The effects of microornamentation on the relationship between pressure and curvature are negligible within the scope of this work. A maximum curvature of 60° was used to ensure all experiments were performed consistently without inducing failure of the actuators.

When the actuators bend, the local interaction between the skin and the soft body produce a strain on the lattice causing out-of-plane buckling. Strain was measured at the center line along the bottom of the actuator as that is the area of highest engagement when the skin is in contact with the terrain. The triangular skin was stiffer than the trapezoidal skin which is why it took a higher pressure to produce the same curvature. Therefore, at each curvature the triangular skin had a lower achieved strain.

5.2.2 Characterization of Frictional Properties

To determine how the frictional properties of the skin were contributing to locomotion, the coefficient of friction (COF), dependent on the angle of attack (AOA) of the scales, needed to be characterized for each skin type. The scales pop out when a strain is applied to the skin. The strain is applied through the bending of the actuator meaning the AOA of the scales is determined by how much the actuators bend. Before the COF of the skin could be measured, the relationship between the curvature of the actuator and the resulting AOA of the scales needed to be characterized.

5.2.2.1 Characterizing Angle of Attack

The curvature-AOA relationship was characterized by inflating a skin-wrapped actuator to different curvatures and measuring the resulting AOA of the scales. The trend in Fig. 5.5 shows that as curvature — and therefore strain — increased, AOA increased monotonically and linearly after an initial inflection point. Microornamentation had no observable impact on the AOA. There was a difference in achievable AOA across scale profile geometries as the triangular profile was stiffer than the trapezoidal profile, and therefore produced a lower strain on the skin. The skins could be actuated to the same curvature, but that did not necessarily mean that, between the two shape profiles, the strains would be equivalent. Therefore, comparisons across skin type are made based on curvature, with additional x-axes on the plots showing the difference in applied strain.

When the skin was wrapped around the elliptical actuator, the scales' orientation changed depending on their position along the perimeter of the elliptical cross section, as well as changing when the actuator was at different curvatures. Therefore, the characterization and testing of a planar skin sample was used as a baseline to ensure all scales had the same orientation with respect to surface asperities. Characterization of the AOA of the scales on a planar sample can be seen in Fig. 5.6. A geometric model for the opening angle of a widely-used kirigami lattice with a pattern of linear cuts [87, 88, 89, 90] has been

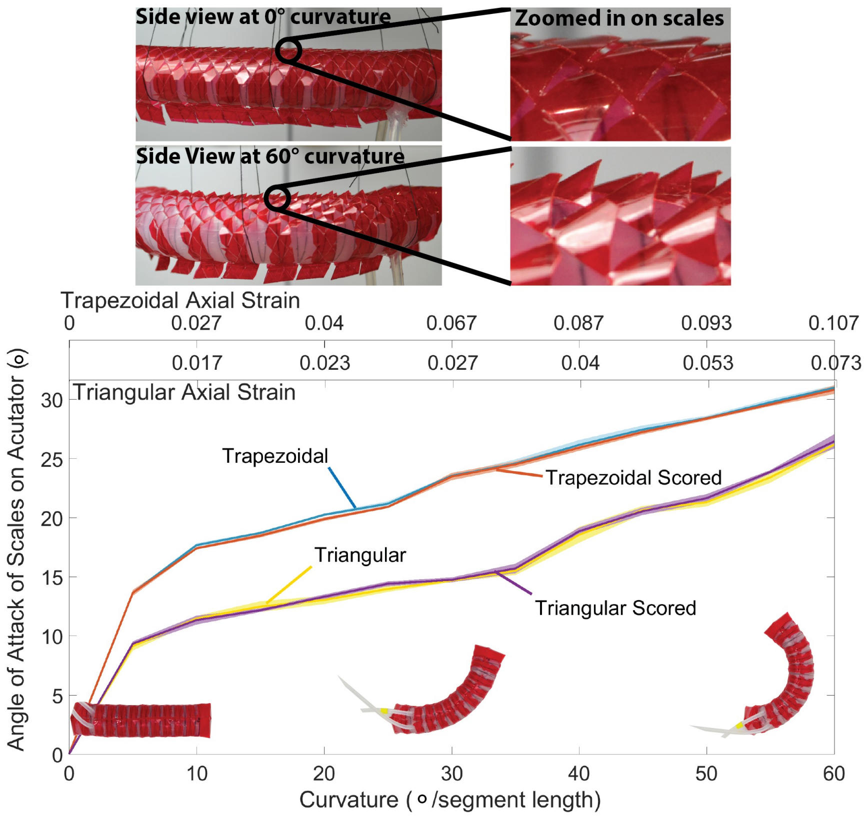

Figure 5.5: Experimentally determined relationship between curvature of the actuator and the resulting AOA.

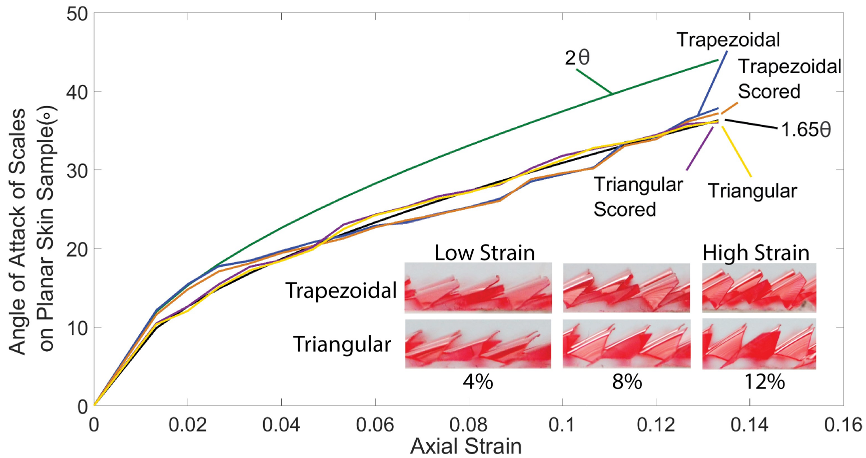

Figure 5.6: Planar AOA measurements from the four types of skin compared to the model shown in Equation 5.1.

previously derived, but not experimentally validated [87]. The model,

$$2\theta(\epsilon_x) = \arccos\left[\sin\left(2\arccos\frac{1+\epsilon_x}{\sqrt{2}}\right) * \tan\left(\frac{\pi}{4} + \arccos\frac{1+\epsilon_x}{\sqrt{2}} - \arccos\frac{1+\epsilon_x}{\sqrt{2}}\right)\right], \quad (5.1)$$

represents the opening angle of the pop-out structure as 2θ, and is a function of the applied uniaxial strain, ϵ_x.

The function, plotted as 2θ in Fig. 5.6, has a similar shape as the observed experimental data, in that the angle increases with increasing strain at a decreasing rate, but was overestimating the AOAs measured. This is likely due to the model being derived for a linear cut pattern which produces both positive and negative (z-axis) out-of-plane buckling (x-y plane). The patterns used in this work only have one direction of out-of-plane buckling (either + or - z-axis). They also have different cut profiles which could be contributing to the reduction of AOA as well. Since the function has the right shape, we can include a scalar multiplier to better fit the experimental data. The new function, represented as 1.65θ in Fig. 5.6), was produced by multiplying the function described in Equation 5.1 by

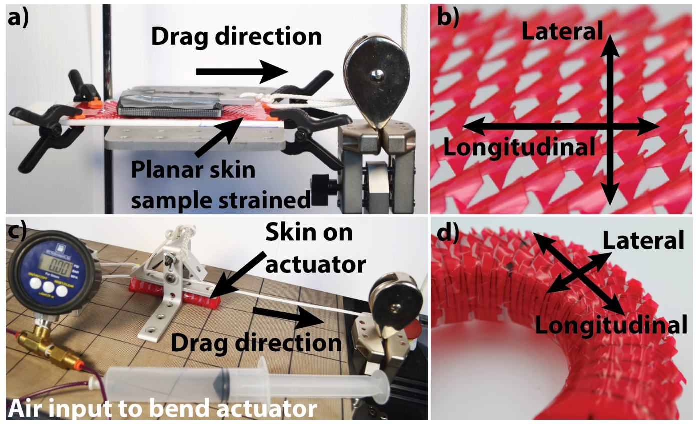

Figure 5.7: Apparatus for measuring the COF of planar skin samples **a)**, and for skin on actuator **c)**. Drag directions of planar skin samples **b)**. and of actuators with skin **d)**

a scalar value of 0.825. It closely approximates the triangular profile relationship between strain and AOA. Examining the stress at the hinges upon uniaxial loading was outside the scope of this work, but could be used to identify why the original model does not accurately represent the magnitude of AOA.

5.2.2.2 Measuring the Coefficients of Friction

The COFs of the skin were characterized to determine the effects of scale profile, microornamentation, and angle of attack on locomotion. The frictional properties of the four skins were measured both in the planar case, where a skin sample was stretched to different strains, and in the curved case, where the skin was wrapped around the actuator and strained by the deformation of the actuator. These two cases were selected to determine if the curvature of the actuator, as well as the orientation of the scales interacting with asperities, had an effect on the COFs measured.

The planar case was tested by stretching a sample of each skin, and dragging a weighted surface sample across the scales (see Fig. 5.7a). The surface tested was a woven fiberglass mesh with an #18x#16 mesh size and a 0.011" wire diameter (McMaster-Carr, #1017A87). A mesh pattern was used so that each opening in the mesh would be considered an asperity with which a scale on the skin could engage. The skin samples were stretched to different strains to produce an AOA corresponding to the AOAs measured at the selected curva-

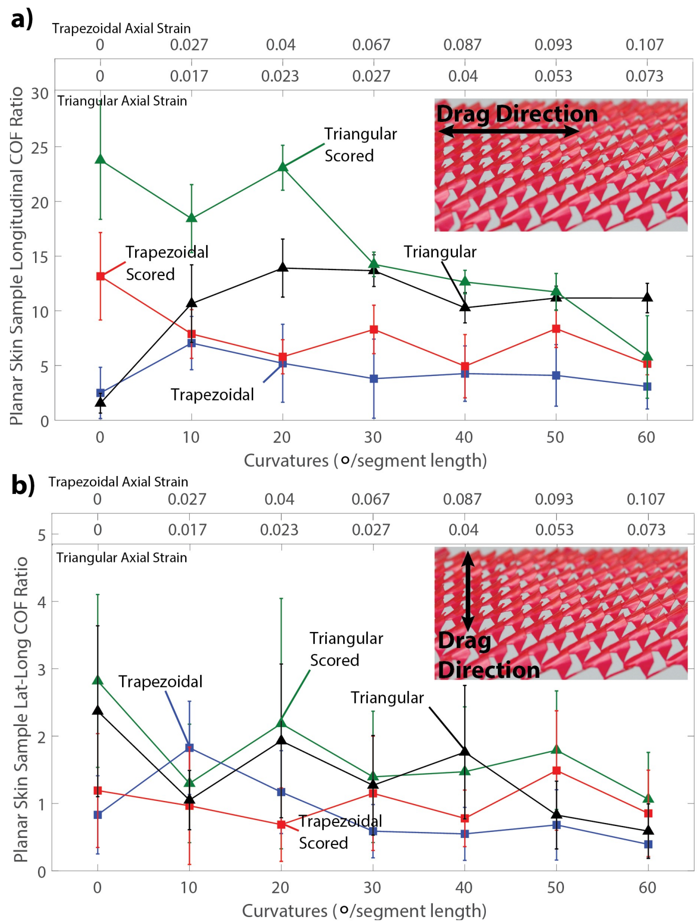

Figure 5.8: a) Longitudinal COF ratio (against scales:with scales) for planar skin sample. b) Lateral-longitudinal COF ratio (across scales:with scales) for planar skin sample.

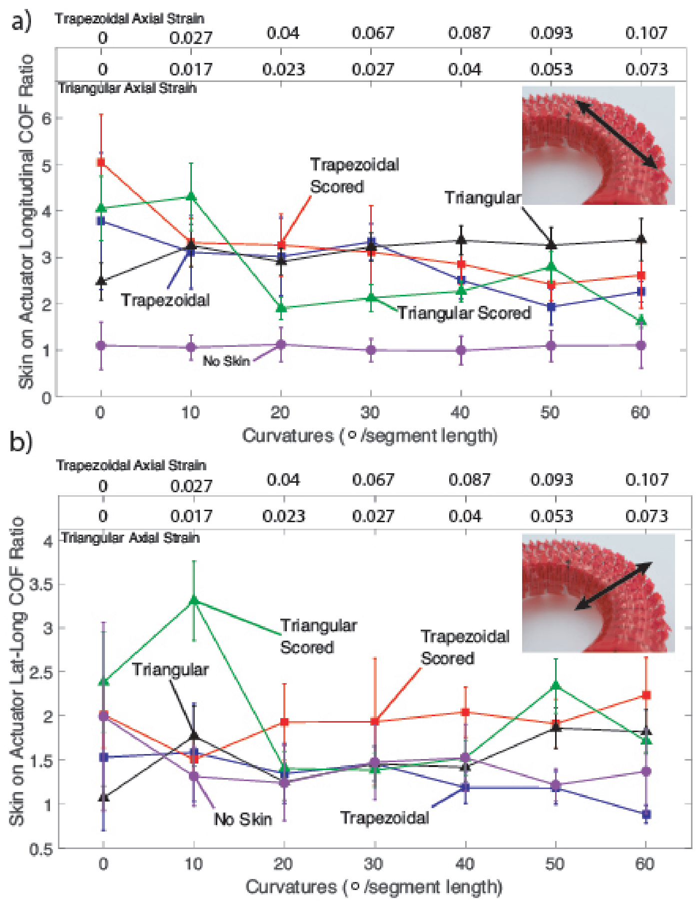

Figure 5.9: a) Longitudinal COF ratio (against scales:with scales) for skin on actuator. b) Lateral-longitudinal COF ratio (across scales:with scales) for skin on actuator.

tures. The curved case was tested by inflating the actuators to the selected curvatures, and dragging them across the surface (see Fig. 5.7c). A force profile was recorded using a Mark10 and 10 N load cell. The skins were tested in 3 configurations to determine the ratio of anisotropy; forwards (cranially, with the scales), backwards (caudally, against the scales), and laterally (across the scales) (see Figure 5.7b and d). The effective COFs in each direction (forwards f, backwards b, and laterally l),

$$\mu_f = \frac{\left\langle F_f \right\rangle}{F_N}, \quad \mu_b = \frac{\left\langle F_b \right\rangle}{F_N}, \quad \mu_l = \frac{\left\langle F_l \right\rangle}{F_N}, \tag{5.2}$$

were needed rather than just comparing the frictional forces because the dragging apparatuses used for the actuator longitudinal tests and lateral tests, and the planar friction tests were different weights. The calculations were performed using the average frictional force $\langle F \rangle$ and the total weight of the dragging apparatus F_N. The dragging apparatus for the planar tests was 1.05N. The actuator tests had a longitudinal dragging apparatus that weighed 2.07N and a lateral dragging apparatus that weighed 1.75 N for actuator tests. The anisotropic COF ratios are defined as μ_b/μ_f for the longitudinal ratio, and μ_l/μ_f for the lateral-longitudinal ratio.

The results of the anisotropic friction ratios for the planar skin samples are plotted in Fig. 5.8. The x-axis is shown in terms of curvature because curvature is the controlled parameter during locomotion. In the planar case, the skin was strained to match the AOA measured at those curvatures. The triangular skin produced higher frictional coefficients. Due to the coupling of the scale shape and axial stiffness of the skin, the higher friction force could be caused by either the geometry of the scale, or the overall axial stiffness of the kirigami lattice. The friction ratio at the highest curvature (60°), and therefore highest strain (7.3% for triangular and 10.7% for trapezoidal) and AOA (26° for triangular and 30° for trapezoidal), is lower than at some of the lower to mid-range curvatures (10°- 30°). At low to mid-range AOAs (11.3° - 14.7° for triangular, and 17.4° - 23.7° for trapezoidal), the scales are less geometrically stiff, and flex backwards while interlocked with an asperity, increasing the time spent interlocked with that asperity. At higher AOAs the scales are stiffer, and upon empirical examination during testing, have a shorter interaction period with surface asperities. Further investigation is required to interrogate this interaction, as the micro-mechanics of skin-surface interactions were outside the scope of this work.

However, based on empirical examinations, though maximizing geometric stiffness increases the applied force of the scale on the asperity, it disengages with the asperity sooner than a less stiff scale, decreasing the total time in which the scale is anchored to the surface.

The anisotropic friction ratios for the skin on actuators are shown in Figure 5.9. Again, at the highest curvature, and therefore highest AOA, the longitudinal ratio is lower compared to mid-range curvatures for most of the skins. The lateral-longitudinal ratio at the highest curvature is maximized for most of the skins. This is likely due to the scales being oriented over a range of angles relative to the asperities, increasing the number of scales interlocking, or partially interlocking with the asperity.

Figs. 5.8 and 5.9 show that microornamentation had an effect on both the longitudinal (forwards:backwards) and the lateral-longitudinal (lateral:forwards) anisotropic ratios. The presence of microornamentation on the skin increased the lateral-longitudinal anisotropy at the majority of curvatures enacted by the actuator. However, it also increased the longitudinal anisotropy. The ridges plastically deformed into the skin increase the longitudinal stiffness of the scales similar to how paper is stiffer when there are folds present.

The frictional anisotropy of terrestrial snakes has been widely studied across different species and testing surfaces, resulting in a range of ratios. From the literature, the ranges were: 1.0 to 3.0 for the longitudinal anisotropic ratio, and 0.99 to 1.46 for the lateral-longitudinal anisotropic ratio [91, 80, 92, 93, 81]. For all four kirigami skins, the range for the longitudinal anisotropic ratios was 1.9 to 5.1. The range of the lateral-longitudinal anisotropic ratios was 0.9 to 3.3. Therefore, we have successfully developed a snake-inspired skin with similar frictional properties as observed in nature.

5.2.3 Locomotion Results

All four skins were tested using a lateral undulation gait, varying only the amplitude of the curvature waves. Due to the coupling between actuator deformation and scale AOA, the AOA would change depending on the driven curvature, which alters the frictional properties of the robot. All robots, at curvatures from 10° to 60° in 10° increments, were tested on top of a metal block covered in a woven fiberglass mesh with an #18x#16 mesh size and a 0.011" wire diameter (McMaster-Carr, #1017A87). The grid was aligned with the longitudinal axis of the robot. Displacement data was collected using an OptiTrack Prime 13 motion capture system and used to calculate the velocity of each robot. A robot with no skin was tested

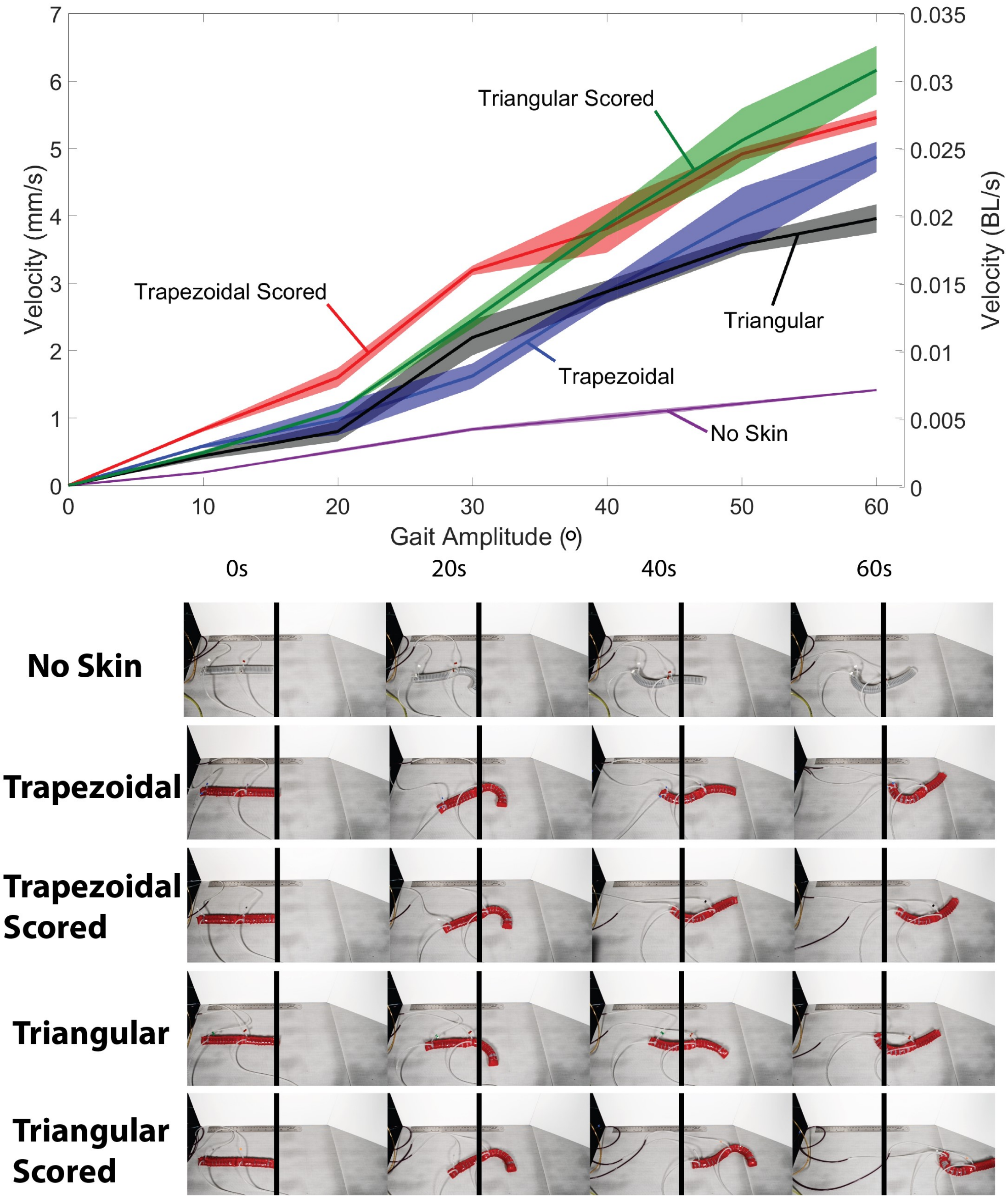

Figure 5.10: Velocity of soft robot using a lateral undulation gait comparing the four types of skin to a robot with no skin.

as a control case to compare against each skin.

The results of the locomotion study are presented in Fig. 5.10. As noted in Chapter 4, all five robots achieved their maximum displacement per cycle (and thus maximum speed for a fixed cycle time) in the gaits with the maximum achievable curvature amplitude.

The scored skin on both scale profile geometries produced a larger velocity than their smooth counterparts. All skins improved velocity of the robot when compared to a robot with no skin, which produced some displacement likely caused by adhesion during surface interactions. The best performing skin, triangular profile with microornamentation, improved the velocity of the robot with no skin by 335% and improved the velocity of the robot with the triangular profile with no microornamentation by 55%. The trapezoidal skin with microornamentation improved velocity of the robot with no skin by 285% and improved velocity of the trapezoidal profile with no microornamentation by 10%.

Beyond our observation that scored skins outperformed unscored skins, and that both provided significantly better performance than no skin, we were not able to identify a clear correlation between the measured COFs and the locomotive performance. Further investigation of this correlation will require a better understanding of how variations in the COFs at different parts of the gait (as the scales are activated and deactivated across the body) and of the role that the longitudinal COF ratio plays in undulatory motion, both at the system level and at the level of individual scales. For example, as the actuator curves more, it reduces the number of scales ideally interacting with asperities as the robot pushes forwards, but as the robot pushes laterally, there are more scales interlocking with asperities.

5.2.4 Conclusions

The first proof-of-concept skin for lateral undulation shows that kirigami can be used for biaxial strains as seen from bending actuators. However, The method employed here relies heavily on the local strains produced by the soft body of the actuator interacting with the skin. These local interactions ensure that all scales buckle accordingly. The negative space in the lattice also prevented the scales on the inner side of the curved actuator from bunching up, crinkling the skin, and preventing full curvature. However, a nonuniform lattice reduces the viability of any kirigami models as a generalized definition is not possible. Therefore, the next design iteration of skin attempts to maintain a fully formed lattice, and uses other kirigami techniques to allow for bending. Although microornamentation improves the overall lateral friction produced by the skin, as well as its locomotion capabilities, there were too many coupled parameters within our system to single out exactly what is happening. The kirigami lattice itself has coupling between the hinge widths and the shape/size of the profiles. There is also an interaction between the soft body of the actuator and the skin, which can be varied depending on the looseness of skin. This was briefly explored in the original kirigami skin developed for crawling locomotion [57], but was not considered in this work. The introduction of micro-ridges on the surface of the skin coupled the interaction between the ridges and the surface, but also weakened the polyester plastic material (making it less stiff) by plastically deforming the ridges into the material. The effect of the scoring on the material properties of the polyester plastic is outside the scope of this work. The micro-mechanics of the micro-ridges interacting with the surface are likely extremely important, but studying this interaction is not within the scope of this work. To remove some of these coupled parameters, a new lattice structure is created for the second skin prototype that increases lateral friction through the modification of the kirigami parameters.

5.3 Kirigami Skin with Radial Lattice Structure

Typical kirigami lattices, as used for the first skin prototype, are defined by a parallel grid structure with hinges and buckled profiles oriented in the direction of applied strain. This makes it ideal for robots using locomotion strategies with a deformation cycle in only one axis. Introducing a feature, such as microornamentation, to a typical lattice allows for the production of force in the desired direction, independent of the underlying lattice structure. However, lateral undulation requires strain in two axes. Current kirigami lattices, with uniform properties, cannot operate under biaxial strain. The first skin prototype removed sections of the lattice, reducing the longitudinal-axis stiffness in a narrow region so when wrapped around the actuator, it could bend. Though this works in practice, it breaks down the kirigami lattice definition. Without a soft body that can provide local, axial strain to the hinges surrounding the negative space of the lattice, the scales attached to those hinges would not buckle. The performance of a kirigami skin with an inconsistent lattice cannot be easily modeled, and the identical buckling of scales and equivalent stresses at the hinges cannot be guaranteed. Therefore, this second prototype aims to define a skin that allows for bending, produces high lateral friction upon interaction with a surface, and maintains

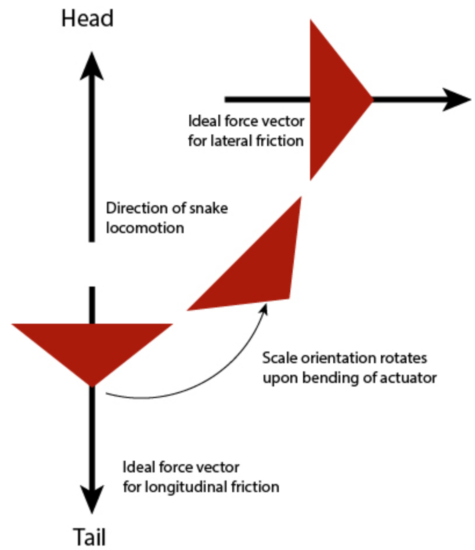

Figure 5.11: Showing how scales rotate upon bending with respect to ideal force vectors.

a lattice definition that can be generalized for all kirigami structures.

The primary purpose of this second skin design is to approach an ideal interaction between the scale and a surface asperity to maximize lateral pushing of the bends of the snake's body. We introduce here a novel set of kirigami lattices, that, rather than following a rectilinear pattern, use a radial pattern specifically meant for bending actuators. As observed with the previous skin design, the scales have an in-plane rotation w.r.t the surface asperities as the body of the actuator bends. Fig. 5.11 shows how the scales rotate during bending. An uninflated actuator has scales oriented along the longitudinal axis (along the backbone of the robot). As the actuator bends, the scales rotate away from their original vertical orientation towards a more horizontal orientation (along the lateral axis). We can utilize this phenomenon to increase lateral friction. However, as the scales rotate more horizontally, the longitudinal anisotropy of the system will decrease as few scales are oriented ideally with the asperity to provide an axial reaction force. Because the goal of this second prototype is to continue to maximize the lateral friction, due to the initial increase seen when implementing microornamentation, the more horizontal the scales can rotate, the more ideal the interaction with the asperity for producing a high tangential reaction force becomes.

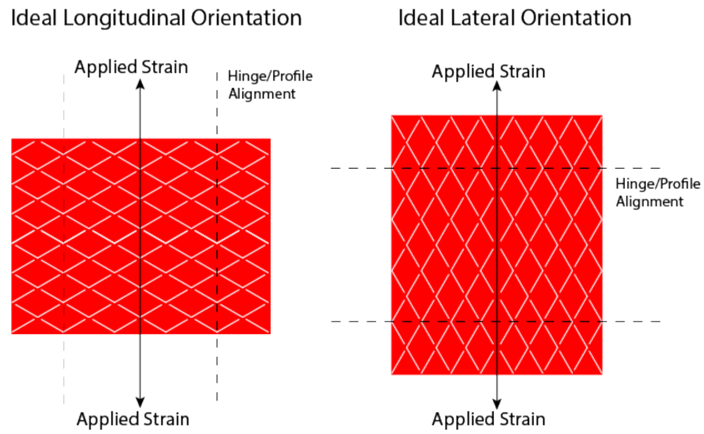

Figure 5.12: Orientation of scales on lattice for different force vectors. The lateral ideal is not possible as the hinges are too far off alignment with the applied strain.

The obvious solution would be to rotate the initial orientation of the scales on the original lattice by 90° as shown in Fig. 5.12. However, out-of-plane buckling can only occur if the hinges are mostly aligned with the direction of applied strain. If the scales are rotated by 90°, then they are too misaligned with the direction of applied strain to present any buckling. Therefore, a solution in between the fully parallel alignment and the fully perpendicular alignment can be found by redefining the kirigami lattice.

By using a radius to define the scale patterning, the scale tips fan out along the radius moving more towards the horizontal position than the vertical. Therefore, the radial lattice, in its neutral state will have scales not all aligned along the vertical axis as is inherent with a rectilinear lattice. Upon bending, these off-vertical scales will rotate even more towards the horizontal, approaching the ideal force vector for lateral pushing. The alignment of hinges will also be close to parallel to the direction of applied strain, which will still allow for out-of-plane buckling. The combination of positioning the scales along a radius, and the already apparent scale rotation during bending allows for increased lateral friction built into the design of the lattice.

5.3.1 Design of New Kirigami Lattices

Three lattices were designed and tested to determine their effects on lateral friction and the overall locomotion capabilities of the robot. The definitions of these lattices are shown in

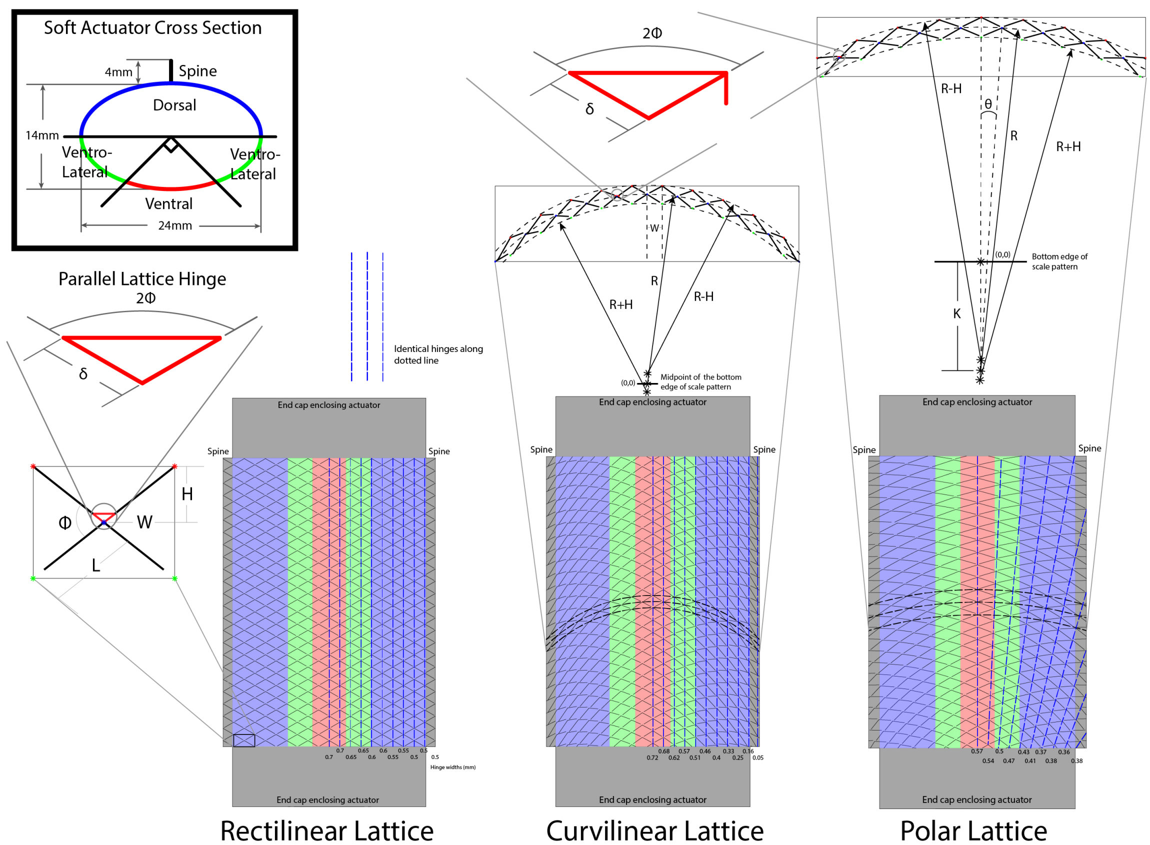

Figure 5.13: Summary of lattice definitions.

Fig. 5.13. Algorithms used to generate the lattice patterns can be found in the appendix. The rectilinear lattice refers to the typical kirigami lattice structure of a parallel grid aligning the hinges and profiles with the direction of the applied axial strain. This lattice is defined by a lattice length, L, lattice angle, ϕ, and a hinge width, δ. The geometric relationship between these parameters result in a uniform column width, $W = l\cos(\phi/2)$ and a row height of scales $H = l\sin(\phi/2)$. The hinge locations can be identified by (x, y) coordinates based on the values of the described parameters. As this is the standard kirigami pattern, there is no strategy for increasing lateral friction other than the rotation of the scales with respect to surface asperities inherent upon the bending of the actuator. Since we are comparing this standard kirigami lattice to our newly created lattices, maintaining consistent parameter values is key. The following lattices are built based on these described parameter values.

The polar lattice is defined by polar coordinates rather than rectilinear coordinates. A radius R defines the shape of the rows which are offset by the same row height H defined by the rectilinear lattice. An angle, θ defines the orientation and spacing of the columns. The hinge locations are defined by the (R, θ) coordinates. An additional parameter, K, defines a negative y-displacement from the origin of the polar lattice in which to define the center point of the radius. This is necessary because as you move axially along the lattice, the columns get closer together. This parameter K controls the smallest and largest scale size along the length of your lattice. It cannot be zero because if K is too small, then the bottom rows of scales will intersect one another, and the lattice structure would breakdown.

The curvilinear lattice is a combination of the rectilinear and polar lattices. In kirigami, the shape, size, and placement of the hinges is extremely important. To keep with typical kirigami standards of aligning hinges with the axis of applied strain (which the polar lattice does not adhere to), the parallel columns from the rectilinear lattice were maintained while radial rows were implemented. The rows of scales are defined by a radius, R and the columns are defined by the same column width W from the rectilinear lattice. Hinge locations are defined by the intersection of the radius, with the parallel columns. This lattice also maintains scale size and shape axially as the rectilinear lattice does, whereas the polar lattice varies scale size and shape along the longitudinal axis. This complicates our implementation of a soft snake robot as this creates a gradient of stiffness along the longitudinal axis which results in non-constant curvature. More importantly, the larger the scale, the less stiff it is, so interactions with an asperity on a surface will be relatively weak

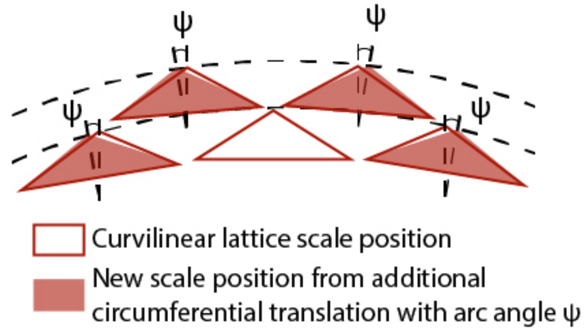

Figure 5.14: Additional circumferential translation of scale tip with an arc angle, ψ along the circumference on the curvilinear lattice.

as the scale size increases.

As the goal is to maximize lateral friction by orienting the scales as close to horizontal as possible, an additional circumferential translation of the scales is possible with the curvilinear lattice. Therefore, a fourth skin with a curvilinear lattice and an addition circumferential translation defined by arc angle $\psi = 5°$ of the scale tip is implemented as well. As the ventral and part of the ventro-lateral portions of the skin are the only parts in contact with surface asperities, that was the only area of the curvilinear lattice where additional scale tip circumferential translations were implemented. Performing a circumferential translation of the scales caused a decrease in hinge width, that would lead to the intersection of cuts if propagated across the entire width of the skin. By keeping the additional circumferential translation of the scales to high interaction locations, the integrity of the skin is maintained.

5.3.2 Design and Characterization of Bending Capabilities

In addition to redefining kirigami lattices to allow for ideal scale orientation, we also needed to ensure the new skins allow for bending of the actuators upon inflation. As described for the first skin prototype, a basic rectilinear lattice with a triangular scale profile does not allow for curvature greater than 35° unless a strategy for decreasing longitudinal stiffness is employed. In kirigami, the hinge width (smallest distance between cut profiles) and the size of the cut profile drive the longitudinal stiffness of the lattice [87]. Ideally, making the hinge width as small as possible, and the cut profile large, would make the longitudinal stiffness of

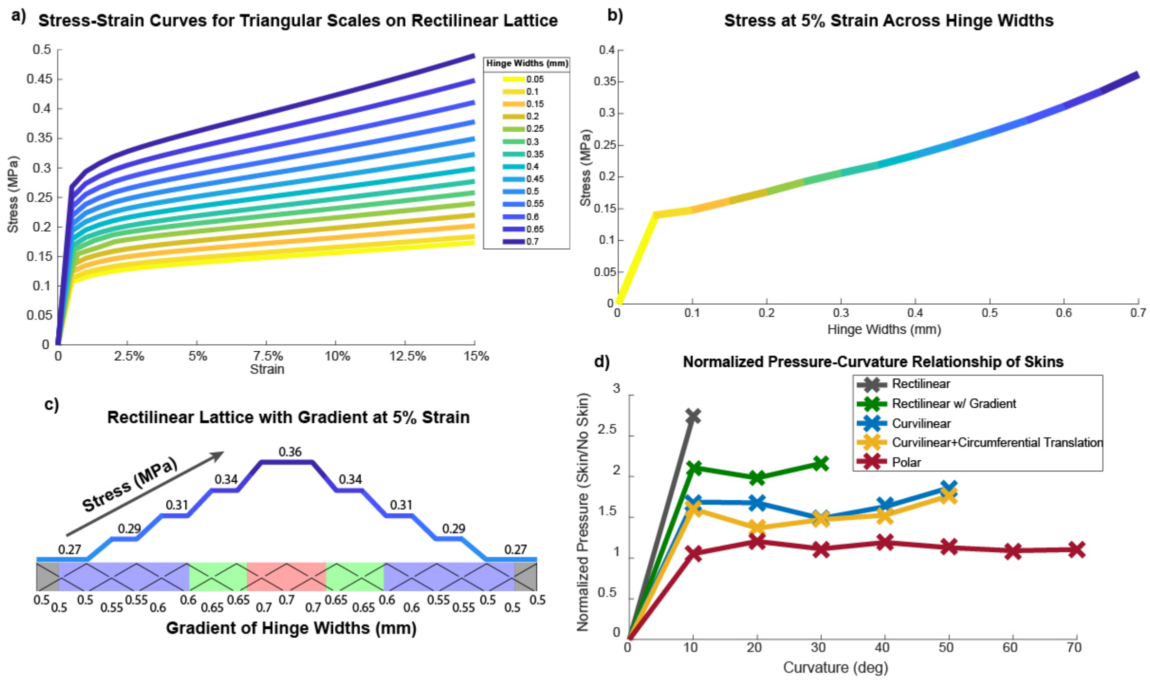

Figure 5.15: Bending capabilities of actuators with different skins. Gradient of hinge widths allow for larger actuator curvatures. Normalized pressure-curvature relationship based on pressure required to bend the same actuator with and without skin to the same curvature.

the skin fairly low, allowing for bending. However, if the hinge width is too small, the lattice will easily rip. Also, since the skin is implemented on a robot for interactional purposes, the scales (cut profile) need to have a relatively high geometric stiffness when engaged with a surface asperity to provide adequate reaction forces to push off against. The geometric stiffness of the scales is also dependent on the hinge width so will decrease with hinge size.

If a typical, rectilinear lattice is used, and the hinge sizes are small enough to allow for bending, then the scales will not be stiff enough to provide frictional force, and would likely rip immediately upon interacting with a surface asperity. If the hinge size is large enough for the scales to interact suitably with asperities, the bending capabilities of the actuator would be minimal. If a gradient of hinge widths is implemented the scales along the bottom of the actuator will be geometrically stiff enough to engage with asperities while the overall bending stiffness of the skin is reduced. This gradient of hinge sizes can be implemented on a typical, rectilinear lattice to allow for bending while maintaining the integrity of the lattice. The gradient is defined by decreasing the hinge width in ventro-lateral and dorsal sections of the skin. The radial lattices have an inherent gradient of hinges sizes as well as changes in scale size and shape ensuring bending capabilities without any additional design modifications.

The stress-strain characterization, determined using finite element analyses, of a recti-linear lattice with triangular scale profiles at different hinge widths is shown in Fig. 5.15a. Fig. 5.15b shows the stress across hinge widths when strained at 5% which is about half the maximum strain achieved on the skins. The gradient of hinge widths and the stress distribution along the width of the rectilinear skin at 5% strain is shown in Fig. 5.15c. The largest hinge widths are in the ventral and ventro-lateral portions of the skin as those areas interact with surface asperities whereas the dorsal section of the skin does not. Finally, Fig. 5.15d shows the normalized pressure-curvature relationship of the four skins designed. Despite the gradient of hinge widths allowing for curvature, the radial lattices, which have a more dramatic gradient of hinge widths and varying scale shape and size, still allowed for more curvature. The maximum curvature achieved by the rectilinear lattice was 30°. The curvilinear lattice with and without the additional circumferential translation had a maximum curvature of 50°, while the polar lattice had a maximum curvature of 70°. The polar lattice had the most curvature due to the large scale size, as well as an axial stiffness gradient caused by increasing the scale size for each additional row of scales.

We have designed radial lattices to ensure the orientation of scales approach the ideal configuration for maximizing lateral pushing. Fig. 5.16 shows the difference in angles of the horizontal (ideal) vector for each skin type on a scale located in the ventro-lateral section of the skin. The smaller the angle shown, the more ideal the interaction with the asperity should be for lateral pushing. The curvilinear lattice has the smallest angle, which means it should produce the highest lateral friction. The additional circumferential translation of the scales on the curvilinear lattice resulted in a 2° reduction in the angle of scale rotation. This is likely not enough to show significant differences in friction with the experiments performed, but shows that addition circumferential translation can be used to vary skin parameters.

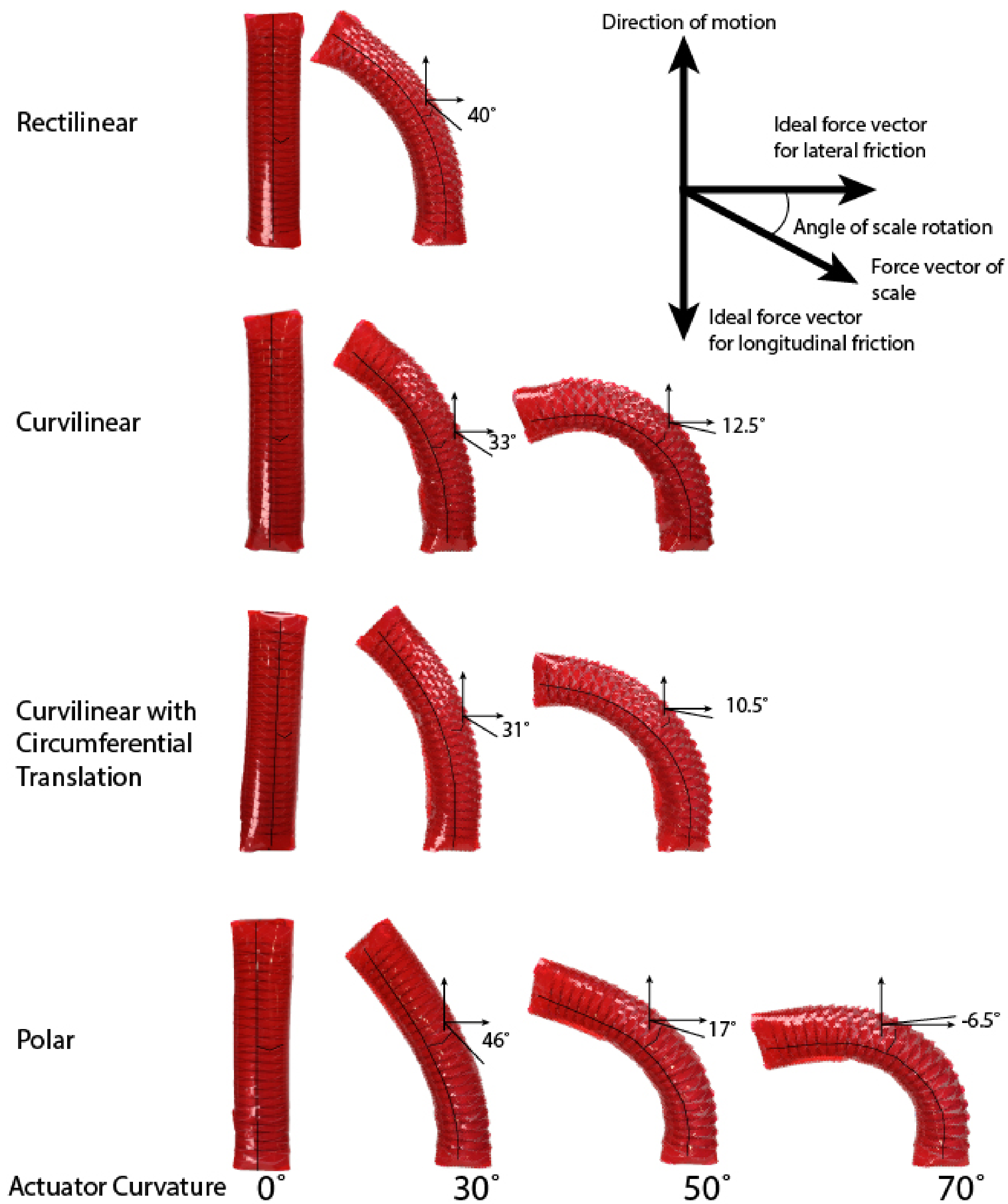

Figure 5.16: Angle between ideal lateral force vector and actual force vector of rotated scales upon bending for each lattice type. The smaller the angle, the closer it is to the ideal force vector for the production of lateral resistance.

5.3.3 Experimental Design

Similar directional friction tests were performed on the new skin designs as described for the first skin prototype earlier in this chapter. A dragging apparatus was attached to a 10N load cell on the Mark10 and dragged the actuators with skin across a textured surface, measuring the tension in the line pulling the actuators. The dragging apparatus was modified to account for the non-constant curvature of the polar lattice caused by the longitudinal stiffness gradient caused by the change in scale size. The new dragging apparatus is shown in Fig. 5.17. It could be adjusted in both the x and y axes to the right size for each curvature. Fishing line was used this time in an attempt to reduce the push back on the sensor. As the skin transfers from stick to slip as it is dragged across the surface, the line dragging the apparatus would kick back causing some positive readings (compression) rather than negative force readings (tension). 3mm of slack were introduced to the line at the start of each trial to improve the consistency of the initial stick-slip interaction.

Planar friction tests, as performed on the first skin prototype were not repeated for this new skin design. The new skin lattices were designed specifically for bending actuators, where the change in scale orientation w.r.t surface asperities was intentional and desired. Planar friction tests were originally performed to determine how scale orientation affected longitudinal friction forces. Since we have designed a skin to utilize the change in scale orientation as the actuator bends, there was no need to decouple the effect using a planar test as a control.

All friction tests were performed on three surfaces varying in surface roughness. The surfaces are a 3D printed (PLA, MeltInk, printed on a LulzBot Taz 6) grid with spacing defined by the scale length (4.15mm) of the scales which are equal across lattices as determined by the row height (H). The three surfaces are 0.5x (2.075mm), 1x (4.15mm), and 2x (8.3mm) scale length. Grid structures were used to test surface interactions because the parameters could be systematically varied and asperity size, shape, and orientation would be known for each interaction. This method is used when randomly rough surfaces, or natural substrates are too complex to determine exactly the dynamics of the interaction of interest [94]. Each skin was wrapped around an actuator, inflated to a specific curvature, and dragged across each surface, in each direction (forwards, backwards,and sideways) five times. These five trials were then averaged to calculate the friction ratios. As not all skins could enact the same curvature, each skin was tested in increments of 10° to its maximum

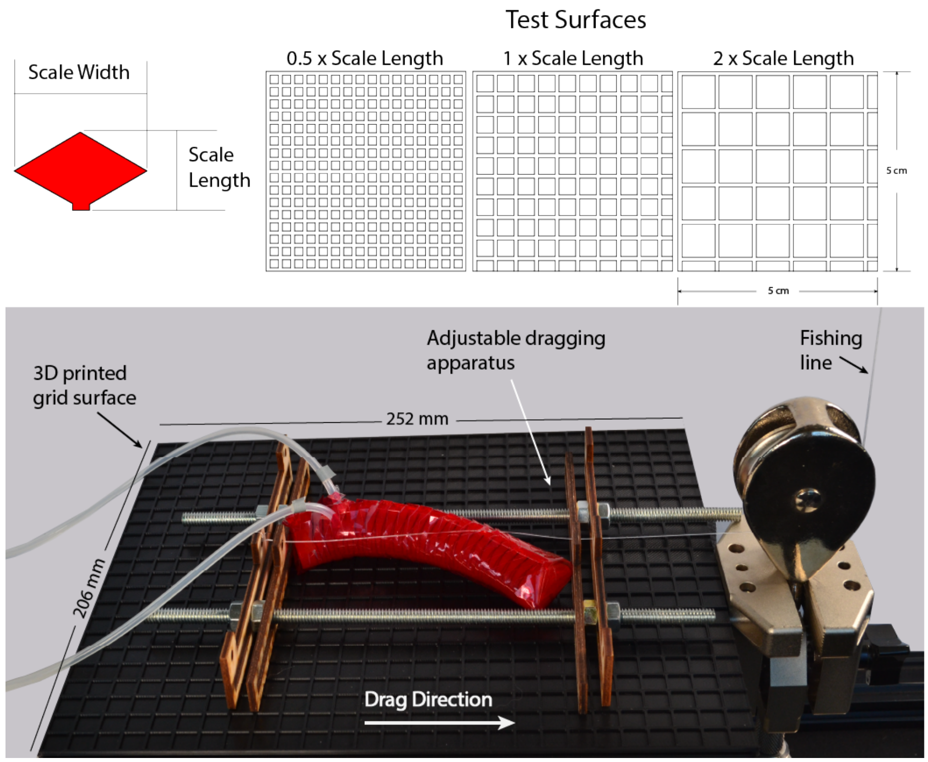

Figure 5.17: Updated dragging apparatus to account for non-constant curvature and reduce compression readings on the load cell. Actuator with polar lattice skin on 2x scale length surface.

curvature: 30° for rectilinear, 50° for curvilinear and curvilinear with the additional circumferential translation, and 70° for polar. This was done to compare the skins against one another, as well as to see how scale rotation affected lateral friction.

5.3.4 Friction

The results of the friction experiments described above are shown in Fig. 5.18. The lateral-longitudinal friction ratio was targeted this time as compared to the first skin prototype where the longitudinal friction ratio was of more interest. Originally, the longitudinal friction ratio was of more interest because that is the axis of frictional anisotropy most commonly investigated for both robotics and snake biology papers. The initial lateral friction augmentation using microornamentation was also simply proof-of-concept, acting as a binary state. The friction ratios are reported in terms of frictional force rather than COF because the new apparatus was used for all tests meaning all weights were equal across tests. The first skin prototype required two separate appartuses for the longitudinal and lateral dragging directions, meaning the frictional forces could not be directly compared because the normal forces were not equivalent. With the new apparatus, the, frictional forces in all direction could be compared directly because the normal force was the same across all tests. As seen in the plots, both curvilinear skins (with and without additional circumferential translation) produced the highest lateral-longitudinal friction ratios across all surfaces. The additional $2°$ of scale rotation achieved by the curvilinear lattice with additional circumferential translation did show improvements over the plain curvilinear lattice, especially on the larger asperities.

The polar skin, although having scale rotation approaching the ideal vector for lateral pushing did not perform well on the small grid-spacing (smaller asperity) surfaces. Despite the scales having the same length, the width of the scale mattered in how many scale could interact with asperities. The large scales on the polar lattice meant that only one or two columns of scales could engage with asperities, and only with the largest asperities. As a consideration for future work, it would be interesting to add microornamentation to the polar lattice. The polar lattice scales are large, so many ridges could be embedded on the scale, and a larger surface area of ridges could interact with asperities in the surface.

The curvilinear lattices produced a much higher lateral-longitudinal friction ratio compared to the rectilinear lattice that had no explicit design intent for increasing lateral resistance. The polar lattice, when on the 2x surface with asperities large enough to engage with, also produced high lateral-longitudinal ratios at high curvatures. Therefore, the radial designs, causing the scale tips to oriented closer to the ideal vector for lateral pushing, were successful in increasing the skins ability to create a lateral resistance.

As expected, the rectilinear skin had the highest longitudinal friction ratio as there were more scales pointed axially w.r.t the surface asperities. The radial designs make a trade off to increase lateral friction by decreasing longitudinal anisotropy. Despite decreasing the number of scales oriented axially for longitudinal pushing, the radial lattices did fairly well in producing a greater than 1 ratio for longitudinal anisotropy.

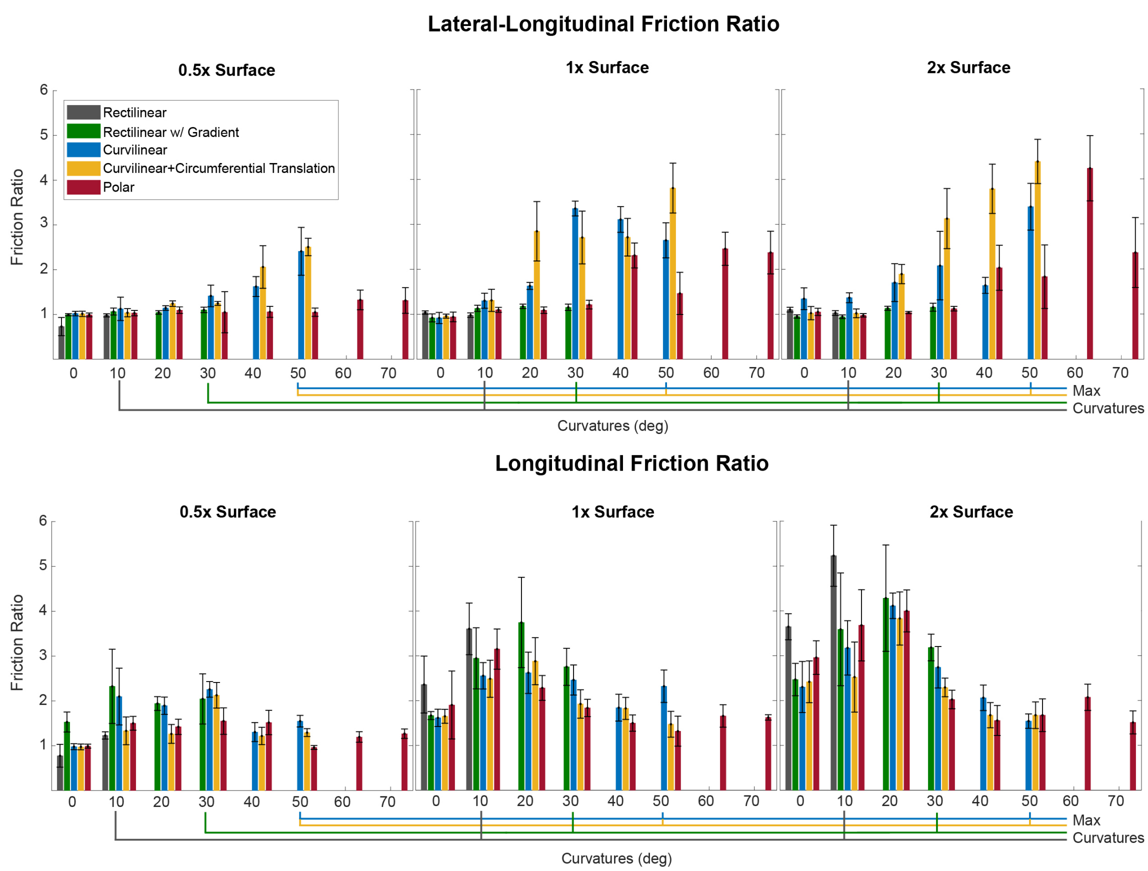

Figure 5.18: Average frictional ratios of skins on varying surfaces. Error bars show one standard deviation.

5.3.5 Locomotion

Locomotion experiments were performed similarly to the first skin prototype. All skins were put on the soft snake robot and tested at different curvatures. Motion capture data was collect by the OptiTrack Prime system and used to calculate the velocity of the robot. All skins and a robot with no skin were tested at 30° to compare skin performance. The curvilinear and polar lattices were also tested at their max curvatures and compared to a robot with no skin. All skins were tested on all three surfaces at each curvature.

Our hypothesis that lateral-longitudinal anisotropy is not only necessary, but just as important as longitudinal anisotropy holds up based on the locomotion results. The curvilinear lattices, which had good rotation of scales and good geometric stiffness of scales performed best. As the polar lattice was not effective on the surfaces with small asperities, it performed best on the 2x surface. At higher curvatures, as has been noted throughout the dissertation, the robot does best. Therefore, future iterations of the skin should continue to reduce axial stiffness to promote further bending. Despite only reaching 50° curvature, the curvilinear skin increased the velocity of a robot with no skin by 530% at it's maximum velocity which occurred on the 1x surface. Comparing to the rectilinear skin at 30°, both the rectilinear and curvilinear skins did best on the 2x surface with a 25% increase in velocity of the curvilinear skin over the rectilinear skin. When comparing the curvilinear lattice skin, to the first skin prototype with microornamentation, the curvilinear lattice skin improved velocity by 75% at 50° on the 1x surface.

5.4 Summary

In the literature regarding both snake biology and snake robots, it has been noted that lateral friction is likely important in the successful production of lateral undulation. However, other than using wheels on snake robots to provide some lateral resistance, no further exploration of the topic has been performed. Since we are using a soft robot, the interactions between the body of the robot and its environment have a significant impact on the behavior of the robot. If those interactions are not specifically designed to produce positive behaviors, there is a chance that, despite producing a desired body action, the overall locomotive progress of the robot is impeded by poor environmental interactions.

The most important interaction with snakes in producing lateral undulation is the ability

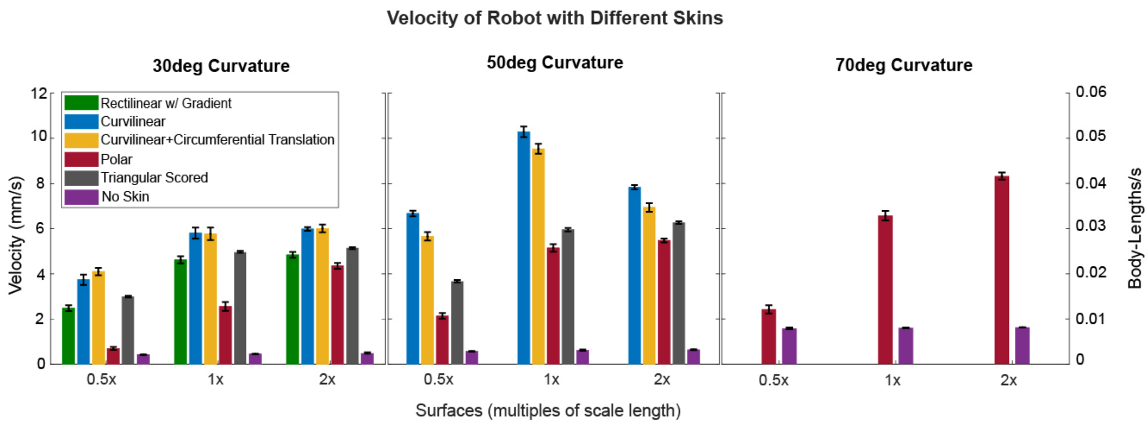

Figure 5.19: Average velocities of skins on varying surfaces. New lattices are compared to the highest performing, first prototype of skin. Error bars show one standard deviation.

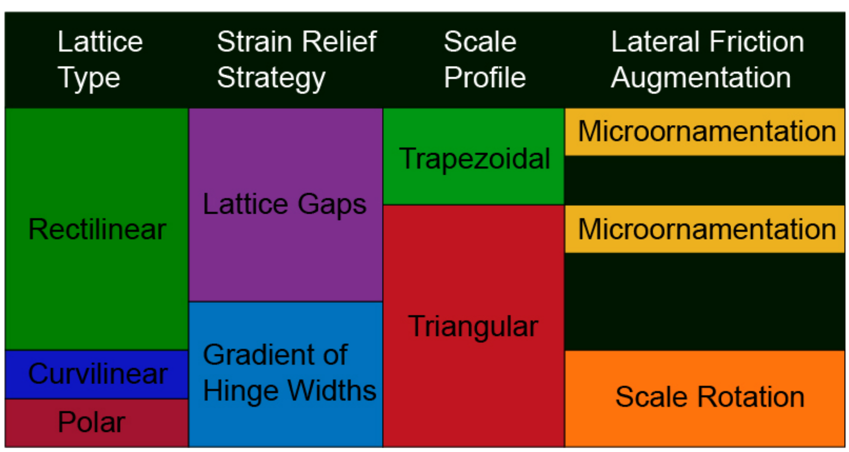

Figure 5.20: Features matrix of all skins tested on robot.

to push off the bends of their body as they undulate. This pushing can be accomplished by bracing against obstacles, or in many cases, through the frictional properties between the snake's skin and environmental surfaces. Both skin prototypes were designed in an attempt to increase lateral friction. Fig. 5.20 shows all skins, and the combination of different characteristics, tested in this chapter. The first skin prototype used the typical, rectilinear lattice and varied scale shape. Strain relief gaps in the lattice were introduced to achieve bending, and microornamentation, a heavily bioinspired strategy for augmenting the production of lateral friction. The microornamentation created a binary state for the skin to determine if velocity could be increased by employing a strategy was implemented for increasing lateral friction. Microornamentation increased lateral resistance (from about 20-80% across curvatures), and certainly improved the overall velocity of the robot (55% improvement), but there were too many coupled parameters, and the micro-mechanics of the textured skin were outside the scope of this work.

In an attempt to further increase lateral resistance, simplify the mechanics of the interaction, and decouple some parameters, a second skin prototype was developed by introducing a completely new set of kirigami lattices. These new radial lattices took advantage of the bending actuator to further orient scales along the ideal vector for lateral pushing. By fanning out the scale tips, and relying on shift in orientation w.r.t surface asperities, lateral friction was significantly increased. These new lattices were compared to the typical rectilinear lattice, and only one scale shape, triangular, was implemented. The 530% increase in velocity over a robot with skin, and a 25% increase in velocity over a skin with no increased lateral friction, shows that lateral friction is indeed an important parameter that must be considered when designing robots meant to enact lateral undulation.

Chapter 6: Conclusion

6.1 Retrospective

The goal of this dissertation was to illustrate how improvements to a bioinspired soft robot's locomotion could be achieved by targeting a specific environmental interaction. There are three main areas of design in bioinspired robotics that can be tuned to make improvements; morphology of the robot's body, the gait design, and the design of any external mechanisms that interact with the environment. Most improvements to robots are performed on an individual basis. One area of design is selected in which to make improvements with little consideration given in how those changes propagate to the other areas of design. By taking a holistic approach, in which all three areas of design are considered in tandem, it is possible to develop a robot that performs targeted behaviors at a high level, while also remaining adaptable to unknown disturbances it might encounter when deployed.

The work presented in this dissertation is centered around increasing the velocity of the first, fully-soft, snake-inspired robot's locomotion through a variety of environments. Each chapter reviewed one area of design focused on how the interaction between the robot and its selected environment can produce both positive and negative behaviors. Each design iteration of the robot looked to increase positive behaviors and decrease negative behaviors by considering the effects of changing one area of design on the other areas.

The first design area, morphology, required understanding the kinematic requirements of the desired gait, lateral undulation. At its core, lateral undulation requires a specific shape space the robot must enact to successfully locomote. Additionally, lateral undulation requires a specific environmental interaction to produce the necessary reaction forces to propel the robot through its environment. In the two environments tested throughout this work — granular media and solid, textured, surfaces — a significant lateral resistance is necessary for the bends of the robots body formed during lateral undulation to push against. In granular media, a directional drag ratio (lateral:longitudinal) is necessary, and for a hard, textured surface, it is a directional friction ratio.

6.1.1 Chapter 3 Review

Chapter 3 focused on the initial design of the soft, snake-inspired robot meant, first to prove that a fully soft snake robot was possible, and second, to determine if a geometric mechanic strategy for designing gaits could be employed on soft robots. The gait was developed based on a kinematic representation of a snake's backbone and its production of lateral undulation in a low Reynolds number environment (viscous fluid). The design of the robot was driven by the shape space necessary to produce lateral undulation, as well as environmental considerations such as increasing the drag ratio necessary for granular media, and preventing rolling of the robot when deployed.

Another major consideration that had a significant impact on the first prototype was the manufacturing process of soft robots. Building soft robots is its own open research problem as the nonlinearities of the material, and the sensitivity of soft materials responding to disturbances in the environment can make reproducible robots and behaviors difficult. Therefore, for the first prototype, a strain-limiting layer, used for bending actuators, was not embedded in the actuators. The complexity of embedding the strain-limiting layer resulted in an increase in actuator failure. The actuators could still bend without a strain-limiting material as the strain differential between the inflated and uninflated chambers was large enough. Therefore, a compromise was made to ease manufacturing. However, without a strain-limiting layer, the actuators could also extend upon inflation, which was not kinematically represented in the model of the circular gait used to represent lateral undulation.

A fully soft snake robot with a mode of extension was developed and the circular gait was used to test its locomotion capabilities. The locomotion results showed that the developed robot displaced further per gait cycle than the model used to develop the gait predicted. As the only major kinematic difference between the robot and the model was the extensibility of the robot, is was determined necessary to develop a robot that did not extend upon inflation. This required redesigning the manufacturing method to allow for the insertion of a strain-limiting material, while maintaining the efficacy of the actuators.

The second prototype of the robot was inextensible, and therefore a better kinematic representation of the model used to develop the circular gait. When the new prototype was tested using the same gait in the same environment as the first, it proved to perform even better than the original robot. The initial consideration that the extensibility of the robot was the reason it was producing a displacement/cycle greater than the model predictions proved false. Even though the second prototype of the robot was closer to the kinematics used in the geometric mechanics model, it only increased the disparity between the experimental results and the model predictions. This is likely caused by assumptions made in the model that could not be maintained on a physical robot. There are likely environmental interactions between the soft body of the robot and the granular media that are not captured by the model. Specifically, the deformability of the robot meant that although the robot could act on its environment (pushing the granular media around), the environment could also impact the behavior of the robot (altering the shapes enacted by the robot). Future gaits and control strategies for soft robots need to consider how the environment can act on the robot. A rigid snake robot is less likely to be impacted by the environment as the rigid materials are less sensitive to reaction forces from contact. Although the model driving the design of the gait and the design of the robot did not fully capture the "softness" of the robot or its interaction with the environment, the gait itself is still an excellent representation of lateral undulation, and can continue to be used to drive the robot.

6.1.2 Chapter 4 Review

Chapter 4 focused on the gait design of our bioinspired framework. Knowing the requirements to produce lateral undulation, and knowing that we would be targeting a granular media as our environment, adjustments to the gait could be made to further increase the robot's velocity. During initial testing of the inextensible robot we observed that the robot slid backwards for part of every forward cycle. On top of normal slip during each gait cycle, piles of millet formed by the robot during shape change would become large, and more dense than the robot, producing too large of a reaction force in the wrong direction. As we cannot control the granular media, nor did we have a closed feedback loop to detect unwanted directional changes or prevent slip, the backwards motion of the robot could be reduced by modifying the gait directly.

Lateral undulation, as represented by the circular gait, is produced by two sine waves separated by a phase offset, driving the two actuators that make up the robot. The amplitude of the sine wave represents the amount of curvature enacted by the robot, and the phase offset controls when the two actuators curve relative to one another. These two parameters could be adjusted, as is seen with biological snakes in different media, to decrease the negative interactions with the environment.

The main contribution presented in Chapter 4 is the custom gait referred to as the "half-activation" gait. "Half-activation' refers to both the curvature and length of activation of the back actuator in comparison to the front. This produces an asymmetric gait, which is contrary to most gaits seen in nature. Most gaits are symmetric and rely on contact forces to break symmetry and produce positive behaviors. As was observed with the inextensible robot, the breaking of symmetry through the interactions with ridges of granular media did not always result in positive behaviors. Therefore, if symmetry is broken at the gait level, we can force more positive interactions with the environment.

By inflating the back actuator half as much as the front, the production of ridges in the granular media large enough to push the actuator backwards upon contact were reduced. By activating the back actuator half as often as the front meant that the actuator was in its uninflated state more often. The actuator's drag ratio is maximized in its uninflated state. Therefore, the back actuator was able to provide a larger push-off force, preventing further backward sliding. Chapter 4 also showed demonstrations of the inextensible robot, enacting the new gait, in a variety of environments representing a range of granular media as well as a flat, hard surface for comparison.

The design of the robot, and the design of the gait were targeting locomotion in a granular media to negate the need for directional friction. However, testing the inextensible robot with the half-activation gait on a solid surface resulted in the highest velocity of the robot achieved across all tested terrains. The success of the robot on a solid surface, without directional friction employed in the design, was surprising. Based on empirical evidence, it was determined that the adhesion between the elastomeric surface of the robot's body and the relatively smooth surface of the terrain provided some anchoring for the robot to push against. It was also observed that the robot was much more dynamic on packed and solid surfaces in comparison to more fluidic surfaces. The looser granular media tested seemed to damp out some of the push-off forces that were evident on more packed surfaces.

6.1.3 Chapter 5 Review

Chapter 5 introduces a kirigami skin that provides directional friction, further improving the robot's capabilities on solid, textured surfaces. Where previously a drag ratio was necessary to successfully engage with the environment, a friction ratio was now necessary. However, snake skin has two axes of frictional anisotropy that are important to consider when using lateral undulation. The longitudinal axis (along the snake's body) has been the primary axis in which frictional strategies have been employed in the literature. Both for robotics, as well as for biological snake studies. However, many of these studies cite the importance of a second axis, lateral (across the snake's body), that although not investigated, likely has significant contributions to the snake's ability to generate proper reaction forces. Therefore, the two skin prototypes presented in Chapter 5 included mechanisms for producing a high lateral-longitudinal friction ratio.

Both skin prototypes use kirigami, a Japanese art form of patterning cuts, to create a lattice structure that would produce out-of-plane buckling upon uniaxial tension. The specific pattern used for the first skin prototype is a rectilinear pattern of cuts that when axially strained, produced out-of-plane buckling of the cut profiles. This lattice pattern was used previously for soft robots using crawling gaits that deformed only in one axis [57]. The first skin prototype extended this idea into biaxial deformation present upon bending. Strain-relief areas were patterned into the lattice to allow for biaxial deformation. The removal of parts of the lattice meant that upon uniaxial strain, not all scales buckled. However, because the body of the robot is soft, and deformation is continuous along its length, enough local uniaxial strain was provided at each hinge to ensure buckling of all scales.

With the skin altered to ensure bending was still achievable, and therefore lateral undulation could be enacted properly, a strategy for lateral resistance that did not interfere further with the lattice or deformation of the robot was necessary. As has been observed in the biological study of snake skin, scales have texturing, or microornamentation, on their surface. Texturing the polyester plastic material used to make the skin would not interfere with the pop-out of the scales, or impede the deformation of the actuators. Ridges were scored into the polyester plastic material along the longitudinal axis of the skin. Upon inflation, the actuator would bend, and theoretically the ridges would provide lateral resistance, increasing the lateral-longitudinal friction ratio.

Skins with and without microornamentation were tested to determine if lateral friction increased, and whether the subsequent increase in the lateral-longitudinal friction ratio improved the velocity of the robot across a hard, textured surface. It became apparent that the kirigami lattice, with its coupled parameters, on top of the coupling of the interaction between the soft body and the skin, and the skin and the surface were extremely complex. However, it was shown that lateral friction did increase and the velocity of the robot when using the original lateral undulation gait increase when using the skin with microornamentation.

Although the skin with microornamentation was successful, and provided preliminary evidence that this lateral-longitudinal friction ratio is important in maximizing the effect of lateral undulation, the interplay between parameters were too convoluted to point to any single contributor. To reduce the amount of coupled parameters, and to continue to explore how increasing lateral friction could result in a high velocity, a new strategy for producing a high lateral-longitudinal friction ratio was necessary.

The second prototype of skin described in Chapter 5 uses the properties of the kirigami lattice, as well as the bending of the actuator to increase lateral friction. The scales remain in a fixed orientation w.r.t the body of the robot, but shift orientation w.r.t the surface asperities in which the scales interact. As the actuator bends, the scales rotate (w.r.t surface asperities) away from the axial orientation. For maximizing the longitudinal friction ratio, it would be ideal to have a strictly axial orientation of the scales. However, for maximizing lateral friction, it would be ideal to have a scale-asperity orientation transverse to the longitudinal axis. This shift towards the transverse orientation is inherent in the coupling of the skin to the body. Therefore, by changing the parameters of the kirigami lattice, it is possible to further push the scale-asperity orientation more transverse to the longitudinal axis.

Altering the parameters of the original, rectilinear kirigami lattice to further increase the transverse scale-asperity orientation was not possible. The second prototype of skin required the creation of a completely new kirigami lattice. The new lattice required not only patterning the cut profiles in a way that permitted out-of-plane buckling, but could also rotate the tips of the scales laterally, so that upon bending, they would approach the ideal force vector for generating a large lateral reaction force. The major characteristic of this new kirigami lattice is that the cut profiles are patterned along a radius, rather than a straight line, forcing the tips to rotate a small amount across each column of profiles.

To compare the new radial lattices to the original rectilinear lattices meant that a bending strategy, that did not require removing parts of the lattice, was necessary. The axial stiffness of the skin was determined by the coupling of the hinge width and size of the cut profiles. If the skin had a low axial stiffness, it would increase the biaxial deformation capabilities of the actuator. However, decreasing axial stiffness, decreased the geometric stiffness of the scales. The scales had to be sufficiently stiff to have a useful interaction with surface asperities. Therefore, minimizing the axial stiffness was not an option. A gradient of axial stiffness around the perimeter of the elliptical cross section, achieved by reducing the hinge size in steps across the columns of cut profiles allowed for the high geometric stiffness along the ventral scales, while allowing for less axial stiffness along the dorsal scales. This gradient of hinge sizes allowed for bending without decreasing the interactional capabilities of the skin. The radial lattices had an inherent gradient of hinge sizes caused by patterning the cut profiles along a radius.

Three lattices were generated to compare the production of lateral friction. The original rectilinear lattice with the gradient of hinge sizes, a radial lattice defined by polar coordinates, and a hybrid between the two coordinate systems referred to as the curvilinear lattice. The polar lattice while having a gradient of stiffness in both the longitudinal and lateral axes. This meant that the stiffness at one end of the actuator was different than at the other, resulting in non-constant curvature. This curvilinear lattice maintained the radial spanning of scales, but carried over the parallel column structure of the rectilinear lattice. By defining hinge locations at the intersection of the radius and the parallel column, the scales would still have a lateral rotation while maintaining constant longitudinal stiffness (constant curvature). A fourth skin was included in the comparison to further push the scale-asperity orientation towards the ideal lateral force vector. Using the curvilinear lattice, a circumferential translation of the scale tip was added. These four skins were then tested to measure their production of lateral friction as well as their locomotion capabilities.

The skins using the curvilinear lattice produced the most lateral friction, increasing the subsequent lateral-longitudinal friction ratio. The polar lattice, due to the increase in scale size along the longitudinal axis of the skin, was only effective on surfaces with large asperities. There was not a large enough difference in the performance of the curvilinear lattice and curvilinear lattice with local scale rotation to determine if the small increase in rotation was helpful. Both radial lattices, when compared to the rectilinear lattice, produced much greater lateral-longitudinal ratios. However, there is a trade off in using the radial lattices. By rotating the scales transverse to the longitudinal axis, the scale-asperity orientation for longitudinal forces was reduced. Therefore, the rectilinear lattice, which had the most ideal scale-asperity orientation for longitudinal forces had the highest longitudinal friction ratio.

The second question, whether the production of a high lateral-longitudinal friction ratio was better for increasing velocity, was answered by the locomotion study. Most robots employing frictional anisotropy focus on the longitudinal axis. The first skin prototype showed that employing a strategy for lateral-longitudinal frictional anisotropy was helpful. However, it is unclear whether maximizing this lateral-longitudinal anisotropy is ideal, or whether maximizing the longitudinal anisotropy is enough. The results of the locomotion study for the second skin prototype showed that the lateral-longitudinal friction anisotropy is just as important that the longitudinal frictional anisotropy. The curvilinear lattice skins, which produced the highest lateral-longitudinal anisotropy, produced the highest velocities on each surface tested. We could not decouple the lateral-longitudinal frictional anisotropy from the longitudinal anisotropy so we cannot say if the lateral-longitudinal frictional anisotropy is more important in increasing velocity than the longitudinal anisotropy, but it should not be ignored when designing interactional mechanisms for snake robots.

6.2 Future Work

Although the best performing skin designed showed an improvement of velocity over a robot with no skin by 530%, there are many limitations to the design of robot, skin, and gait that can be addressed in future work. The control of the robot is open loop, as no sensors were used to adjust the gait in any way. Ideally, a sensor placed in the backbone of the robot to measure curvature and make necessary adjustments would have been the simplest method for providing feedback. This feedback would ensure that the shape space enacted by the robot approached the commanded shapes. Another immediate improvement to the system would be the pneumatic control board. The use of one-way valves meant there were no degassing capabilities, causing the robot to work against itself in enacting shape changes. If the phase of the sine wave driving the gait was small enough, the chambers in each actuator would inflate while the other side was deflating. This meant that the driven curvature was not always achieved because part of the inflation time to reach that curvature would be spent pushing air out the other half of the actuator.

One of the major limitations of the system is the tethering requirement. Most soft robots are tethered as they require pneumatic systems that are large and comprised of rigid parts that would be difficult to integrate physically into the body itself. However, the tubes attached to the actuators to deliver air from the microcompressor on the control board were the weakest point of the actuator and had to be managed to prevent them from affecting the locomotion of the robot. Untethering is an open problem in the field of soft robotics. Some efforts in untethering soft robots have been made by increasing the size of the robot so it is strong enough to carry the compressor and valves on them [20]. Others utilize microfluidics and maintain a completely soft robot that pushes fluids around during deformation [95]. The development of soft valves has recently begun [96], but the next major roadblock becomes reducing the stiffness, or at least the size of a compressor.

The polyester plastic material used to make the skin presented in this work needed to be thin and compliant enough to not impede the shape changing capabilities of the actuators. The geometric stiffness of the scales relative to the weight of the robot was high enough to provide large enough reaction forces to work effectively. However, if the system was any heavier, or the surface too rough, the skin would rip during locomotion. Ideally, a tougher material would be used, but again, it needs to be compliant enough to not interfere with the deformation of the actuators. The method of adhering the skin to wrap the actuator needs to also be improved. The spine, adhered out-of-plane to the perimeter of the actuator, was one of the weakest points of the system. Curvature of the actuators was limited by the skin and if the actuators were further pressurized, either the spine would pull apart, or the junction of the tubing on the actuator would pop. Increasing the robustness of the skin while maintaining high compliance will definitely require further effort.

There are many natural extensions to this work in all three areas of our bioinspired design framework. Further modifications to the robot's cross section and aspect ratio could be performed and tested in a variety of environments to gauge their usefulness in the production of positive behaviors. Gaits that utilize the softness of the robot's body could also be developed. Few gaits in the literature have been designed specifically for soft robots. They are standard crawling or legged gaits that have simply been employed using a soft body. Advances to gaits will of course require better modeling of soft-bodied actuators as well as the development of soft sensors that can be embedded to close the feedback loop. The addition of a head or tail to a soft snake robot would be useful in targeting other environments or interactions that are uniquely addressed by the presence of a head or tail of a biological snake (e.g. swimming or burrowing).

Further optimization of a skin designed to provide directional friction would continue to improve the locomotion the soft snake robot. Ideally, the skin would be able to maximize both axes of anisotropy depending on the curvature of the actuator and the orientation of the scale w.r.t surface asperities. Further investigation of the micro-mechanics of microornamentation as well as exploring other forms of microornamentation would be useful. An immediate experiment that could be tried with the current state of this work would be to place microornamentation on the radial lattices. The polar lattice produced larger scales, that if microornamentation were employed, would provide more surface area to produce interactions between the micro-ridges on the scales and the asperities on the surface. The curvilinear lattice would also benefit from microornamentation as the rotation of scale tips towards the ideal force vector for lateral pushing is limited by the width of the skin. A larger, flatter cross section of the actuator would also be helpful to maximize interactions with the surface.

6.3 Major Contributions and Broader Impact

The major contributions of this dissertation are:

- The development of the first fully-soft, snake-inspired robot
- A skin for lateral undulation that had both longitudinal and lateral-longitudinal frictional anisotropy
- A set of new kirigami lattices
- A framework in which to investigate bioinspired design of robots in three areas of design: morphology, gait, and interfacial mechanisms.

Soft robot technology has the potential to make robots in the real world more robust and adaptable to perform complex tasks in unstructured environments. The nonlinear materials used to build these robots make them difficult to model and control, but as advances in the field are made, we will further harness the inherent properties of these soft materials as is seen in nature. The softness of the materials also make the internal states of the robot extremely sensitive to external disturbances. Therefore, the successful development of useful soft robots will require understanding how the design of the robot, the actions it takes (gaits), and the way in which it interacts with its environment can all affect one another and the robot's overall behavior. By looking to nature, where most systems are a hybrid of soft and rigid structures, we can pull inspiration on what morphological characteristics are important in producing positive behavior, and how those can be refined by targeting a specific environmental interaction.

Using this bioinspired framework of tuning three separate knobs of design while investigating how they are coupled, we have developed a fully soft snake robot that can produce lateral undulation to navigate both granular media and solid, textured environments. The key interaction used to focus design efforts was the lateral reaction forces enacted on the bends of the robot as they propagate down the robot's backbone. In granular media, this lateral reaction force is controlled by the drag ratio and requires navigating an environment that is constantly shifting between ideal and non-ideal interaction states. By understanding that achieving the drag ratio was not enough to guarantee ideal interactions, we were able to make modifications to the gait to further emphasize the lateral forces.

Expanding the robot's capabilities into other environments required a shift in how potential lateral reaction forces could be produced. On solid surfaces, friction becomes the central interaction to optimize. Although the concept was the same, increase lateral resistance, the method in which it was employed had to change entirely. Due to the robot's softness, any method used to increase lateral friction needed to also be compliant enough to not impede the deformation of the actuators. To achieve these requirements, it was necessary to invent a new set of kirigami lattices that would allow for suitable deformation of the actuator while also utilizing this shape change to further promote lateral friction.

These improvements to the robot's design and performance were made possible by understanding how the robot and its environment are coupled in an action-reaction partnership. The robot not only affects its environment, but its environment affects the robot's performance as well. The environment in which the robot is employed is not something that can be ignored or generalized, but is something, that if utilized properly, can advance the progress of the robot's tasks. Snakes are an excellent model in which to explore the coupling between a system and its environment because all it's locomotion strategies are dependent on positive interactions with characteristics of the environment. The fact that snakes exist in almost all environments around the world, and have all evolved different morphological traits and behaviors to work with characteristics unique to those environments show how integral the partnership between organism and its habit is in nature.

The framework in which three areas of design, morphology, gait, and interfacial mechanisms are used to improve the performance of a system by targeting a specific environmental interaction can be extended to other areas of robotics and engineering. Any system that must complete a task in an unstructured environment would benefit from this holistic approach. As the exact conditions in which the system will operate cannot be predicted, it is possible to breakdown unstructured environments into likely environmental interactions.

For example, planetary rovers will navigate a wide range of unknown situations, but must adapt to them nevertheless. Therefore, by targeting a specific interaction like rolling wheels interacting with granular media, they can increase the robustness of the robot in a range of environments by simply targeting one interaction. Understanding the geometry and kinematics of the wheels, how they are expected to actuate, what strategies can be added to the wheels to directly interface with a granular medium, and how each area will affect the others, the functionality of the mechanism can be improved. Focusing on only one area of design improvements, without considering the others, can potentially lead to an overall decrease in functionality. Using the environment as a tool rather than treating it as an obstacle, and making design considerations through the lens of a specific interaction can increase the system's robustness and adaptability as a whole.

Chapter 7: Appendix

The algorithms shown below outline the method for generating the hinge locations for both the unit cell, and the full lattice, of each lattice type. The values of R and θ are used to determine which lattice is being used. If $R \to \infty$ that implies that the rows are horizontal lines rather than radii, and therefore reference the typical rectilinear lattice. Any other value of R can be used to generate one of the radial lattices. θ is then used to determine whether the desired lattice is curvilinear or polar. If $\theta = 0$ then tat means the columns are vertical as they are in the rectilinear lattice, which then determines that the desired lattice is curvilinear. Any other value of θ can be used to generate the polar lattice.

Algorithm 1: Hinge Locations for all Lattices

Input: $l, \phi, R, \theta, M, N, K$

Output: (X,Y) Coordinates for the hinge locations for selected lattice

Parameters

l = lattice spacing ϕ = lattice angle

R = radius θ = angle between columns

M = skin width N = skin length

K = negative y-displacement from origin for center of radii

$X_{off} = 2l\cos(\phi/2)$: distance between columns

$Y_{off} = l\sin(\phi/2)$: distance between rows

(X,Y) Output Arrays

Top_Hinges [ ] : array of hinge locations for middle row

Middle_Hinges [ ] : array of hinge locations for middle row

Bottom_Hinges [ ] : array of hinge locations for middle row

if $\theta = 0$ *&&* $R \to \infty$ **then**

| rectilinear_lattice(X_{off}, Y_{off}, M, N)

end

if $\theta = 0$ **then**

| curvilinear_lattice($R, X_{off}, Y_{off}, M, N$)

end

else

| polar_lattice($R, \theta, Y_{off}, M, N, K$)

end

Algorithm 2: rectilinear_lattice (X_{off}, Y_{off}, M, N)

Result: (X,Y) Coordinates for the hinge locations on the rectilinear lattice

Unit Cell Definition

Middle Hinge [1] = (0 , 0)

Top_Hinges [1] = ($X_{off}/2, Y_{off}$);
Top_Hinges [2] = ($-1 * X_{off}/2, Y_{off}$);
Bottom_Hinges [1] = ($X_{off}/2, -1 * Y_{off}$);
Bottom_Hinges [2] = ($-1 * X_{off}/2, -1 * Y_{off}$);

Pattern unit cells along width and length of skin

for *m = 1:M (rounded to nearest integer)* **do**
  for *n = 1:N (rounded to nearest integer* **do**
    (Middle_Hinges [1]_X += $X_{off} * m$, Middle_Hinges [1]_Y += $2Y_{off} * n$) ;
  end
end

Algorithm 3: curvilinear_lattice ($R, X_{off}, Y_{off}, M, N$)

Result: (X,Y) Coordinates for the hinge locations on the curvilinear lattice

Unit Cell Definition

Middle_Hinges [1] = (0 , r)

for *i = 1:1/2M / X_{off} (rounded to nearest integer)* **do**

  Middle_Hinges_Right [i+1] = $(X_{off} * i, \sqrt{R^2 - (X_{off} * i)^2})$;
  Middle_Hinges_Left [i+1] = $(-X_{off} * i, \sqrt{R^2 - (X_{off} * i)^2})$;
  Top_Hinges_Right [i+1] =
  $(X_{off} * i - X_{off}/2, \sqrt{R^2 - (X_{off} * i - X_{off}/2)^2} + Y_{off})$;
  Top_Hinges_Left [i+1] =
  $(-X_{off} * i - X_{off}/2, \sqrt{R^2 - (X_{off} * i - X_{off}/2)^2} + Y_{off}$;
  Bottom_Hinges_Right [i+1] =
  $(X_{off} * i - X_{off}/2, \sqrt{R^2 - (X_{off} * i - X_{off}/2)^2} - Y_{off})$;
  Bottom_Hinges_Left [i+1] =
  $(-X_{off} * i - X_{off}/2, \sqrt{R^2 - (X_{off} * i - X_{off}/2)^2} - Y_{off})$;

end

Middle_Hinges = [Middle_Hinges_Right Middle_Hinges_Left];
Top_Hinges = [Top_Hinges_Right Top_Hinges_Left];
Bottom_Hinges = [Bottom_Hinges_Right Bottom_Hinges_Left];

Pattern unit cells along length of skin

for *i = 1:N (rounded to nearest integer)* **do**

  (Middle_Hinges [1]_X, Middle_Hinges [1]_Y += $2 * Y_{off}$);

end

Algorithm 4: polar_lattice $(R, \theta, Y_{off}, M, N, K)$

Result: (X,Y) Coordinates for the hinge locations on the polar lattice

Full lattice pattern generation (unit cell undefinable)

for *n = 0:N (round to nearest integer)* **do**
  $R = R + Y_{off} * n$;
  for *m = 0:1/2M /* $R \sin\theta$ *(rounded to nearest integer)* **do**
    i = odd numbered m's;
    Middle_Hinges_Right [m] =
      $((R - Y_{off}) \sin(\theta/2 * i), (R - Y_{off}) \cos(\theta/2 * i) - K)$;
    Middle_Hinges_Left [m] =
      $((R - Y_{off}) \sin(-\theta/2 * i), (R - Y_{off}) \cos(\theta/2 * i) - K)$;
    Top_Hinges_Right [m+1] = $(R \sin(\theta * m), R \cos(\theta * m) - K)$;
    Top_Hinges_Left [m+1] = $(R \sin(-\theta * m), R \cos(\theta * m) - K)$;
    Bottom_Hinges_Right [m+1] =
      $((R - Y_{off} * 2) \sin(\theta * m), (R - Y_{off} * 2) \cos(\theta * m) - K)$;
    Bottom_Hinges_Left [m+1] =
      $((R - Y_{off} * 2) \sin(-\theta * m), (R - Y_{off} * 2) \cos(\theta * m) - K)$;
  end
end

Middle_Hinges = [Middle_Hinges_Right   Middle_Hinges_Left];
Top_Hinges = [Top_Hinges_Right   Top_Hinges_Left];
Bottom_Hinges = [Bottom_Hinges_Right   Bottom_Hinges_Left];

Notes for Algorithms 2 and 3: Technically nested FOR loops, as used for the polar lattice algorithm, can be used for patterning the unit cells for the other two lattices. I left them broken out as most kirigami work is defined by unit cells not the full patterned structure. Using the nested FOR loops simplifies the definition of the Middle_Hinges[1](X,Y) as the first (X,Y) pair in the Middle_Hinges array is the center point of the unit cell that then gets translated to make the rest of the tessellated structure. However, leaving the unit cell as a separate definition helps to show that only the curvilinear and rectilinear lattices have unit cells whereas the polar lattice does not. Since this diverges from the norm in kirigami literature, it's important that this point is very clear in defining a brand new lattice structure.

Notes for Algorithms 3 and 4: The curvilinear lattice is a hybrid of the rectilinear lattice and the polar lattice. That means that the linear columns from the rectilinear lattice are maintained with curvilinear rows. Because I started with the rectilinear lattice, I carry over the column and row spacing as defined there ($X_{off} = 2l\cos(\phi/2)$ and $Y_{off} = l\sin(\phi/2)$) to compare them directly in muse on the robot. However, this is arbitrary. Both the column and row spacing can be chosen at will. The rectilinear lattice is defined by a lattice width l and lattice angle ϕ, which then define the column and row spacing. The selection of l and ϕ is arbitrary though. There is no reason the column and row spacing have to be the same across lattices, that's just what I did to make a proper comparison in performance. For those not starting from the rectilinear lattice, using l and ϕ doesn't make sense. Instead, X_{off} and Y_{off} values can be defined directly. This is also true for the polar lattice which departs even further from the original rectilinear lattice strategy.

Bibliography

[1] Shigeo Hirose. *Biologically inspired robots: snake-like locomotors and manipulators.* Oxford University Press, 1993.

[2] Modular Snake Robots, 2013.

[3] Snake Movement — HowStuffWorks.

[4] M Calisti, G Picardi, and C Laschi. Fundamentals of soft robot locomotion. *Journal of the Royal Society, Interface*, 14(130), 5 2017.

[5] Callie Branyan, Chloe Fleming, Jacquelin Remaley, Ammar Kothari, Kagan Tumer, Ross L. Hatton, and Yigit Menguc. Soft snake robots: Mechanical design and geometric gait implementation. In *2017 IEEE International Conference on Robotics and Biomimetics (ROBIO)*, pages 282–289. IEEE, 12 2017.

[6] James K Hopkins, Brent W Spranklin, and Satyandra K Gupta. A survey of snake-inspired robot designs. *Bioinsp. Biomim*, 4, 2009.

[7] David Rollinson, Yigit Bilgen, Ben Brown, Florian Enner, Steven Ford, Curtis Layton, Justine Rembisz, Mike Schwerin, Andrew Willig, Pras Velagapudi, Howie Choset, Ben Brown, Florian Enner, Steven Ford, Curtis Layton, Justine Rembisz, Mike Schwerin, Andrew Willig, Pras Velagapudi, and Howie Choset. Design and Architecture of a Series Elastic Snake Robot. In *International Conference on Intelligent Robots and Systems*, pages 4630–4636, 2014.

[8] Cagdas D Onal and Daniela Rus. Autonomous undulatory serpentine locomotion utilizing body dynamics of a fluidic soft robot. *Bioinspiration & Biomimetics*, 8:26003–10, 2013.

[9] Marie-Christin G Klein and Stanislav N Gorb. Epidermis architecture and material properties of the skin of four snake species. *Journal of the Royal Society*, 2012.

[10] Bruce C Jayne, Steven J Newman, Michele M Zentkovich, and H Matthew Berns. Why arboreal snakes should not be cylindrical: body shape, incline and surface roughness have interactive effects on locomotion. *The Journal of experimental biology*, 218(Pt 24):3978–86, 12 2015.

[11] Fumiya Iida and Cecilia Laschi. Soft Robotics: Challenges and Perspectives. *Procedia Computer Science*, 7:99–102, 2011.

[12] Sangbae Kim, Cecilia Laschi, and Barry Trimmer. Soft robotics: a bioinspired evolution in robotics. *Trends in Biotechnology*, 31:287–294, 2013.

[13] Deepak Trivedi, Christopher D. Rahn, William M. Kier, and Ian D. Walker. Soft robotics: Biological inspiration, state of the art, and future research. *Applied Bionics and Biomechanics*, 2008.

[14] Cecilia Laschi, Barbara Mazzolai, and Matteo Cianchetti. Soft robotics: Technologies and systems pushing the boundaries of robot abilities. 2016.

[15] G.K. Klute, J.M. Czerniecki, and B. Hannaford. McKibben artificial muscles: pneumatic actuators with biomechanical intelligence. In *1999 IEEE/ASME International Conference on Advanced Intelligent Mechatronics (Cat. No.99TH8399)*, 1999.

[16] Fluidic Control Board — Soft Robotics Toolkit.

[17] Bobak Mosadegh, Panagiotis Polygerinos, Christoph Keplinger, Sophia Wennstedt, Robert F. Shepherd, Unmukt Gupta, Jongmin Shim, Katia Bertoldi, Conor J. Walsh, and George M. Whitesides. Pneumatic Networks for Soft Robotics that Actuate Rapidly. *Advanced Functional Materials*, 24(15):2163–2170, 4 2014.

[18] Panagiotis Polygerinos, Zheng Wang, Johannes T B Overvelde, Kevin C. Galloway, Robert J. Wood, Katia Bertoldi, and Conor J. Walsh. Modeling of Soft Fiber-Reinforced Bending Actuators. *IEEE Transactions on Robotics*, 2015.

[19] Fionnuala Connolly, Panagiotis Polygerinos, Conor J Walsh, and Katia Bertoldi. Mechanical Programming of Soft Actuators by Varying Fiber Angle.

[20] Citation Tolley, Robert F Shepherd, Bobak Mosadegh, Kevin C Galloway, Michael Wehner, Michael Karpelson, Michael T Tolley, Robert J Wood, and George M Whitesides. A Resilient, Untethered Soft Robot. *Soft Robotics*, 1(3):213–223, 2014.

[21] Ailish O'Halloran, Fergal O'Malley, and Peter McHugh. A review on dielectric elastomer actuators, technology, applications, and challenges. *Journal of Applied Physics*, 104(7):071101, 10 2008.

[22] M. Cianchetti, V. Mattoli, B. Mazzolai, C. Laschi, and P. Dario. A new design methodology of electrostrictive actuators for bio-inspired robotics. *Sensors and Actuators B: Chemical*, 142(1):288–297, 10 2009.

[23] Sangbae Kim, Elliot Hawkes, Kyujin Cho, Matthew Jolda, Joe Foley, and Robert Wood. Micro artificial muscle fiber using NiTi spring for soft robotics. In *2009 IEEE/RSJ International Conference on Intelligent Robots and Systems, IROS 2009*, 2009.

[24] F Harvey Pough, R M Andrews, J E Cadle, M L Crump, A H Savitzky, and K D Wells. Herpetology Prentice Hall. *Upper Saddle River, NJ*, 1998.

[25] Craig Guyer and Maureen A Donnelly. Length-Mass Relationships Among an Assemblage of Tropical Snakes in. *Journal of Tropical Ecology*, 6(1):65–76, 1990.

[26] Carl Gans. Approaches to the Evolution of Limbless Locomotion. *Cuadernos de Herpetología*, 8(1):12–17, 1194.

[27] Franç Brischoux and Richard Shine. Morphological Adaptations to Marine Life in Snakes. 272:566–572, 2011.

[28] Ronald C Rozar. *The Role of Morphology in the Locomotor Performance of Arboreal Snakes*. PhD thesis, 2010.

[29] R. Shine and S. Shetty. Moving in two worlds: aquatic and terrestrial locomotion in sea snakes (Laticauda colubrina, Laticaudidae). *Journal of Evolutionary Biology*, 14(2):338–346, 12 2001.

[30] Bruce C Jayne and Albert F Bennett. The Effect of Tail Morphology on Locomotor Performance of Snakes: A Comparison of Experimental and Correlative Methods. Technical report, 1989.

[31] Coleman M Sheehy Iii, James S Albert, and Harvey B Lillywhite. The evolution of tail length in snakes associated with different gravitational environments. 2015.

[32] Hamidreza Marvi, James P. Cook, Jeffrey L. Streator, and David L. Hu. Snakes move their scales to increase friction. *Biotribology*, 5:52–60, 3 2016.

[33] David Rollinson. *Control and Design of Snake Robots*. PhD thesis, Carnegie Mellon University, 2014.

[34] Daniel I Goldman and David L Hu. Wiggling Through the World The mechanics of slithering locomotion depend on the surroundings. *American Scientist*, 98, 2010.

[35] Carl Gans. Terrestrial Locomotion Without Limbs. *American Zoologist*, 2:167–182, 1962.

[36] J Gray. Undulatory Propulsion. *Journal of Cell Science*, 1953.

[37] Z V Guo and L Mahadevan. Limbless undulatory propulsion on land.

[38] Bruce C Jayne and James D Davis. KINEMATICS AND PERFORMANCE CAPACITY FOR THE CONCERTINA LOCOMOTION OF A SNAKE (COLUBER CONSTRICTOR). *J. exp. Biol*, 156:539–556, 1991.

[39] Michael Walton, Bruce C. Jayne, and Albert F. Bennet. The Energetic Cost of Limbless Locomotion. *Science*, 249(4968):524–527, 1990.

[40] Hamidreza Marvi and David L Hu. Friction enhancement in concertina locomotion of snakes. *Journal of the Royal Society, Interface*, 9(76):3067–80, 11 2012.

[41] Raymond B Cowles. Sidewinding Locomotion in Snakes. *Source: Copeia*, 1956(31):211–214, 1956.

[42] J Gray. STUDIES IN ANIMAL LOCOMOTION I. THE MOVEMENT OF FISH WITH SPECIAL REFERENCE TO THE EEL. *Journal of Experimental Biology*, 1933.

[43] Gary B Gillis. Undulatory Locomotion in Elongate Aquatic Vertebrates : Anguilliform Swimming since Sir James Gray 1. 36:656–665, 1996.

[44] J Michael Heffernan and Stephen A Wainwright. LOCOMOTION OF THE HOLOTHURIAN EUAPTA LAPPA AND REDEFINITION OF PERISTALSIS. *Reference : Biol. Bull*, 147:95–104, 1974.

[45] K J Quillin. Kinematic Scaling of Locomotion by Hydrostatic Animals: Ontogeny of Peristaltic Crawling by the Earthworm Lumbricus Terrestris. *Journal of Experimental Biology*, 202:661–674, 1999.

[46] Yoshimi Tanaka, Kentaro Ito, Toshiyuki Nakagaki, and Ryo Kobayashi. Mechanics of peristaltic locomotion and role of anchoring. *Journal of the Royal Society, Interface*, 9(67):222–33, 2 2012.

[47] Barry A Trimmer, Ann E Takesian, Brian M Sweet, Chris B Rogers, Daniel C Hake, and Daniel J Rogers. Caterpillar locomotion: A new model for soft- bodied climbing and burrowing robots.

[48] Barry A. Trimmer, Huai-Ti Lin, Amanda Baryshyan, Gary G. Leisk, and David L. Kaplan. Towards a Biomorphic Soft Robot: Design Constraints and Solutions. In *IEEE International Conference on Biomedical Robotics and Biomechatronics*, pages 599–605, Rome, 2012.

[49] Ariel A Calderón, Joakin C Ugalde, Juan Cristóbal Zagal, and Néstor O Pérez-Arancibia. Design, Fabrication and Control of a Multi-Material–Multi-Actuator Soft Robot Inspired by Burrowing Worms.

[50] Alexander S Boxerbaum, Kendrick M Shaw, Hillel J Chiel, and Roger D Quinn. Continuous wave peristaltic motion in a robot. *The International Journal of Robotics Research*, 31(3):302–318.

[51] Sangok Seok, Cagdas D. Onal, Robert Wood, Daniela Rus, and Sangbae Kim. Peristaltic locomotion with antagonistic actuators in soft robotics. In *Proceedings - IEEE International Conference on Robotics and Automation*, 2010.

[52] Sangok Seok, Cagdas Denizel Onal, Kyu-Jin Cho, Robert J Wood, Daniela Rus, and Sangbae Kim. Meshworm: A Peristaltic Soft Robot With Antagonistic Nickel Titanium Coil Actuators. *IEEE/ASME TRANSACTIONS ON MECHATRONICS*, 18(5), 2013.

[53] Kathryn A. Daltorio, Alexander S. Boxerbaum, Andrew D. Horchler, Kendrick M. Shaw, Hillel J Chiel, Roger D. Quinn, Hillel J Chiel, Alexander S Boxerbaum, Kendrick M Shaw, and Roger D Quinn. Efficient worm-like locomotion: slip and control of soft-bodied peristaltic robots. *Bioinspir. Biomim*, 8:35003–23, 2013.

[54] K. H. Low, Yang Jie, Anjan P. Pattathil, and Zhang Yonghua. Initial prototype design and investigation of an undulating body by SMA. In *2006 IEEE International Conference on Automation Science and Engineering, CASE*, 2007.

[55] A Westphal, N F Rulkov, J Ayers, D Brady, and M Hunt. Controlling a lamprey-based robot with an electronic nervous system. *Smart Structures and Systems*, 8(1):39–52, 2011.

[56] Andrew D Marchese, Cagdas D Onal, and Daniela Rus. Autonomous Soft Robotic Fish Capable of Escape Maneuvers Using Fluidic Elastomer Actuators. *Soft Robotics*, 1(1):75–87, 2014.

[57] Ahmad Rafsanjani, Yuerou Zhang, Bangyuan Liu, Shmuel M. Rubinstein, and Katia Bertoldi. Kirigami skins make a simple soft actuator crawl. *Science Robotics*, 3(15):eaar7555, 2 2018.

[58] Matthew Tesch, Kevin Lipkin, Isaac Brown, Ross Hatton, Aaron Peck, Justine Rembisz, and Howie Choset. Parameterized and Scripted Gaits for Modular Snake Robots. *Advanced Robotics*, 23(9):1131–1158, 1 2009.

[59] Ross L. Hatton and Howie Choset. Generating gaits for snake robots: Annealed chain fitting and keyframe wave extraction. *Autonomous Robots*, 28(3):271–281, 2010.

[60] Keyan Ghazi-Zahedi, Raphael Deimel, Guido Montúfar, Vincent Wall, and Oliver Brock. Morphological Computation: The Good, the Bad, and the Ugly.

[61] William M. Kier and Kathleen K Smith. Tongues, Tentacles and Trunks.

[62] L Margheri, C Laschi, and B Mazzolai. Soft robotic arm inspired by the octopus: I. From biological functions to artificial requirements. *BIOINSPIRATION & BIOMIMETICS Bioinspir. Biomim*, 7:25004–12, 2012.

[63] Mariangela Manti, Vito Cacucciolo, and Matteo Cianchetti. Stiffening in soft robotics: A review of the state of the art. *IEEE Robotics and Automation Magazine*, 2016.

[64] E. Brown, N. Rodenberg, J. Amend, A. Mozeika, E. Steltz, M. R. Zakin, H. Lipson, and H. M. Jaeger. Universal robotic gripper based on the jamming of granular material. *Proceedings of the National Academy of Sciences*, 107(44):18809–18814, 11 2010.

[65] Yingtian Li, Yonghua Chen, Yang Yang, and Ying Wei. Passive Particle Jamming and Its Stiffening of Soft Robotic Grippers. *IEEE TRANSACTIONS ON ROBOTICS*, 33(2), 2017.

[66] E Steltz, A Mozeika, N Rodenberg, E Brown, and H M Jaeger. JSEL : Jamming Skin Enabled Locomotion.

[67] Yashraj S. Narang, Joost J. Vlassak, and Robert D. Howe. Mechanically Versatile Soft Machines through Laminar Jamming. *Advanced Functional Materials*, page 1707136, 2 2018.

[68] Yang Yang, Yingtian Li, and Yonghua Chen. Principles and methods for stiffness modulation in soft robot design and development. *Bio-Design and Manufacturing*, pages 1–12, 2 2018.

[69] Takuya Umedachi, Vishesh Vikas, and Barry A Trimmer. Highly Deformable 3-D Printed Soft Robot Generating Inching and Crawling Locomotions with Variable Friction Legs. *IEEE International Conference of Intelligent Robots and Systems*, 2013.

[70] Huai-Ti Lin, Gary G Leisk, and Barry Trimmer. GoQBot: a caterpillar-inspired soft-bodied rolling robot. *Bioinspiration & Biomimetics*, 6(2):026007, 6 2011.

[71] Vishesh Vikas, Paul Templeton, and Barry Trimmer. Design and control of a soft , shape - changing , crawling robot.

[72] Alan T. Asbeck, Sangbae Kim, M. R. Cutkosky, William R. Provancher, and Michele Lanzetta. Scaling Hard Vertical Surfaces with Compliant Microspine Arrays. *The International Journal of Robotics Research*, 25(12):1165–1179, 12 2006.

[73] Suresh Ramasamy and Ross L. Hatton. Soap-bubble Optimization of Gaits. 2016.

[74] Ross L Hatton and Howie Choset. Geometric Swimming at Low and High Reynolds Numbers. *IEEE TRANSACTIONS ON ROBOTICS*, 29(3), 2013.

[75] R. L. Hatton and H. Choset. Geometric motion planning: The local connection, Stokes' theorem, and the importance of coordinate choice. *The International Journal of Robotics Research*, 30:988–1014, 2011.

[76] R. L. Hatton and H. Choset. Nonconservativity and noncommutativity in locomotion: Geometric mechanics in minimum-perturbation coordinates. *European Physical Journal: Special Topics*, 224(17-18):3141–3174, 2015.

[77] Jin Dai, Hossein Faraji, Chaohui Gong, Ross L Hatton, Daniel I Goldman, and Howie Choset. Geometric Swimming on a Granular Surface. *Proceedings of Robotics: Science and Systems*, 2016.

[78] Ross L. Hatton, Yang Ding, Howie Choset, and Daniel I. Goldman. Geometric visualization of self-propulsion in a complex medium. *Physical Review Letters*, 110(7), 2013.

[79] B R Moon and C Gans. KINEMATICS, MUSCULAR ACTIVITY AND PROPULSION IN GOPHER SNAKES. *The Journal of Experimental Biology*, 201:2669–2684, 1998.

[80] David L Hu, Jasmine Nirody, Terri Scott, and Michael J Shelley. The mechanics of slithering locomotion. *Proceedings of the National Academy of Science*, 106(25):10081–10085, 2009.

[81] Hisham A. Abdel-Aal. On surface structure and friction regulation in reptilian limbless locomotion. *Journal of the Mechanical Behavior of Biomedical Materials*, 2013.

[82] Kristin Y Pettersen. Snake robots R. *Annual Reviews in Control*, 44:19–44, 2017.

[83] S. Hirose. *Biologically Inspired Robots (snake-like locomotor and manipulator)*. Oxford University Press, Oxford, 1993.

[84] Miguel M. Serrano, Alexander H. Chang, Guangcong Zhang, and Patricio A. Vela. Incorporating frictional anisotropy in the design of a robotic snake through the exploitation of scales. In *Proceedings - IEEE International Conference on Robotics and Automation*, volume 2015-June, pages 3729–3734. Institute of Electrical and Electronics Engineers Inc., 6 2015.

[85] Toen Castle, Yigil Cho, Xingting Gong, Euiyeon Jung, Daniel M Sussman, Shu Yang, and Randall D Kamien. Making the Cut: Lattice Kirigami Rules. *Physical Review Letters*, 113(24):245502, 2014.

[86] Bangyuan Liu, Yasemin Ozkan-Aydin, Daniel I Goldman, and Frank L Hammond Iii. Kirigami Skin Improves Soft Earthworm Robot Anchoring and Locomotion Under Cohesive Soil. In *IEEE International Conference on Soft Robotics*, pages 828–833, 2019.

[87] Ahmad Rafsanjani, Katia Bertoldi, and John A Paulson. Buckling-Induced Kirigami. *Physical Review Letters*, 118(8), 2017.

[88] Terry C. Shyu, Pablo F. Damasceno, Paul M. Dodd, Aaron Lamoureux, Lizhi Xu, Matthew Shlian, Max Shtein, Sharon C. Glotzer, and Nicholas A. Kotov. A kirigami approach to engineering elasticity in nanocomposites through patterned defects. *Nature Materials*, 14(8):785–789, 8 2015.

[89] Aaron Lamoureux, Kyusang Lee, Matthew Shlian, Stephen R. Forrest, and Max Shtein. Dynamic kirigami structures for integrated solar tracking. *Nature Communications*, 6:8092, 9 2015.

[90] Midori Isobe and Ko Okumura. Initial rigid response and softening transition of highly stretchable kirigami sheet materials. *Scientific Reports*, 6(1):24758, 2016.

[91] J Gray and H W Lissmann. The Kinetics of Locomotion of the Grass-Snake. *Journal of Experimental Biology*, 26(4):354–367, 1950.

[92] Berthe R. A., , G. Westhoff, and Bleckmann H., and and Gorb S N. Surface structure and frictional properties of the skin of the Amazon tree boa Corallus hortulanus (Squamata, Boidae). *Journal of Comparative Physiology A*, 195(3):311–318, 3 2009.

[93] Martina J. Baum, Alexander E. Kovalev, Jan Michels, and Stanislav N. Gorb. Anisotropic friction of the ventral scales in the snake lampropeltis getula californiae. *Tribology Letters*, 54(2):139–150, 2014.

[94] J C Spagna, D I Goldman, P-C Lin, D E Koditschek, and R J Full. Distributed mechanical feedback in arthropods and robots simplifies control of rapid running on challenging terrain. *Bioinspiration & Biomimetics*, 2(1):9–18, 3 2007.

[95] Michael Wehner, Ryan L. Truby, Daniel J. Fitzgerald, Bobak Mosadegh, George M. Whitesides, Jennifer A. Lewis, and Robert J. Wood. An integrated design and fabrication strategy for entirely soft, autonomous robots. *Nature*, 536(7617):451–455, 8 2016.

[96] Philipp Rothemund, Alar Ainla, Lee Belding, Daniel J Preston, Sarah Kurihara, Zhigang Suo, and George M Whitesides. A soft, bistable valve for autonomous control of soft actuators. Technical report, 2018.